General Disclaimer

One or more of the Following Statements may affect this Document

- This document has been reproduced from the best copy furnished by the organizational source. It is being released in the interest of making available as much information as possible.

- This document may contain data, which exceeds the sheet parameters. It was furnished in this condition by the organizational source and is the best copy available.

- This document may contain tone-on-tone or color graphs, charts and/or pictures, which have been reproduced in black and white.

- This document is paginated as submitted by the original source.

- Portions of this document are not fully legible due to the historical nature of some of the material. However, it is the best reproduction available from the original submission.

Produced by the NASA Center for Aerospace Information (CASI)

SQT

NASA CR-151956
NA-76-863

SMALL-SCALE TEST PROGRAM TO DEVELOP A MORE EFFICIENT SWIVEL NOZZLE THRUST DEFLECTOR FOR V/STOL LIFT/CRUISE ENGINES

(NASA-CR-151956) SMALL-SCALE TEST PROGRAM TO DEVELOP A MORE EFFICIENT SWIVEL NOZZLE THRUST DEFLECTOR FOR V/STOL LIFT/CRUISE ENGINES (Rockwell International Corp., Los Angeles) 112 p HC A06/MF A01 CSCL 21E G3/07

N77-23110

Unclas
28867

By Donald W. Schlundt

November 1976

Prepared under Contract NAS 2-8972 by
ROCKWELL INTERNATIONAL
Los Angeles Aircraft Division

for

AMES RESEARCH CENTER
NATIONAL AERONAUTICS AND SPACE ADMINISTRATION

MAY 1977
RECEIVED
NASA STI FACILITY
INPUT BRANCH

NASA CR-151956
NA-76-863

SMALL-SCALE TEST PROGRAM TO DEVELOP A MORE EFFICIENT SWIVEL NOZZLE THRUST DEFLECTOR FOR V/STOL LIFT/CRUISE ENGINES

By Donald W. Schlundt

November 1976

Prepared under Contract NAS 2-8972 by
ROCKWELL INTERNATIONAL
Los Angeles Aircraft Division

for

AMES RESEARCH CENTER
NATIONAL AERONAUTICS AND SPACE ADMINISTRATION

TABLE OF CONTENTS

LIST OF ILLUSTRATIONS (Continued)

PRECEDING PAGE BLANK NOT FILMED

LIST OF ILLUSTRATIONS (Continued)

LIST OF ILLUSTRATIONS (Continued)

SMALL-SCALE TEST PROGRAM TO DEVELOP A MORE EFFICIENT SWIVEL NOZZLE THRUST DEFLECTOR FOR V/STOL LIFT/CRUISE ENGINES

By Donald W. Schlundt
Los Angeles Aircraft Division
Rockwell International

SUMMARY

The test program was performed under NASA contract NAS 2-8972 to investigate and improve the installed performance degradation of a swivel nozzle thrust deflector system obtained during increased vectoring angles of a large-scale test program conducted under contract NAS 2-7656. The program used small-scale models to generate performance data for analyzing selected swivel nozzle configurations. A single-swivel nozzle design model with five different nozzle configurations and a twin-swivel nozzle design model, scaled to 0.15-size of the large-scale test hardware, were statically tested at low exhaust pressure ratios of 1.4, 1.3, 1.2, and 1.1 and vectored at four nozzle positions from 0° cruise through 90° vertical used for the VTOL mode.

The small-scale model and large-scale hardware test data both show that the swivel nozzle deflector systems have low internal pressure losses in all nozzle positions. Significant thrust degradation obtained during the large-scale hardware tests when the nozzle vectoring angle was increased, however, did not occur during the small-scale model testing. Each of the small-scale models tested, including the single-swivel nozzle A configuration that represents a scaled 0.15 size of the large-scale test hardware, showed relatively constant total gross thrust for a selected airflow inlet pressure ratio as the nozzle was rotated from 0° cruise through 90° vertical positions. The small-scale test data substantiate the analysis that the degradation in thrust for increased vectoring angles during the large-scale tests was not due to the swivel nozzle deflector system internal performance. Figure 83 shows the thrust coefficients obtained from the large-scale swivel nozzle system testing, with and without internal flow vanes installed, as a function of nozzle position. The large-scale data in figure 83 are compared to the small-scale model test data of the single-swivel nozzle A, nozzle C with and without flow vanes, and the twin-swivel configurations. The thrust coefficient values for the nozzle A configuration with the estimated losses for the exit rake and base drag extracted, as presented in figure 82, are shown with the large-scale data in figure 83 to illustrate the estimated static performance of a swivel nozzle deflector system.

The small-scale static test program for the single- and twin-swivel nozzle configurations provided data to evaluate the thrust deflector concept for low-pressure ratio propulsion systems. The exit discharge coefficients along with the pressure loss through the swivel nozzle system would be used to determine the effective exit area of the nozzle. Design changes to provide an even exhaust pattern at the nozzle exit and to reduce exhaust flow losses, such as exit base drag, would improve the performance obtained from the small-scale tests. A change in the design of the twin-swivel nozzle divider section used in the scale tests to reduce the internal pressure losses would provide performance of the twin-swivel nozzle configuration to be comparable to the single-swivel nozzle configurations.

This report was prepared for NASA-Ames Research Center, Moffett Field, California, by the Los Angeles Aircraft Division of Rockwell International Corporation.

INTRODUCTION

A LF336/A lift-cruise fan exhaust deflector system was designed, built, and tested under a previous contract NAS 2-7656, dated 21 June 1973, to determine the design and performance characteristics of a large-scale single-swivel nozzle thrust vectoring system for V/STOL aircraft. The LF336/A lift fan system with the exhaust deflector nozzle, installed on the static test facilities at NASA-Ames, is shown in figure 1.

Procedure and results of the static test program are presented in the report NASA CR-137682 (NA-75-227), dated March 1975, entitled, "Testing of Lift/Cruise Fan Exhaust Deflector." The test hardware, that was designed to represent a typical aircraft installation for aerodynamic considerations and also designed with minimum complexity to allow for manufacture and assembly without high cost or difficulty, effectively vectored the fan exhaust flow from 0° through 130° with no structural problems during the entire test period. The performance characteristics obtained during thrust vectoring, however, were not as good as anticipated. The force measurements taken during the zero-degree vectoring cruise position indicated a thrust loss of less than 3 percent with the incorporation of turning vanes, but a substantial decrease in performance was measured in all tested configurations as the vector angle was increased. The thrust loss of approximately 15 percent obtained in the 90° nozzle position did not provide efficient propulsion system performance system performance to use for V/STOL aircraft design criteria. Based on a preliminary analysis of the test data indicating that the single-swivel system can be designed to provide higher performance during increased vectoring angles, a follow-on design investigation and small-scale model test program was recommended.

The small-scale model test program was conducted under contract NAS 2-8976, dated 6 August 1975, to develop a more efficient single-swivel thrust deflector for V/STOL lift/cruise engines. The purpose of the program was to investigate the single-swivel nozzle system performance degradation during increased thrust vectoring angles with additional analysis of the large-scale test data, explore configuration refinements to correct these deficiencies, and substantiate performance improvements with small-scale model testing. Changes in V/STOL aircraft requirements and design at LAAD, after the single-swivel nozzle program was initiated, resulted in a propulsion system installation outboard from the fuselage using an underwing nacelle concept. The most favorable method of thrust deflection for the nacelle installation proved to be a swivel nozzle system with the exhaust flow divided into two swivel nozzles rather than a single-swivel nozzle. The twin-swivel nozzle exhaust system (bifurcated swivel) appears to have an advantage of a shorter exhaust nozzle for higher ground clearance, negligible side forces, and is analyzed to have performance comparable to the tested large-scale single-swivel design. Based on the change in the V/STOL aircraft design, a twin-swivel nozzle configuration was included as one of the small-scale model designs for the test program.

This report presents the results of the small-scale swivel nozzle thrust deflector test program conducted at the Los Angeles Aircraft Division facilities of Rockwell International.

NOMENCLATURE AND SYMBOLS

A_2	sonic nozzle throat area, cm^2 ($in.^2$)
A_8	model nozzle exit area, cm^2 ($in.^2$)
C_D	sonic nozzle discharge coefficient
C_{D8}	model nozzle discharge coefficient
$(C_{D8})_5$	model nozzle discharge coefficient using total pressure into diffuser
C^*	critical flow coefficients
d	sonic nozzle throat diameter, cm (in.)
F_g	actual thrust, Newtons (lb)

F_{gi5}	ideal thrust, based on diffuser inlet conditions Newtons (lb)
F_{gi8}	ideal thrust, based on nozzle exhaust conditions Newtons (lb)
g	gravitational constant, m/sec^2 (ft/sec^2)
g_u	sonic nozzle upstream viscosity, kg/m-sec (lb/ft-sec)
H_T	ground plane height, cm (in.)
lrc	rolling moment about model reference center, cm-Newtons (in.-lb)
M_5AVE	average mach number, station 5
M_8AVE	average mach number, station 8
m_{r_c}	pitching moment about model reference center, cm-Newtons (in.-lb)
N	total normal force, Newtons (lb)
n_{r_c}	yawing moment about model reference center, cm-Newtons (in.-lb)
P_A	ambient pressure, Newtons/cm^2 (psia)
P_D	sonic nozzle downstream pressure, Newtons/cm^2 (psia)
$P_{T_{5_i}}$	diffuser rate total pressure, Newtons/cm^2 (psia)
P_{T_U}	sonic nozzle upstream total pressure, Newtons/cm^2 (psia)
P_U	sonic nozzle upstream static pressure, Newtons/cm^2 (psia)
$P_{S_{5_i}}$	diffuser rake static pressure, Newtons/cm^2 (psia)
$P_{T_{8_i}}$	nozzle exit total pressure, Newtons/cm^2 (psia)
R	gas constant, m/° K (ft/°R)
R_e	sonic nozzle Reynolds number
S	side force, Newtons (lb)
T	chord force, Newtons (lb)
T_{T_U}	sonic nozzle upstream total temperature, ° K (° R)

T_{T5}	diffuser total temperature (°R) °K
W_a	sonic nozzle weight flow (lb/sec) Kg/sec
W_{ai}	ideal weight flow (lb/sec) Kg/sec
Ψ	swivel nozzle angle, deg refer nozzle exit plane centerline aft = 0°
○	single-swivel nozzle A configuration
△	single-swivel nozzle B configuration
◇	single-swivel nozzle C configuration
◆	single-swivel nozzle C (with vanes) configuration
□	single-swivel nozzle D configuration
[]	twin-swivel nozzle configuration

newtons = 4.4482 x pounds force

kilograms = 0.4536 x pounds weight

centimeters = 2.54 x inches

° kelvin = 5/9 x ° Rankine

OBJECTIVE

The objective of the program was to develop a more efficient single- and twin-swivel thrust deflector for V/STOL lift/cruise engines by using small-scale test models. The three basic tasks required to accomplish the objective of the program, as described in the introduction section, were to analyze the large-scale thrust deflector test data to find the hardware design problem areas, modify the design to improve the nozzle performance, and conduct a small-scale test program to generate performance data for analyzing the selected model configurations.

LARGE-SCALE TEST DATA ANALYSIS

The initial task of the thrust deflector development and test program was to explore the design problem areas. The fan inlet temperature increase from 11° to 17° K (20° to 30° K) when the nozzle was rotated from 0°-cruise position to the 90°-vertical position and the J85 gas generator inlet ingestion of the higher temperature air when the fan system exhaust flow was deflected down into the test stand pit resulted in a net reduction in performance. Although the large-scale test data were normalized for the anlaysis to relate the environmental effects of the ambient temperature and pressure conditions to the fan system, the temperature effect of the J85 gas generator inlet ingestion and the 2- to 3-percent increase in J85 rotor speed to maintain near constant fan speed during thrust vectoring was not accounted for in the exhaust flow analysis. A temperature increase of the gas generator discharge from the tip-turbine flow and the fan exhaust flow was measured by the diffuser discharge rake as the nozzle was rotated down. A typical result was that the tip-turbine discharge temperature increased between 33° and 39° K (60° to 70° R) as the nozzle was rotated to the 90°-nozzle position at 90-percent fan speed. The indication is that the J85 gas generator discharge temperature was increasing due to throttle adjustment required to maintain fan speed as the nozzle was rotated down. This increase in tip-turbine discharge temperature with thrust deflection and the fan exhaust temperature increase due to ingestion and higher fan pressure causes an average nozzle flow temperature increase. Based on the estimated average temperature obtained from correcting the measured values on the diffuser exit rake, the mixed exhaust temperature increased approximately 11 to 17° K (20° to 30° R) when the nozzle was rotated from the 0°- to 90°-position. A temperature increase of this magnitude would require a nozzle exit area increase of approximately 2 percent to exhaust the same flow rate at a constant pressure.

Corrected total exhaust flow rates were calculated from the weight flow/area function values obtained for the total and static pressure data measured at the diffuser exit rake. Actual total exhaust flow rates were calculated from the corrected flow rates, using the estimated average temperatures and average total pressures. From these data the actual flow rates were plotted as a function of nozzle position for selected constant fan speed of 90, 80, and 60 percent, and the trend showed a reduction in total exhaust flow rate as the nozzle was rotated down. Additional internal pressure losses due to flow turning during thrust vectoring and the increase in exhaust temperatures could both cause a reduction of exhaust flow rate when a fixed nozzle area is used. An increase in nozzle exit area would be required to maintain a constant flow rate for a selected fan speed during thrust vectoring to allow for this change in nozzle internal aerodynamics.

Static pressure taps installed on the inside of the small radius bends prior to and aft of the swivel bearing were used on the large-scale hardware to determine the flow condition along the bend wall. The static pressure measurements taken around the small radius bend prior to the bearing in the diffuser section were fairly constant during each of the nozzle positions that were run with or without flow vanes installed. The static pressure data for the small radius bend aft of the bearing in the nozzle section showed a drop in static pressure as the flow passed around the bend and the static to ambient pressure ratio fell below 1.0 during all nozzle positions. The static pressure measurements in the nozzle section tend to increase downstream of the bend as the static to ambient pressure ratio approach 1.0 at the nozzle exit plane. The installation of flow vanes in the nozzle section did increase the static pressures around the bend, compared to the measurements for the same conditions taken without flow vanes, but the static to ambient pressure ratios in the nozzle section bend were always lower than measured just prior to the bend and upstream in the diffuser. The static pressure patterns along the nozzle small radius bend indicate flow separation due to the static pressure reduction throughout the bend. Although flow vanes in the nozzle did provide an improvement in the pressure pattern and performance, a design change in the nozzle section would be required for further improvements.

From this analysis, it appeared that the major portion of the performance losses (other than the high-temperature air ingestion) could be reduced by three changes in the swivel nozzle section design. The primary change would be to increase the exhaust nozzle exit area to allow for a reduction in the nozzle discharge coefficient. A change in flow characteristics as the nozzle is rotated due to an additional pressure reduction, due to separation from high flow bend angles and due to an increase in exhaust temperatures (caused by ingestion or higher turbine discharge temperature) would require a larger exhaust nozzle exit area to compensate for a low discharge coefficient. Different nozzle exit areas would be incorporated in the small-scale model design to investigate the effect on internal performance during thrust vectoring.

A second design change would be to increase the small bend radius of the inner nozzle section aft of the bearing. The analysis of the large-scale test data indicated only a limited improvement in the nozzle bend wall static pressures with the installation of flow vanes due to possible flow separation still occurring. Designing the small-scale test model with a larger bend radius would explore a basic method of reducing this flow separation problem.

A third change would be a modification to the outer shape of the nozzle section aft of the bearing to increase the bend radius. This larger outer bend radius would improve the flow path and reduce the local flow mach number, particularly in the vertical thrust deflection angles where the flow path is turned down.

HARDWARE DESCRIPTION

Models

The thrust deflector configurations selected for building the small-scale test models were analyzed to provide the desired design characteristics for the investigation of the single- and twin-swivel nozzle internal performance. The small-scale models were designed for modular construction to simplify assembly and minimize the amount of test hardware. The single-swivel nozzle configuration with the different nozzle designs and the twin-swivel nozzle configuration are illustrated in figures 2 and 3. Photographs of the assembled test models and separate hardware components are shown in figures 4 through 10. The single-swivel nozzle model was scaled to 0.15-size of the large-scale test hardware used for the thrust deflector test program performed at NASA/Ames in 1974 with the LF336/A lift-fan propulsion system.

The diffuser section for the small-scale models, as shown in figure 4, was common for both the single- and twin-swivel nozzle configurations. The circular diffuser section was designed to provide an effective expansion half-angle of approximately 10° to simulate the large-scale hardware. An exhaust hub cone of an ellipse design that is held in the center of the duct by four support struts and a diffuser duct wall angle of less than 4° combined to provide the desired expansion from the 0.15-scale diffuser inlet area to the maximum duct area. The diffuser inlet flange was designed for mounting to the plenum outlet flange with an inside diameter of 16.5 centimeters (6.5 inches). The upstream portion of the center cone is a half sphere with a 4.064-centimeter (1.6 inch) radius which allows airflow to enter the minimum duct area of the diffuser from the larger plenum duct area with a good flow path. The diffuser section, including the hub cone, was formed and machined from a steel alloy material.

The single-swivel bend section, that ducts the internal flow through the 65° bend to the swivel bearing plane, has a scaled 0.15-size inside diameter of 17.9 centimeters (7.05 inches). The circular duct section was sized to provide a flow velocity of less than 0.3 mach number to minimize internal flow losses. A 2.54 centimeter (1.0 inch) length of constant area straight duct was added to the model design of the 0.15-size bend section prior to the 65° bend to avoid a model interference problem between the swivel bearing flange and the flange mounting the bend and diffuser sections. This additional length would have a negligible effect on internal performance since the diffuser or bend flow conditions would not be changed.

Five nozzles were fabricated for the single-swivel nozzle configuration to investigate thrust vectoring performance with the small-scale models. The nozzles are shown in the schematic in figure 2 and hardware photographs in

figure 6. Model nozzle A represents the basic nozzle design scaled 0.15-size of the large-scale test hardware. The nozzle section shape changes from circular at the swivel bearing to oval at the nozzle exit plane. The shape was formed by maintaining a constant maximum dimension of the bearing in the top and bottom walls, while in the side walls the dimensions were reduced by a half-angle of approximately 10.5 degrees. This nozzle shape was selected to represent a typical aircraft installation for providing a low aerodynamic drag design. The basic model nozzle A exit area was sized for 145.8 centimeters squared (22.6 inches squared).

Model nozzles B, C, and D incorporate the design modifications to the basic nozzle design, each differing in nozzle exit area. These modifications, as described in the analysis section, include an increase in the inner small bend radius, an increase to the outer large bend radius, and a change in exit area. The design changes move the nozzle exhaust centerline from 1.4 centimeters (0.55 inch) to 2.4 centimeters (0.95 inch) further outboard when the basic model nozzle design. Model nozzle B used the same exit area as the basic nozzle A of 145.8 centimeters squared (22.6 inches squared). Model nozzle C has a 9.6-percent larger exit area than the basic nozzle of 159.8 centimeters squared (24.77 inches squared) and model nozzle D has a 18.8-percent larger exit are than the basic nozzle of 173.3 centimeters squared (26.86 inches squared). Two models of the nozzle C were made to allow one of the models to have three equally spaced thin steel vanes installed. The guide flow vanes extend throughout most of the bend portion of the nozzle which is approximately half of the section length.

The twin-swivel nozzle divider section ducts the internal flow through two 12.66 centimeter (4.985 inches) inside diameter swivel bearings, each half the flow area of the single-swivel bearing. The position of the twin-swivel bearing plane was designed to be on the same angle and approximately the same distance to the center of the bearing axis, with reference to the diffuser duct centerline, as used for the single-swivel nozzle configuration. The same 2.54 centimeters (1.0 inch) length of 17.9 centimeters (7.05 inches) constant diameter duct was used for the twin-swivel nozzle divider section prior to the small radius bend of the 65° flow turn into the swivel bearing as was designed for the single-swivel nozzle bend section. A half-sphere contour shape of a 8.95 centimeters (3.525 inches) radius on the duct centerline 5.08 centimeters (2.0 inches) aft of the divider section inlet was used to provide a simple twin arrangement design with minimum base area between the twin nozzles.

The matching model nozzles for both sides of the twin-swivel nozzle configuration, as shown in figure 9, were designed as 0.707 size (0.50-area scale) of the single swivel model nozzle C. The twin model nozzles each have an

exhaust exit area of 79.9 centimeters squared (12.4 inches squared). The flow path from the bearing through the nozzle exit for both of the twin nozzles is the same as the flow path through the single swivel model nozzle C.

The single-swivel bend section, the twin swivel nozzle divider section, and all the model nozzles were made by a laminated fiber glass material process with metal mating flanges. The fiber glass material walls, approximately 0.60 centimeters (0.24-inch) thick, were designed for the stress loads obtained at maximum test conditions. Nozzle swivel variations were accomplished by using an indexed Marman Aeroquip V-band coupling installed over the mating flanges of the nozzle section and the single-swivel bend or twin-swivel divider sections. An O-ring gasket was used between all the model section flanges to provide a pressure/leakage seal.

The test model hardware was mounted to an air plenum section that was mounted on the balance assembly. All the forces from the test model are transmitted through the plenum to the balance. Air flows into the plenum from the balance assembly through four opposing inlets around the section and passes through a screening system in the outer chamber of the plenum before being delivered into the diffuser inlet section of the model. The plenum is a welded steel assembly that was designed and constructed by Rocketdyne Division of Rockwell International to provide an undistorted flow to a test nozzle model with minimum airflow force effects.

Measurement Balance

A six-component measurement balance was used to measure thrust forces and moments acting on the model. The test hardware assembly was mounted on the balance as shown in figures 7, 8, and 10. The balance measures three forces in horizontal, vertical, and side directions and three moments in pitch, yaw, and roll. The balance was designed and constructed by Rocketdyne Division of Rockwell International to provide force measurements of deflector- and vectoring-type exhaust nozzles with a minimum of interference error. System gas flow is brought onboard test hardware through a floating "trombone" arrangement integral to the balance and by this method the induced momentum and pressure corrections are considered negligible. The gas flow is delivered to the balance through eight separate inputs of the floating "trombone" arrangement and are tied together from the balance output to provide the four plenum inputs.

The load cells on the balance were of the dual output type. Both outputs from the load cells were recorded but only one of the outputs was used for data reduction. Three load cells were used to measure the horizontal or axial forces, two load cells were used to measure the vertical or normal forces, and one load cell was used to measure the side force.

The test model hardware was installed on the balance in an inverted position to eliminate ground effects. The air plenum and test model hardware was mounted to the balance assembly on a fixed 30° angle wedge section. This allowed the swivel exhaust nozzle to be positioned 30° down from horizontal for the 0° deflector angle cruise conditions and 60° up from horizontal for the 90° deflector angle VTOL conditions to avoid impingement of the exhaust flow on the balance frame. The test model hardware, the balance system, and the floating "trombone" air tubes were isolated from the nozzle exhaust flow effects by separator sections and cover panels mounted to the ground.

Instrumentation

A 2.2 centimeter (0.865-inch)-diameter sonic nozzle flowmeter was used to measure the airflow rate of the pressurized air supply to the balance. The flow meter had been calibrated and used for other programs prior to the test. Flow meter upstream and downstream pressure levels measured by transducers and upstream temperature levels measured using an exposed junction iron-constantan thermocouple probe were mounted in the air supply line.

The total and static pressures of the flow entering the deflector system were measured at the diffuser inlet plane at station 5, as shown in figure 2, that mounts to the air plenum outlet plane. The diffuser inlet pressure probes were integrated into the fabrication ofthe four diffuser hub support vanes, as shown in the inlet and exit views in figure 4. Three total and one static pressure probes were installed on each of the four vanes in a area weighted profile. A exposed junction iron-constantan thermocouple probe was mounted in the diffuser section to measure the airflow temperature levels in the models. The diffuser section with the installed instrumentation was used for all test model configurations.

The deflector exhaust total pressures were measured at the station nozzle exit plane, as shown in figures 2 and 3. The exhaust total pressure rake assembly for all the single-swivel nozzle deflector models, as shown in figure 11, was an adjustable system to provide a near-area weighted profile for each of the three different oval-shaped nozzle areas included in the test program. Each of the eight cantilevered rakes had three total pressure probes installed to provide a total of 24 pressure measurements in the deflector exhaust stream. The twin nozzle system used a fixed exhaust total pressure rake assembly designed to provide 16 pressure measurements in a near-area weighted profile at the nozzle exit plane. The exhaust total pressure rake assembly for the twin nozzle deflector system was interchangeable for installation on either of the matched exhaust nozzles. Exit probe weighting factors were used to calculate the average total pressure of the nozzle exit area.

Test Facility

The static small-scale model tests were performed in the calibration room of the Trisonic Wind Tunnel facility at the Los Angeles Aircraft Division of Rockwell International.

High-pressure air system. - High-pressure air is supplied to a storage bottle from two compressors with 0.227 kg/sec (0.5 lb/sec) total airflow capacity. The storage bottle has a volume of 13.3 cubic meters (470 cubic feet) and is capable of storing 2,948 kilograms (6,500 pounds) of air at 1,827 Newtons/cm^2 (2,650 psia). The air is dried to a 220° K (400° R) dew point using a twin-bed dryer system at the compressor intake.

The air is supplied to the calibration room through a 10 centimeter (4-inch) diameter line (OD) and metered using a 2.2 centimeter (0.865-inch) diameter sonic nozzle. The airflow is controlled using a servo hydraulic valve upstream of the flow meter.

Data acquisition and processing. - The astrodata automatic data acquisition system used provides filtering, power supplies, and signal amplification for up to 120 channels of instrumentation.

The conditioned analog signals are passed through the system multiplexer and analog to digital converter. These digital data are collected through an IBM 1802-2CB Process Controller and written on magnetic tape. Simultaneously with this collection process those blocks of data which satisfy the data reduction program search routine are stored on disk for immediate processing. The data processing phase automatically follows the collection phase with final computed data available within a few minutes of a test point.

A UCC M-2000 incremental plotter provides work plots with all required annotations and data fairing if desired.

TEST CONDITIONS AND PROCEDURE

Force measurements of the six-component balance system were checked with a static-load calibration after the installation of the balance system was completed in the test room. All the balance load cells proved to be providing accurate force measurements within the level of the design requirements.

A high-pressure leak check of the air supply system, balance air lines, and plenum was performed prior to testing. A pressure blank-off plate was attached to the downstream plenum flange and the leak check was performed with air pressure to ambient pressure ratios up to approximately 30.

A calibrated ASME nozzle was installed to the air plenum on the balance system and a series of checkout tests were made to perform a statistical analysis of actual test data. The ASME nozzle installation is shown in figure 12. The performance runs with the ASME nozzle were made using a varing airflow rate to simulate the range of airflow rates that would be used during the swivel nozzle model testing. Due to the smaller exhaust exit area of the ASME nozzle, compared to the swivel nozzles, the plenum discharge total to ambient pressure ratios were in the 2 to 5 range during the ASME nozzle tests rather than the 1.1 to 1.4 pressure ratio range used for the model testing. A gross thrust coefficient and flow discharge coefficient were computed from the ASME nozzle test data for each run. These data are compared to the predicted values of the calibrated ASME nozzle as shown in figure 13. The ASME nozzle test data proved to be within the desired range of accuracy for the swivel nozzle thrust deflector test program.

The same testing procedure was followed for each of the different swivel nozzle configurations tested. The four nozzle positions selected for the test as measured from the direct aft zero-degree direction used for cruise were 0°, 30°, 60°, and 90° vertical used for the VTOL made. At the 0° nozzle position, a series of four runs with airflow inlet total to ambient pressure ratios of 1:1, 1:2, 1:3, and 1:4 were made. At the 30°, 60° and 90° nozzle positions total to ambient pressure ratios of 1:1, 1:2, and 1:3 were used. To provide ground effect information, the simulated ground plane plate was mounted perpendicular to the nozzle exhaust flow when the nozzle was installed in the vertical 90° nozzle position. The single swivel nozzle C configuration was run with ground heights of 30.48, 25.4, 20.32, and 15.24 centimeters and the twin-swivel nozzle configuration was run with ground heights of 25.4, 20.32, 15.24, and 10.16 centimeters. The ground height tests were run at total to ambient pressure ratios of 1:1, 1:2, and 1:3.

Each of the different nozzle configurations was run with all the test instrumentation listed in the hardware description to provide data for each test condition. In addition to these runs, a series of runs for the single-swivel nozzle configuration C and the twin-swivel nozzle were made without the total pressure rake installed at the exit plane. The data obtained from the runs made with and without the exit total pressure rake can be used to compare what effect the metric installation of the instrumentation has on internal performance.

Immediately before and after each performance run a recording of the measurements was taken with the airflow off to establish the test instrumentation.

A pretest report NA-76-345 was prepared prior to the testing to define and outline the test program procedure. Along with a description of the test hardware and required instrumentation, a complete definition of the method of data processing including test nomenclature and equations was presented in the report.

TEST RESULTS

The five single-swivel nozzle configurations and the one twin-swivel nozzle configuration were each tested as outlined in the testing procedure. The test results were recorded on magnetic tape and stored on disks for immediate processing after each test run. Data from the test instrumentation and data reduction program using the data processing equations were provided as computer printouts. Parameters were selected from the stored data to provide plots for this report and were made by an incremental plotter system. The symbols used in the data plots were consistent in representing each of the tested nozzle configuration as defined under "Nomenclature and Symbols."

The measured force components in the normal (vertical), chord (horizontal), and side directions are shown in figures 14 through 19 for each nozzle configuration. The three curves of force values for each nozzle were measured at diffuser inlet total to ambient pressure ratios of 1:3, 1:2, and 1:1. The larger nozzle exit area used for the configuration produced higher maximum force values, as illustrated by comparing nozzles B, C, and D at the same pressure ratio and angle. The higher thrust is due to an increase in internal airflow through a larger exit area for a given pressure ratio. The force data show a definite pattern for all swivel nozzle models to produce the maximum thrust in the horizontal direction at the 0° cruise nozzle position and the maximum thrust in the vertical direction in the 90° nozzle position. A smooth reduction from maximum to zero force in the horizontal and vertical directional planes is clearly shown in the test data plots as the swivel nozzles are rotated through a 90° arc.

Nozzle A and B configurations show minimum side force at 0° and 90° nozzle positions. As the nozzle exit area was increased, the side force values at 0° and 90° nozzle angles also increased, indicating the exhaust flow from the nozzle was changing outboard in the side direction. These data show that the single-swivel nozzle section would require a design modification for the increase exit area configurations if minimum side force is desired at 0° and 90° nozzle positions.

The side forces for the twin-swivel nozzle configuration (figure 19) are minimized due to the counterforce effect on two nozzles rotating through the same nozzle positions. The resultant side force of the twin-nozzle would normally balance out to zero as the nozzles are rotated together. The test data plots show a slight side force at all nozzle angles due primarily to a reduction in performance of one of the twin nozzles that had the exit total pressure rake installed.

The total gross thrust of the swivel nozzles is defined at the vector summation of the measured horizontal, vertical, and side force components. The total gross thrust values, corrected by the diffuser inlet total to standard ambient pressure ratio, is shown in figures 20 through 25 for each of the swivel nozzle configurations. Again, the slightly higher thrust values for the larger exit area configuration is due to an allowable increase in internal airflow. Using these total thrust values, a thrust coefficient based on an ideal thrust at the diffuser inlet conditions is presented in the same figures.

The most significant fact to be noted from these thrust data is that there was no degradation in performance in the configurations tested as the nozzle was rotated from a 0° cruise to 90° vertical position. The change in thrust coefficient throughout the range of nozzle positions tested was within 2 percent for all configurations without internal flow vanes. The thrust coefficient, based on diffuser inlet ideal thrust, shows a total performance loss for all swivel nozzle configurations, which includes pressure loss and nozzle exit loss, to be within a range of 7 to 12 percent.

The average total to ambient pressure ratios measured at the nozzle exit plane for each configuration are shown in figures 26 through 31. The ratio of average exit plane total pressure to average total pressure at the diffuser inlet, also shown, illustrates the change in total pressure through the entire deflector system. Since pressure loss is a function of duct airflow velocity, the configurations with higher flow rate at constant pressure, due to an increased exit area, show slightly higher pressure losses.

The following is apparent. First, nozzle rotation through 0° cruise to 90° vertical position has little effect on external pressure loss for the same flow conditions. Second, reducing the inlet pressure, which also decreases the airflow and duct velocity, does show an expected decrease in pressure loss. Third, the low-pressure losses through the system, ranging from 1 to 3 percent for all swivel nozzle models tested, indicates good internal aerodynamic characteristics.

Figures 32 through 37 show plots of the corrected flow rates and nozzle exit discharge coefficients for each of the swivel nozzle configurations. The flow rates corrected for the pressure and temperature conditions at the diffuser inlet show the increase in flow rate for the same pressure when the configurations with larger exit areas were tested. A comparison of nozzle C with and without nozzle flow vanes in figures 34 and 35 show that a higher discharge coefficient obtained with flow vanes for the same exit area allows an increase in flow rates. The plots indicate a slight reduction in exit discharge coefficients of 1 to 2 percent when the swivel nozzle was rotated from the 0° cruise to 90° vertical position.

A comparison of exit to diffuser total pressure ratios, discharge coefficients, and thrust coefficients, for all swivel nozzle configurations tested, is presented in figures 38 through 49 as a function of nozzle position for diffuser inlet total pressure ratios of 1:3, 1:2, and 1:1. The same computed test parameters compared at nozzle positions of 0°, 30°, 60°, and 90° as a function of diffuser inlet total pressure ratio are presented in figures 50 through 65.

The data plots comparing the test results of all configurations show the single swivel nozzles A and B designs to have the highest overall performance characteristics. The twin-swivel nozzle test data indicate a slightly higher exit discharge coefficient is obtained with a twin-swivel design compared to the similar single-swivel design of nozzle C, but the overall performance characteristics of higher internal total pressure losses and lower thrust coefficients show the twin nozzle to have the lowest performance of all the configurations tested.

Comparing the data plots of nozzle C configuration tested with and without guide flow vanes in the nozzle section indicates that the vanes cause a slight increase in the exit discharge coefficient values for all nozzle positions. The flow vanes also improved the thrust coefficients when the nozzle was vectored from 30° to 90°. However, the flow vanes caused a reduction in the internal performance of nozzle C when tested in the 0° cruise position.

The test data results plotted in figures 38 through 65 compare the deflector system total thrust coefficient based on the ideal thrust using the diffuser inlet conditions and the nozzle exit thrust coefficients, based on the nozzle exhaust conditions at the station 8 exit plane. The difference between the diffuser inlet and nozzle exit thrust coefficients is attributed to the loss in pressure through the deflector system. The important consideration to be obtained from the coefficient comparison is that the largest portion of the overall performance loss, for each of the configurations tested, is related to the low thrust coefficient derived from internal aerodynamic conditions at the nozzle exit.

The nozzle exit total pressure rake values for each probe are presented in figures 67 through 81 for each of the nozzle configurations tested in the 0° cruise and 90° vertical nozzle positions. The data are shown for diffuser inlet pressure ratios of 1:3, 1:2, and 1:1. A schematic of the single- and twin-swivel exit total pressure rakes is shown in figure 66 to illustrate the location of each probe used to measure the pressure at the nozzle exit plane.

The exit total pressure probe data are useful to explore the condition of the exhaust flow at the exit plane. The single-swivel nozzle exit pressure measurements show a similar pattern for all nozzles tested in the 0° and 90° positions. Measurements taken in the 0° position consistently indicate low-pressure ratios on the outside probes of the horizontal rake. The outside probes on the middle horizontal rake, with the exception of the nozzle C with vanes configuration, maintained the higher pressure of the three horizontal rakes throughout the test. Configurations with the larger exit areas, and higher flow rates at selected inlet pressures, showed lower pressure ratios at the outside probe locations. The probes toward the inside or small radius bend portion of the horizontal rake measured increasing pressure values in the 0° position. Nozzle A, which has a smaller inner bend radius, indicated a fall-off in pressure for the inside probe near the wall at the 1:3 pressure ratio. The nozzle C with flow vanes configuration had slightly lower pressures in the middle portion of the horizontal rakes than nozzles without vanes.

The vertical portion of the exit pressure rake shows a slight fall-off in pressure for the No. 1 probe at the top and No. 3 probe at the bottom near the wall when the nozzle is in the 0° position. This pattern for the vertical rake is common for all configurations without flow vanes. The nozzle C with flow vanes configuration shows low pressures for all six probes on the vertical exit rake in the 0° nozzle position.

The exit pressure measurements taken at the 90° nozzle position show an extreme pressure fall-off for the inside probes on the bottom horizontal rake. The bottom part of the nozzle in the 90° position would be forward toward the diffuser inlet. Nozzle A, with a small inner bend radius, also shows a fall-off in pressure for the inside probe near the wall on the middle horizontal rake. The nozzle C with flow vanes shows less pressure fall-off for the inside probes on the bottom horizontal rake than the nozzles without vanes; however, the nozzle C with vanes showed low pressures in the center portion of all horizontal rakes.

When the nozzle is in the 90° position, the vertical portion of the exit pressure rake shows a trend similar for all single-swivel configurations where the pressures are highest at the top, with a decrease to the lowest pressures at the bottom. In the 90° position, the top is to the rear, and the bottom is forward toward the diffuser inlet.

The twin-swivel nozzle configuration showed similar pressure patterns for the horizontal portion of the exit rake as did the single-swivel nozzle measurements. The pressure measurements of the vertical portion of the exit rake showed low pressures at the top in the 0° position and low pressures in the center in the 90° position, but the pressure fall-off at the bottom peculiar to the single-swivel nozzle was not evident in the twin-swivel data.

The results of the ground height effect tests for the single-swivel nozzle C and the twin-swivel configurations tested in the 90° nozzle position are presented in figures 79 through 81. The plots are shown for the exit-to-inlet pressure ratios, exit discharge coefficients, and diffuser inlet thrust coefficients versus ground height for diffuser inlet pressure ratios of 1:2 and 1:3. The effective diameter of the nozzle C exit area is 14.26 centimeters (5.61 inches), and the effective diameter of each of the twin-nozzle exit areas is 10.11 centimeters (3.98 inches). The nozzles were tested for ground heights in the range of approximately one through two effective nozzle exit diameters.

The nozzle-exit-to-diffuser-inlet total pressure ratios, plotted in figure 79, show relatively no change with ground height. The pressure ratio values obtained from the ground height tests were slightly lower than values obtained from the tests performed in the 90° nozzle position with a ground plane. The exit discharge coefficients, plotted in figure 80, show little change for the single-swivel nozzle C with varing ground height, while the twin nozzle indicated a slight increase as the ground height was decreased.

The diffuser inlet thrust coefficients for the ground height tests, plotted in figure 81, show a slight decrease in values for the single-swivel nozzle C as the ground height was reduced. The nozzle C thrust coefficient at the maximum ground height compared the same as that obtained for the 90° nozzle position tests with a ground plane. The twin-swivel nozzle thrust coefficient data appear irregular with varing ground height. All thrust coefficients values shown in the ground height test data were higher than were obtained during tests performed without a ground plane.

DISCUSSION

The test data presented in figures 14 through 81 and described in the test results section provide selected parameters to investigate the aerodynamic performance of the single- and twin-swivel nozzle configurations. The data plots can be used to compare and analyze internal pressure losses, flow discharge coefficients, force measurements, and thrust losses for swivel nozzles deflecting low-pressure exhaust flow from 0° through 90°.

The side force components of the data plots deserve special attention in the data analyses. The position of the swivel bearing plane with reference to the centerline of the lift/cruise fan or propulsion system exhaust axis determines the side loads obtained as the nozzle is rotated. The position of the swivel bearing used for the model design was selected to provide acceptable side force values for aircraft design requirements and to provide minimum side force at 0° cruise and 90° vertical nozzle positions. Higher side force values at 0° and 90° positions as the size of the single-swivel nozzle exit area was increased indicated a change in the exhaust flow path toward the outboard side direction. The model nozzle designs with the larger exit areas would require exhaust direction modifications to provide minimum side force in the 0° cruise and 90° vertical nozzle positions. Nozzle configurations with varing exit areas must be analyzed for exhaust flow path direction to obtain the desired performance at a selected nozzle position.

The data obtained from the large-scale thrust deflector test program, performed at NASA/Ames using the LF336/A lift-fan system, had shown a significant performance loss during thrust vectoring. The purpose of the small-scale model test program was to investigate the thrust vectoring losses to improve the swivel nozzle performance. Each of the swivel nozzle models tested, including the single-swivel nozzle A configuration that represents a scaled 0.15 size of the large-scale test hardware, showed relatively constant total gross thrust for a selected diffuser inlet pressure ratio as the nozzle was rotated from 0° cruise through 90° vertical positions. The nozzle A configuration test data did show a slight decrease of approximately 1 to 2 percent in exit discharge coefficient between 0° and 90° nozzle positions, which would account for relatively little change in performance.

The nozzle exit to diffuser total pressure ratios averaged from the large-scale model data provided an estimate of the total system internal pressure losses during the test. The large-scale data agreed with the results of the small-scale model tests that swivel nozzle rotation through 0° cruise to 90° vertical position has little effect on internal pressure loss for the same flow conditions. The low-pressure losses obtained in both the large- and small-scale model tests show good internal aerodynamic characteri ics in all nozzle positions. The small-scale single-swivel nozzle test data show the thrust loss due to internal pressure loss was in a constant range of 3 to 4 percent for all configurations tested without flow vanes for 0° through 90° nozzle positions. The substantial decrease in performance measured during the large-scale tests as the vectoring angle was increased is concluded to be a condition that was not caused by pressure losses in the single-swivel nozzle system.

A comparison of the total thrust coefficients, based on the ideal thrust using the diffuser inlet parameters, indicates the performance of the small-scale configurations was as high or higher in the 90° vertical position than

nozzle angles of less thrust deflection. The nozzle exit thrust coefficients of the models, based on the ideal thrust using the nozzle exhaust parameters, also show similar performance trends as shown by the total thrust coefficients. These test data of measured-to-ideal thrust ratios substantiate the analysis that the degradation in thrust for increased vectoring angles during the large-scale tests was not due to the swivel nozzle internal performance.

The difference between the diffuser inlet and nozzle exit thrust coefficients is attributed to the loss in pressure through the deflector system. As stated earlier, the thrust loss due to pressure loss was 3 to 4 percent for the small-scale models tested under static conditions. The thrust loss due to system pressure loss would be reduced to less than 2 percent during forward velocity cruise conditions as the diffuser inlet pressure ratio increases with dynamic pressure. The remainder and largest portion of the overall performance loss of the deflector system is related to the nozzle exit thrust coefficient. The small-scale single-swivel nozzle test data show losses in the range of 4 to 7 percent based on conditions at the nozzle exit.

Part of the losses at the exhaust nozzle can be explained by the uneven total pressure pattern across the nozzle exit plane, as described under "Test Results." The nonuniform pressure distribution would result in some reduction in the thrust coefficient, caused primarily by incomplete flow bending and flow separation through the curved ducting. Another contribution to the exhaust nozzle loss is due to the base drag at the nozzle exit plane. The fiber glass material walls of the small-scale model nozzle sections were designed with a thickness of approximately 0.60 centimeter (0.24 inch) required for stress loads obtained at maximum test conditions. The material thickness created a flat base at the nozzle exit plane of approximately 20 percent of the exhaust exit area. Base pressures were not measured during the test to calculate base drag values, but a thrust loss of approximately 2 percent was estimated from the effect of the base area and flow velocity at the nozzle exit plane.

A series of runs for the single-swivel nozzle C and the twin-swivel configurations were made without the total pressure rake installed on the exit plane, to compare to the test data obtained from runs made with the exit rake. The data comparison showed the rake installation caused a small reduction in effective exit area and decreased the flow rates, at the same test conditions, in the range of 3 to 4 percent. The effect of the metrically installed exit rake on internal performance was an average decrease of approximately 1.5 percent in both the thrust coefficients and discharge coefficients. These average coefficient values can be used to estimate the performance increase required to correct the test data obtained with exhaust instrumentation.

The exit discharge coefficients shown in the data plots and described under "Test Results" are a ratio of measured airflow through the swivel nozzle to calculated ideal airflow based on the nozzle exit parameters. The exit discharge coefficients along with the pressure loss through the swivel nozzle system would be used to determine the effective exit area of the nozzle. The data show only a slight change in discharge coefficients during thrust vectoring for all nozzle configurations. A comparison of nozzle C configurations with and without flow vanes indicates that vanes caused an increase of 1 to 2 percent in discharge coefficient values.

The low performance of the twin-swivel nozzle concept, shown by a total thrust losses in the range of 12 to 14 percent, was due primarily to the higher internal pressure loss through the divider section and a higher percentage of material thickness base drag using two nozzles. The divider section was designed for model fabrication to be a simple half-sphere contour shape with little consideration for internal flow path design. An investigation to improve the divider section design and a reduction of the nozzle exit base drag would provide a twin-swivel nozzle performance comparable to the single-swivel nozzle designs.

CONCLUSIONS

The purpose of the program was to investigate the performance degradation obtained during thrust vectoring of a large-scale single-swivel nozzle system tested at NASA-Ames under a previous contract NAS 2-7656, explore configuration refinements to correct these difficiencies, and substantiate performance improvements with small-scale model testing. The investigation of the test data obtained from the large-scale hardware testing indicated that the fan and gas generator inlet ingestion of higher temperature air when the fan system exhaust flow was deflected down does account for some reduction in performance. An ingestion temperature increase would also require a nozzle exit area increase, or a reduction in flow rate would occur using a fixed-nozzle area. Based on the analysis of the large-scale test data, it appeared that the major portion of the performance losses could be reduced by three changes in the swivel nozzle section design:

(1) Increase the exhaust nozzle exit area to allow for a reduction in the nozzle discharge coefficient due to separation from high flow bend angles and an increase in exhaust temperatures caused by ingestion or higher turbine discharge temperatures

(2) Increase the small bend radius of the inner nozzle section aft of the bearing to reduce flow separation problems

(3) Modify the outer shape of the nozzle section aft of the bearing by increasing the outer bend radius to improve the flow path and reduce the local flow mach number

Small-scale models of the single-swivel nozzle design with five different interchangeable nozzle sections and of the twin-swivel nozzle design were fabricated. Single-swivel model nozzle A represented the basic nozzle design scaled 0.15 size of the large-scale test hardware. Single-swivel model nozzles B, C, and D incorporated the modifications to investigate the design changes for performance improvement with three different nozzle exit areas. Two models of nozzle C were made to allow all models to have three equally spaced thin steel vanes installed.

The five single-swivel nozzle configurations and the one twin-swivel nozzle configuration were each tested in four selected nozzle positions of 0° aft for cruise, 30°, 60°, and 90° vertical used for the VTOL mode. The static tests were run at airflow inlet to ambient pressure ratios of 1:1, 1:2, 1:3, and 1:4 at the 0° nozzle position, and pressure ratios of 1:1, 1:2, and 1:3 at the 30°, 60°, and 90° nozzle positions.

Single-swivel nozzles A and B showed total thrust losses in the range of 7 to 9 percent during all test conditions. Nozzles C and D, with higher flow rates due to increased nozzle exit areas, show higher total thrust losses in the range of 9 to 12 percent. The installation of guide flow vanes improved the performance of nozzle C, with the exception of tests run in the 0° cruise position. The twin-swivel nozzle configuration showed total thrust losses in a range of 12 to 14 percent.

The small-scale single-swivel nozzle test data show the thrust loss due to internal pressure loss was in a constant range of 3 to 4 percent for all nozzle positions. The thrust loss due to pressure loss would be reduced during forward velocity cruise conditions as the diffuser inlet pressure ratio increases with dynamic pressure. The single-swivel nozzle test data show the remainder and largest portion of the overall performance losses, in the range of 4 to 7 percent, is related to the thrust coefficient, based on conditions at the nozzle exit.

Part of the losses at the exhaust nozzle can be explained by the uneven total pressure pattern across the nozzle exit plane, as described under "Test Results." Another contribution to the exhaust nozzle losses is due to the flat base drag at the nozzle model exit plane, of approximately 20 percent of the exhaust exit area, that creates an approximate 2-percent estimated thrust loss. The data comparison of runs made without the total pressure exit rake

installed showed the rake installation caused an average decrease of approximately 1.5 percent in both thrust coefficients and discharge coefficients. The data in figure 82 shows the effect on nozzle A diffuser inlet thrust coefficient at a diffuser inlet total pressure ratio of 1.2 when the estimated exit rake and base drag loss is extracted from the test data obtained during nozzle positions of 0° through 90°.

The small-scale model and large-scale hardware test data both show that the swivel nozzle deflector systems have low internal pressure losses in all nozzle positions. Significant thrust degradation obtained during the large-scale hardware tests when the nozzle vectoring angle was increased, however, did not occur during the small-scale model testing. Each of the small-scale models tested, including the single-swivel nozzle A configuration that represents a scaled 0.15 size of the large-scale test hardware, showed relatively constant total gross thrust for a selected airflow inlet pressure ratio as the nozzle was rotated from 0° cruise through 90° vertical positions. The small-scale test data substantiate the analysis that the degradation in thrust for increased vectoring angles during the large-scale tests was not due to the swivel nozzle deflector system internal performance. Figure 83 shows the thrust coefficients obtained from the large-scale swivel nozzle system testing, with and without internal flow vanes installed, as a function of nozzle position. The large-scale data in figure 83 are compared to the small-scale model test data of the single-swivel nozzle A, nozzle C with and without flow vanes and the twin-swivel configurations. The thrust coefficient values for the nozzle A configuration with the estimated losses for the exit rake and base drag extracted, as presented in figure 82, are shown with the large-scale data in figure 83 to illustrate the estimated static performance of a swivel nozzle diflector system.

The small-scale static test program for the single- and twin-swivel nozzle configurations provided data to evaluate the thrust deflector concept for low-pressure ratio propulsion systems. The exit discharge coefficients along with the pre-sure loss through the swivel nozzle system would be used to determine the effective exit area of the nozzle. Design changes to provide an even exhaust pattern at the nozzle exit and to reduce exhaust flow losses, such as exit base drag, would improve the performance obtained from the small-scale tests. A change in the design of the twin-swivel nozzle divider section used in the scale tests to reduce the internal pressure losses would provide performance of the twin-swivel nozzle configuration to be comparable to the single-swivel nozzle configurations.

EQUATIONS

$$F_g = (N^2 + T^2 + S^2)^{1/2}$$

$$W_a = C_D\, C_*\, A_2 \left(\frac{P_{T_U}}{\sqrt{T_{T_U}}} \right) \frac{g}{R}$$

$$M_5 AVE = 2.236 \left[\left(\frac{P_{T_5}}{P_{S_5}} \right)^{2/7}_{AVE} - 1 \right]^{1/2}$$

$$M_8 AVE = 2.236 \left[\left(\frac{P_{T_8}}{P_A} \right)^{2/7}_{AVE} - 1 \right]^{1/2}$$

$$M_{8_{AVE}\,5} = 2.236 \left[\left(\frac{P_{T_5}}{P_A} \right)^{2/7}_{AVE} - 1 \right]^{1/2}$$

$$W_{a_i} = \frac{P_{T_{8_{AVE}}}\, A_8\, M_{8_{AVE}}}{\left[1 + 0.2\, (M_{8AVE})^2 \right]^3} \left(\frac{\gamma g}{R\, T_{T_5}} \right)^{1/2}$$

$$\left(W_{a_i} \right)_5 = \frac{P_{T_{5_{AVE}}}\, A_8\, (M_{8AVE})_5}{\left[1 + 0.2\, (M_{8AVE})^2_5 \right]^3} \left(\frac{\gamma g}{R\, T_{T_5}} \right)^{1/2}$$

$$C_{D_8} = W_a / W_{a_i}$$

$$\left(C_{D_8}\right)_5 = W_a / \left(W_{a_i}\right)_5$$

$$F_{g_{i_8}} = \frac{3.1305\ M_{8_{AVE}}\ P_{T_{8_{AVE}}}\ A_8\ C_{D_8}}{\left[1 + 0.2\ (M_{8AVE})^2\right]^3} \left[1 - \left(\frac{P_A}{P_{T_8}}\right)^{2/7}_{AVE}\right]^{1/2}$$

$$F_{g_{i_5}} = \frac{3.1305\ (M_{8AVE})_5\ P_{T_{5_{AVE}}}\ A_8\ \left(C_{D_8}\right)_5}{\left[1 + 0.2\ (M_{8AVE})^2_5\right]^3} \left[1 - \left(\frac{P_A}{P_{T_5}}\right)^{2/7}_{AVE}\right]^{1/2}$$

REPRODUCIBILITY OF THE
ORIGINAL PAGE IS POOR

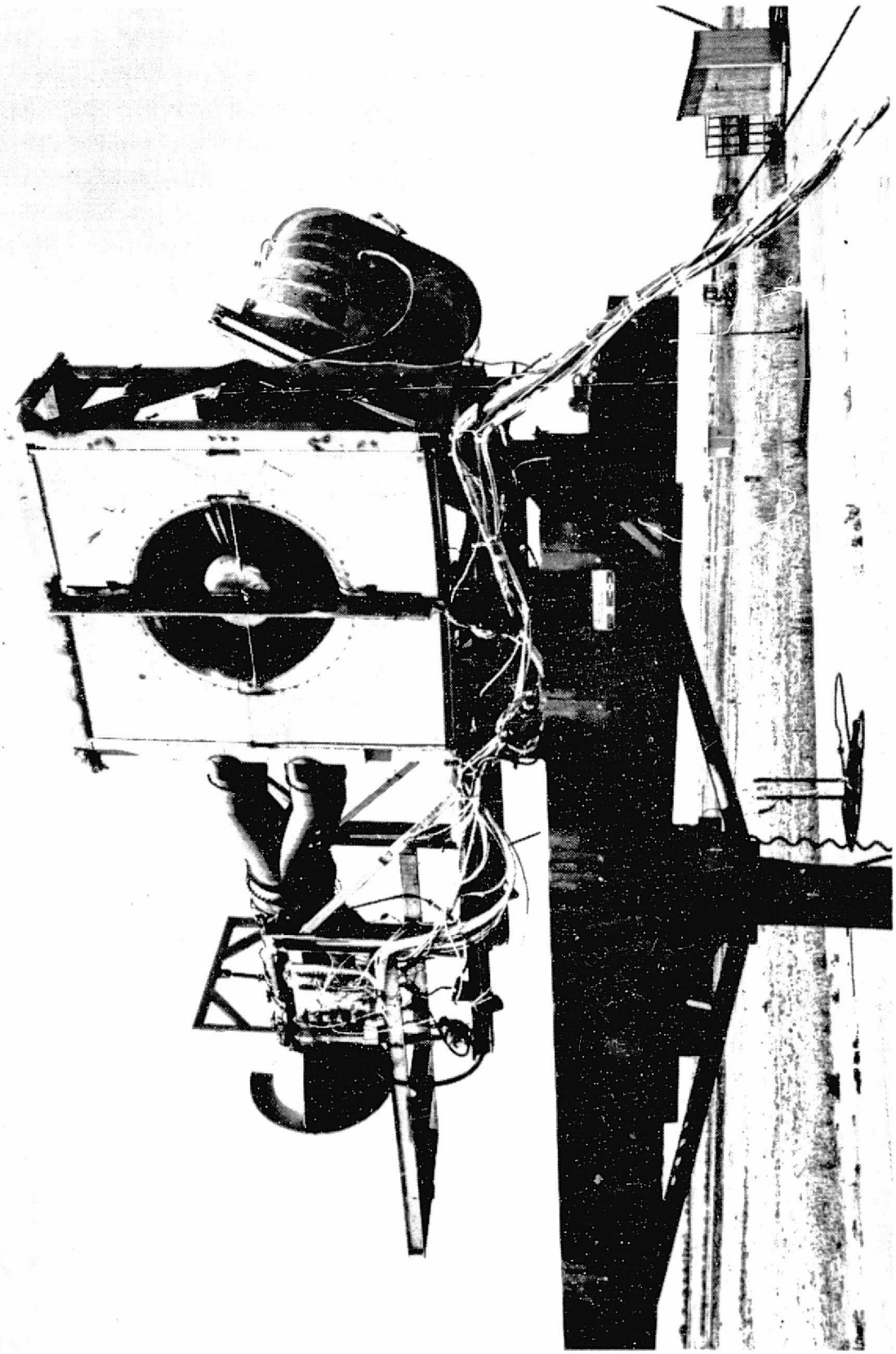

Figure 1. - Front view of the LF336/A lift fan system with exhaust deflector nozzle in 0° cruise position.

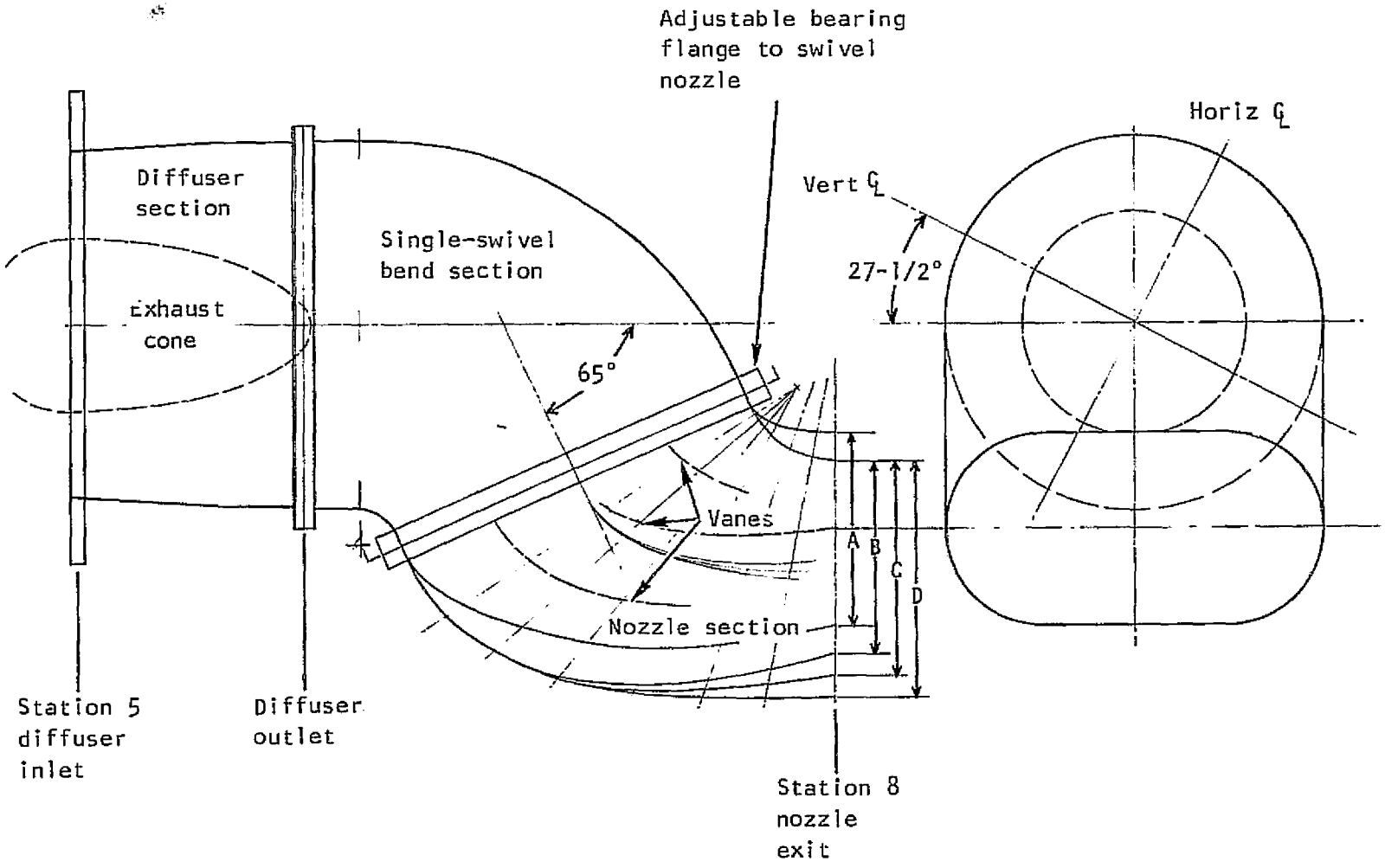

Figure 2. - Single-swivel model schematic.

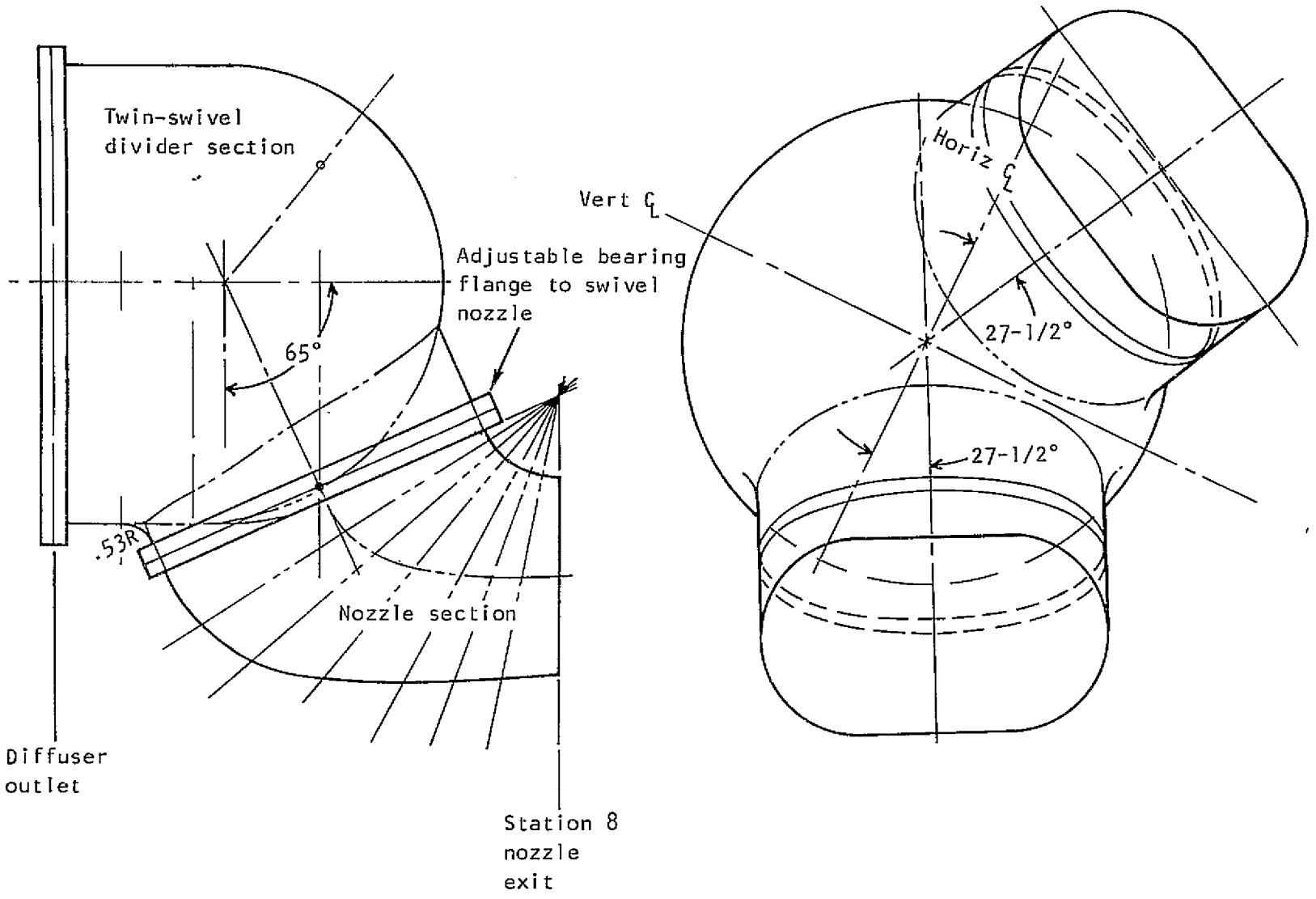

Figure 3. - Twin-swivel model schematic.

REPRODUCIBILITY OF THE
ORIGINAL PAGE IS P

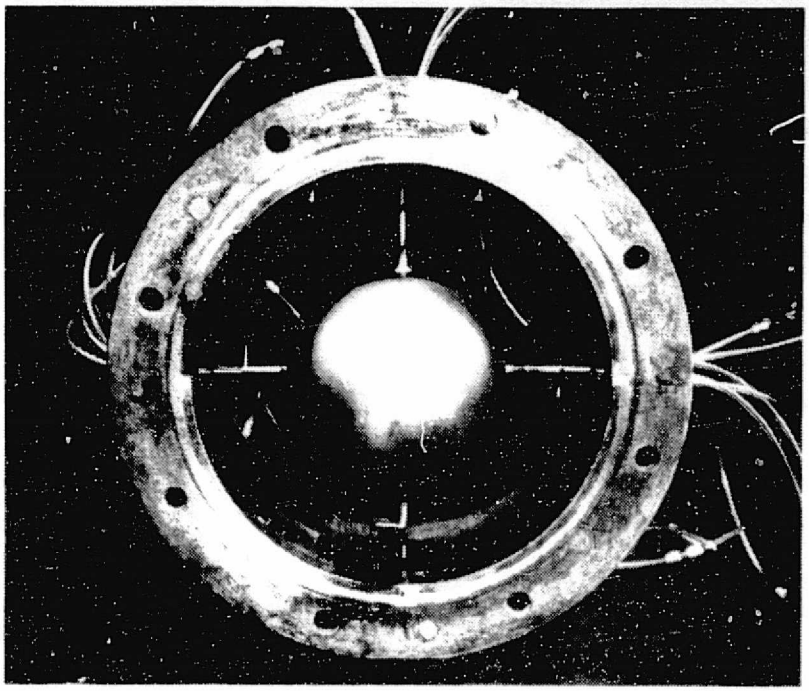

11266-93-1D

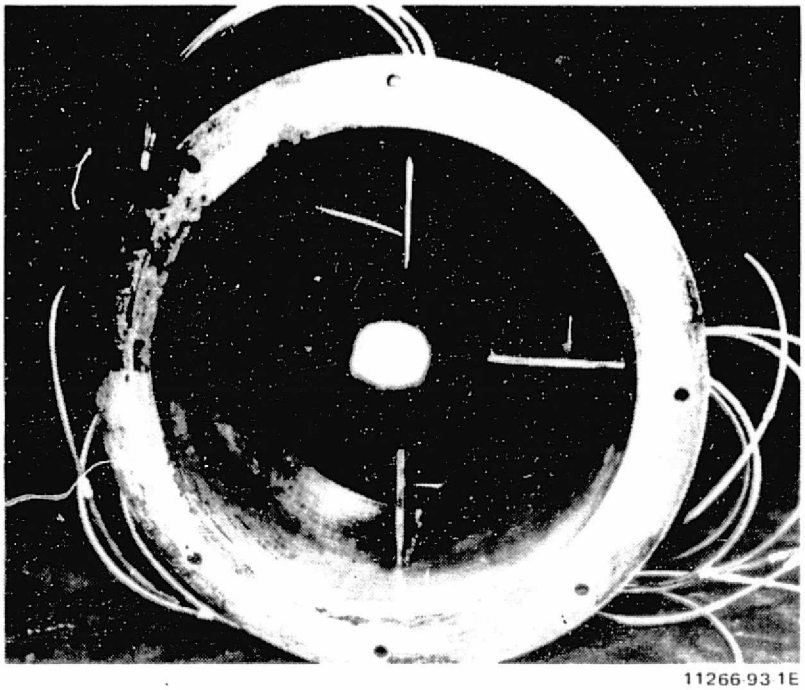

11266-93-1E

Figure 4. - Diffuser section inlet and exit views.

REPRODUCIBILITY OF THE
ORIGINAL PAGE IS POOR

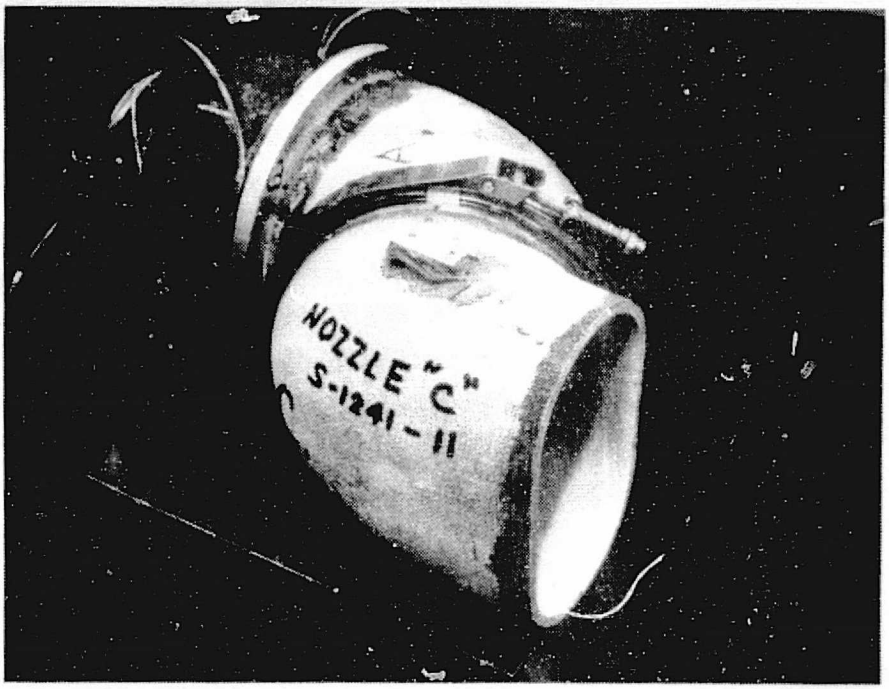

11266-93-1F

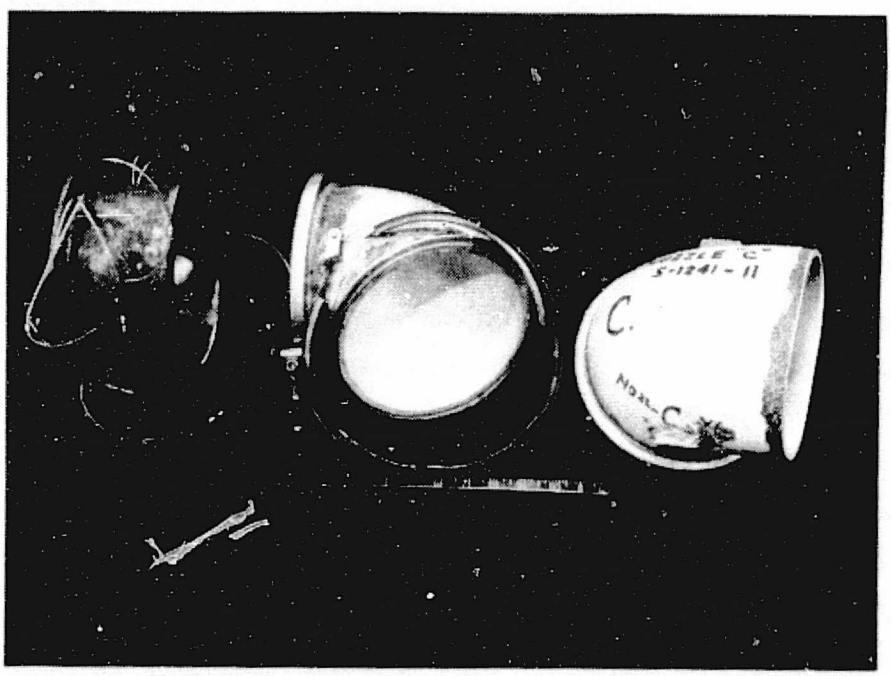

11266-93-1G

Figure 5. - Single-swivel nozzle system assembled and disassembled.

REPRODUCIBILITY OF THE
ORIGINAL PAGE IS POOR

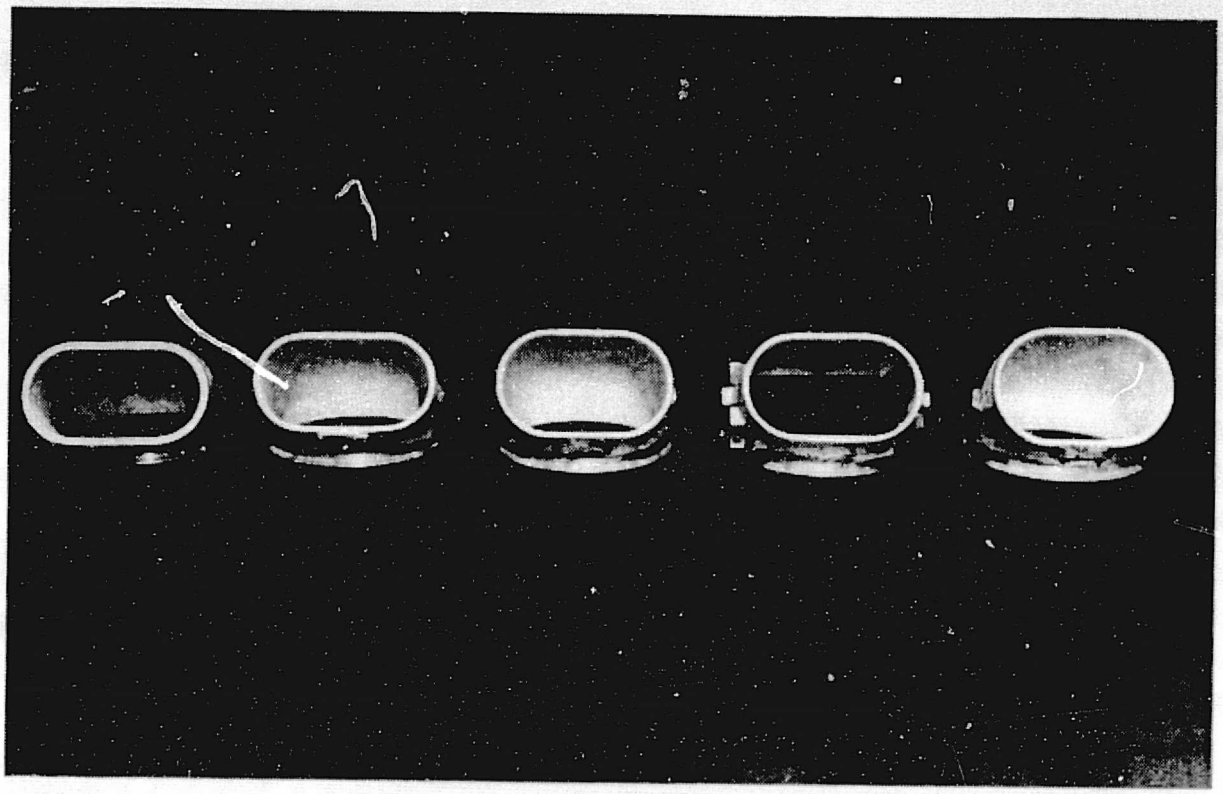

11266-93-1H

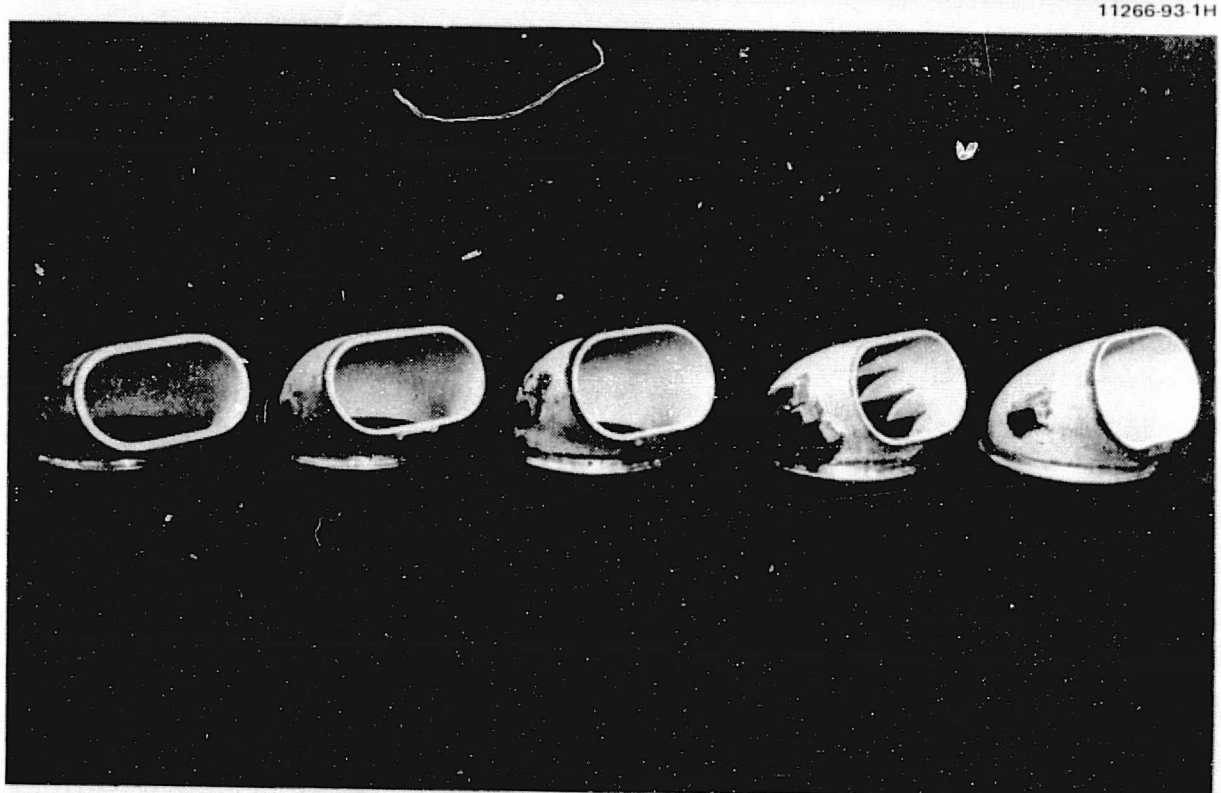

Figure 6. - Single-swivel nozzle configurations.

11266-93-1I

Figure 7. - Single-swivel nozzle model mounted on test balance without exit rake installed.

TWT S-54D

REPRODUCIBILITY OF THE ORIGINAL PAGE IS POOR

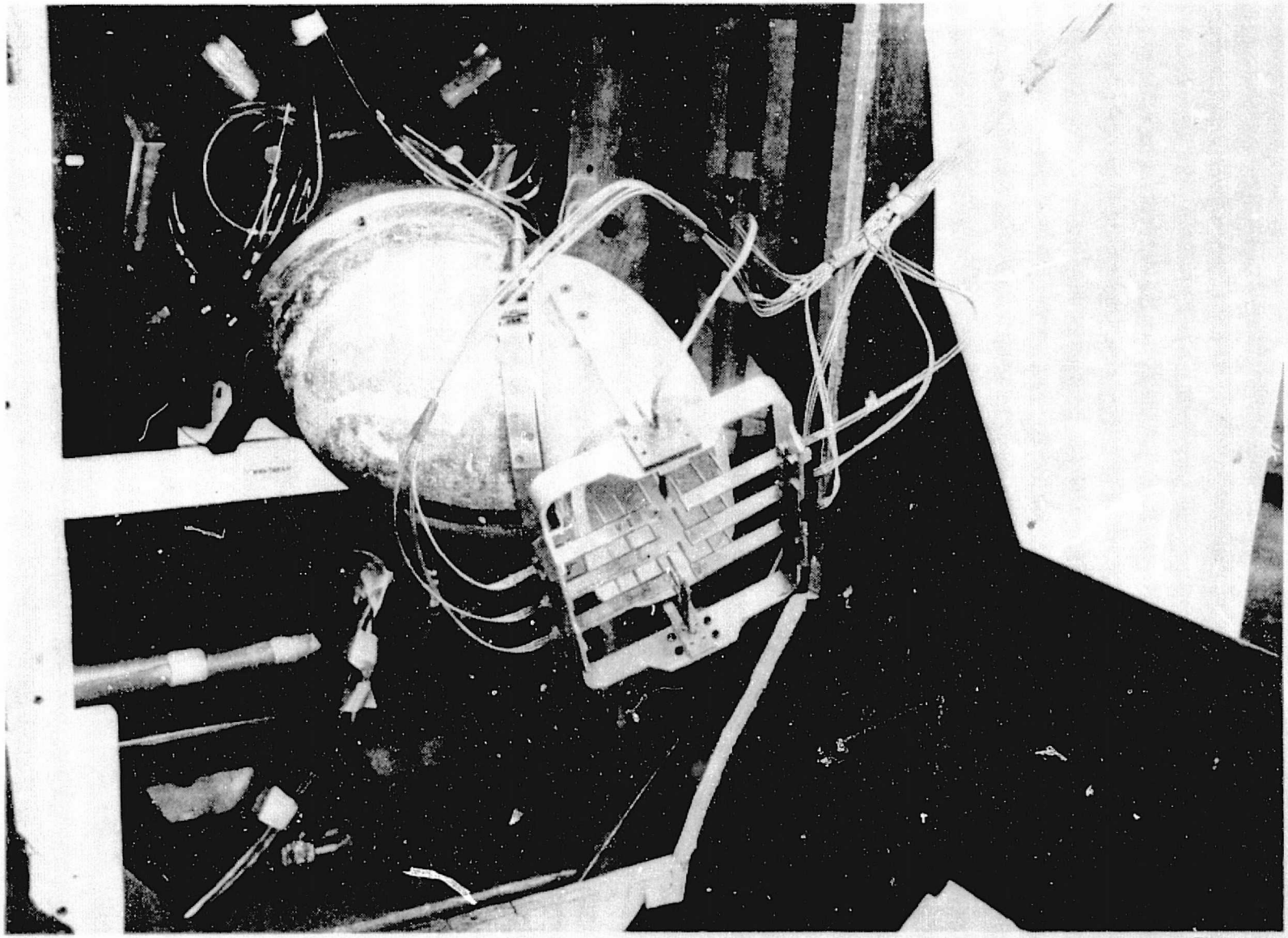

Figure 8. - Single-swivel nozzle model mounted on test balance with exit rake installed.

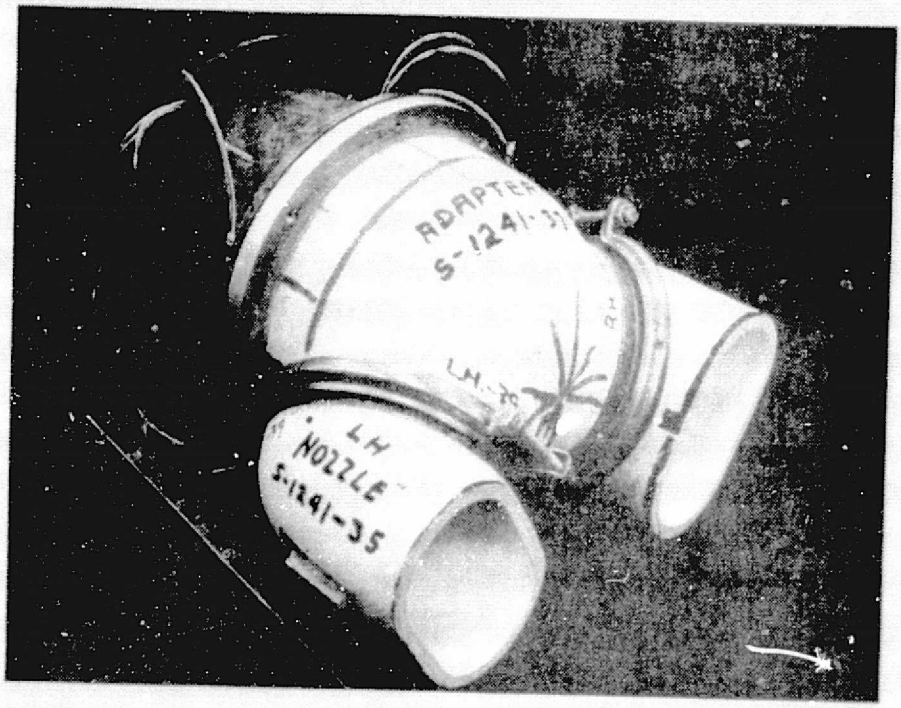

11266-93-1B

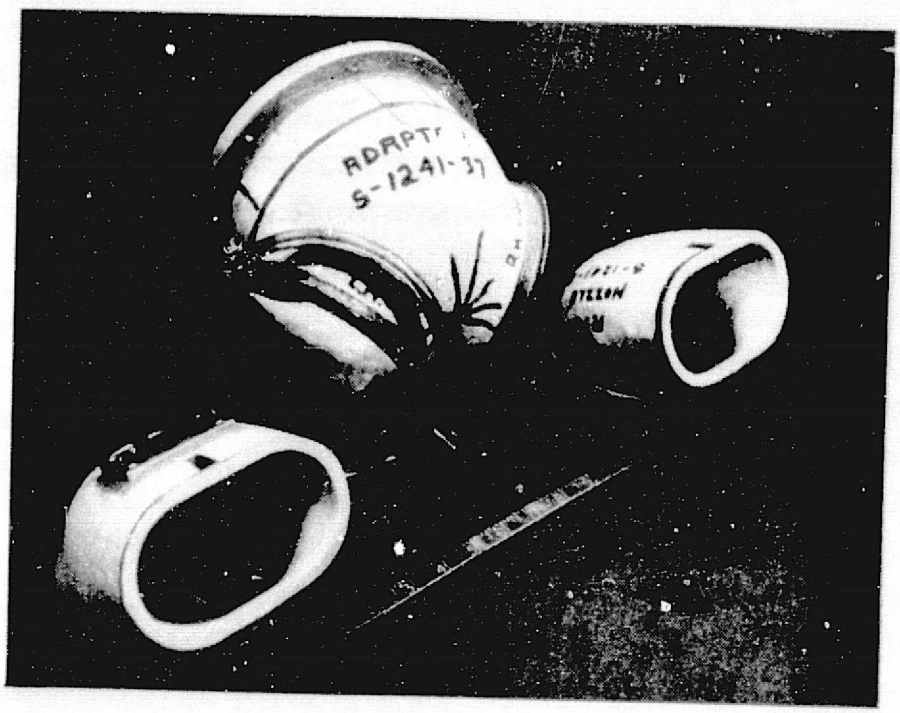

11266-93-1J

Figure 9. - Twin-swivel nozzle system assembled and disassembled.

REPRODUCIBILITY OF THE
ORIGINAL PAGE IS POOR

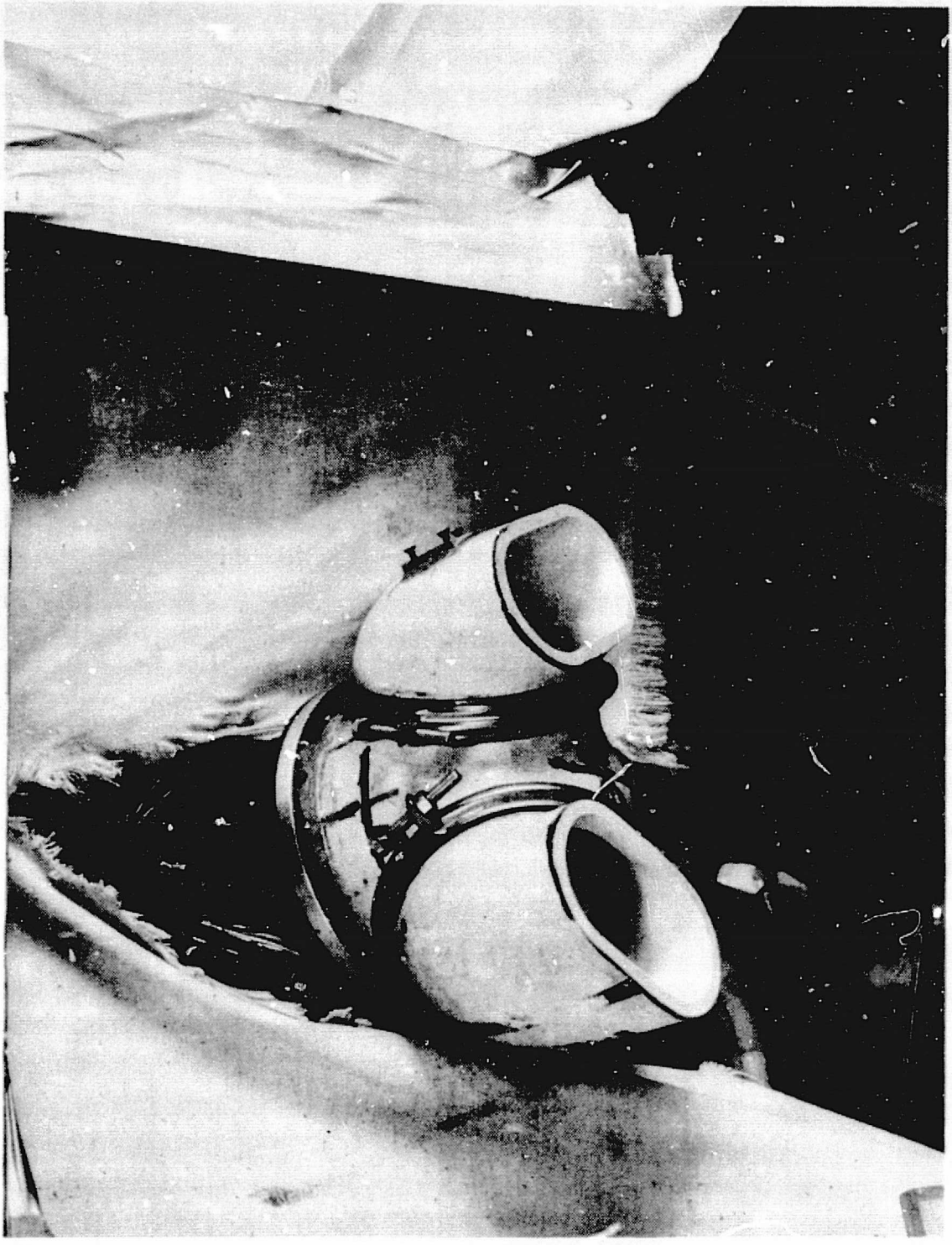

Figure 10. - Twin-swivel nozzle model mounted on test balance system without exit rake installed.

REPRODUCIBILITY OF THE
ORIGINAL PAGE IS POOR

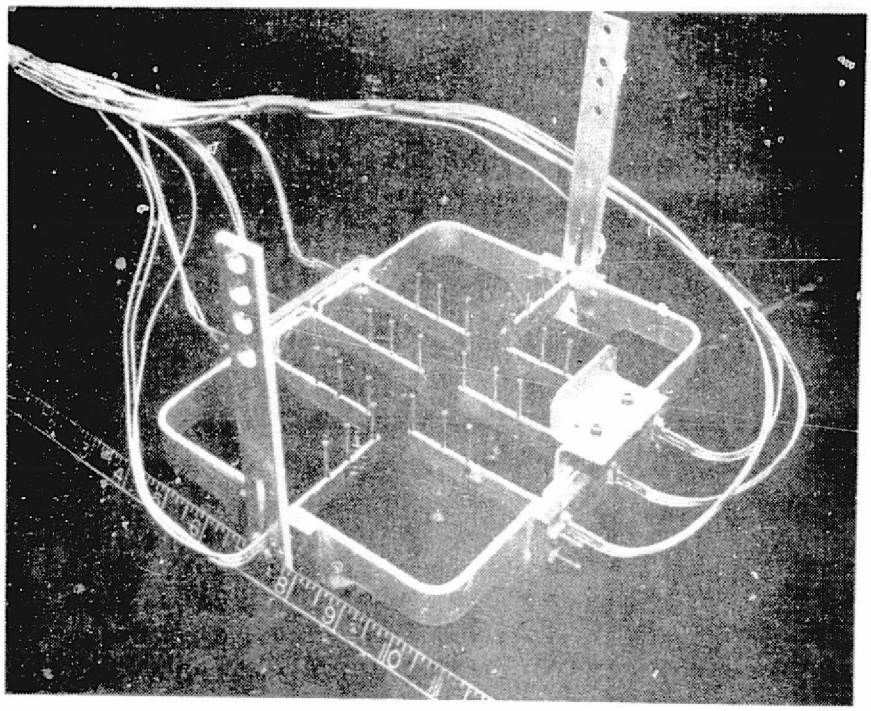

11266-93-1A

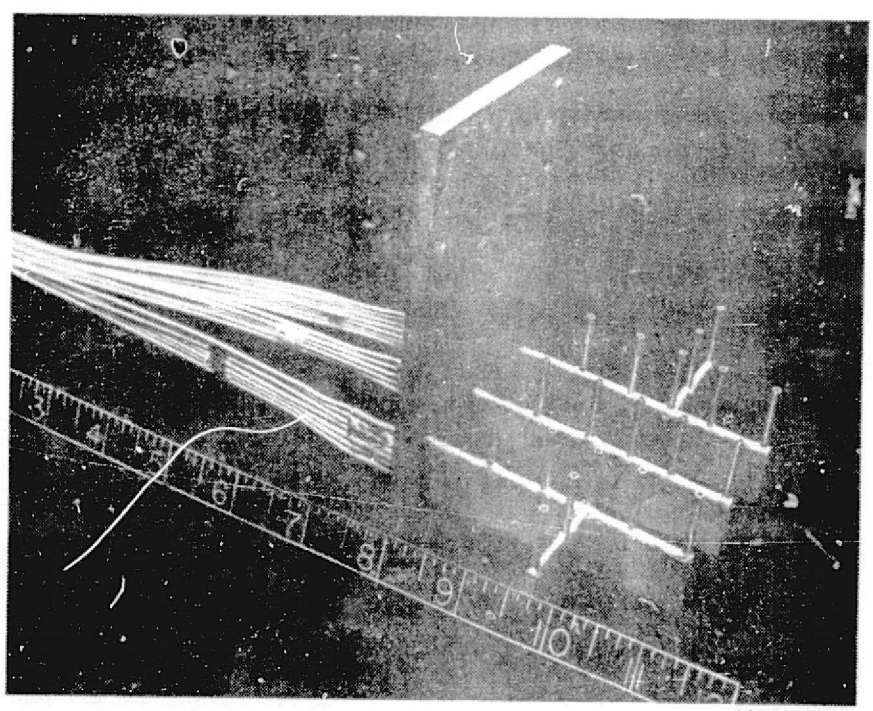

11266 93-1C

Figure 11. - Single-and twin-swivel nozzle exit rakes.

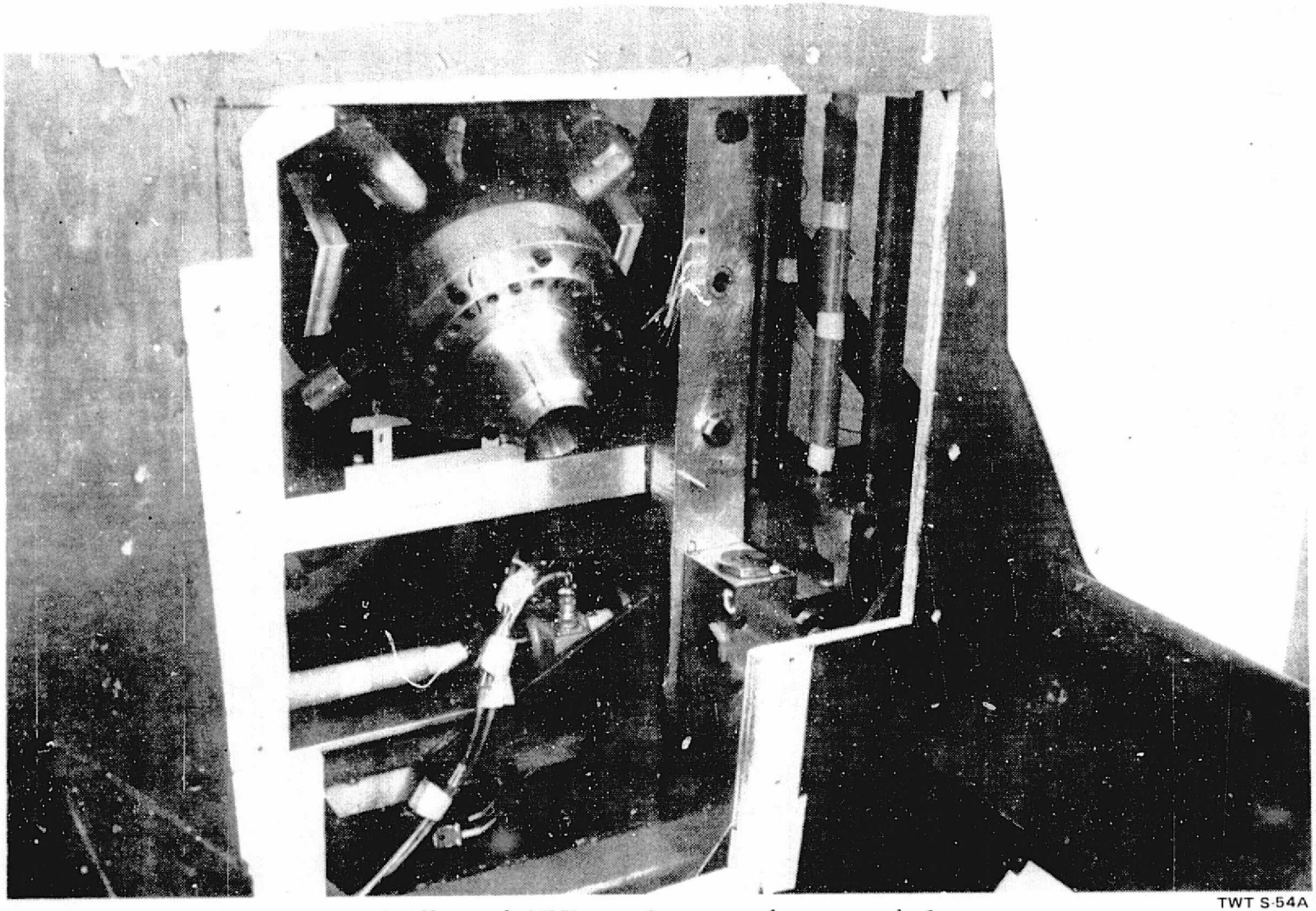

Figure 12. - Calibrated ASME nozzle mounted on test balance system.

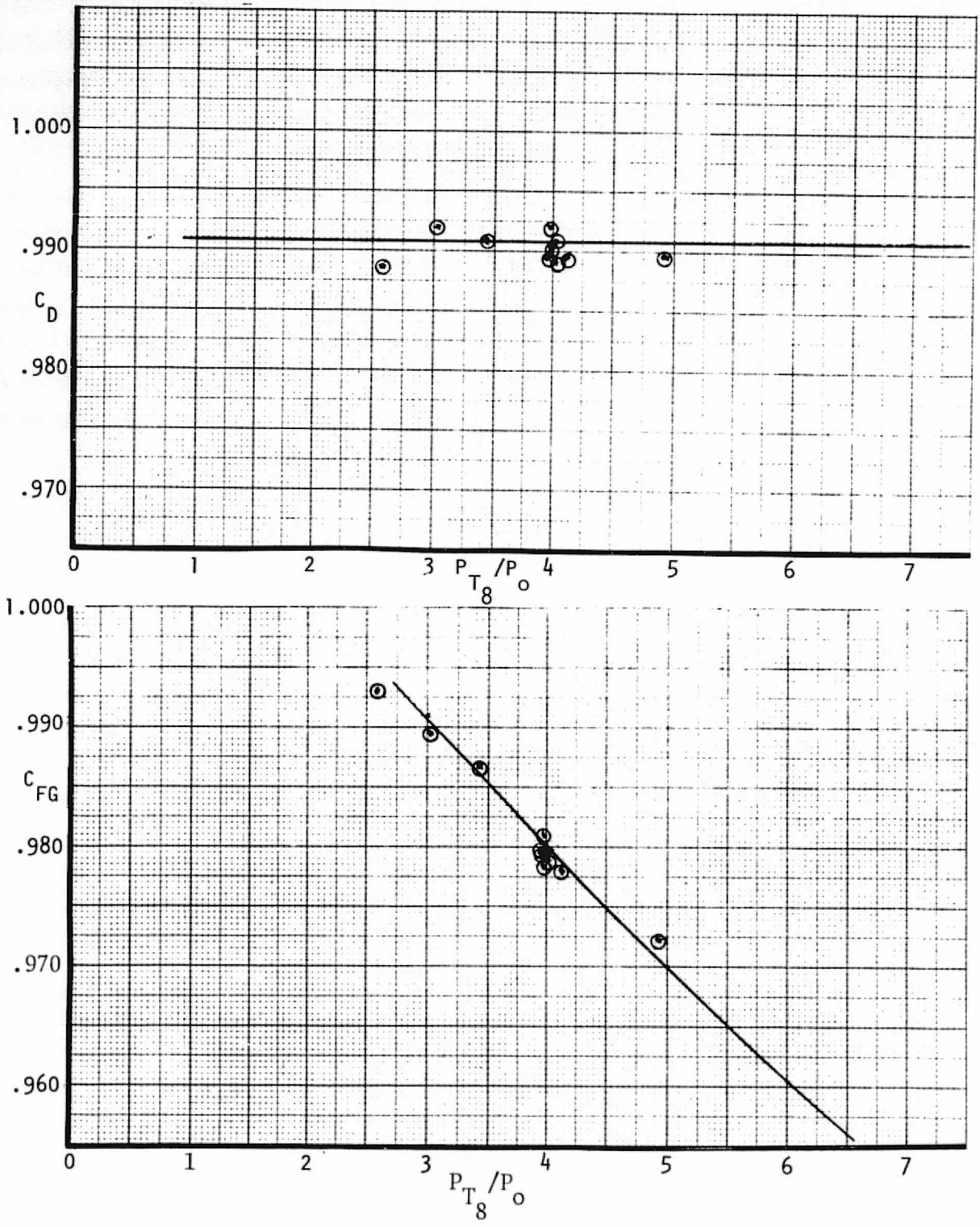

Figure 13. - Discharge and thrust coefficient versus pressure ratio and for ASME nozzle.

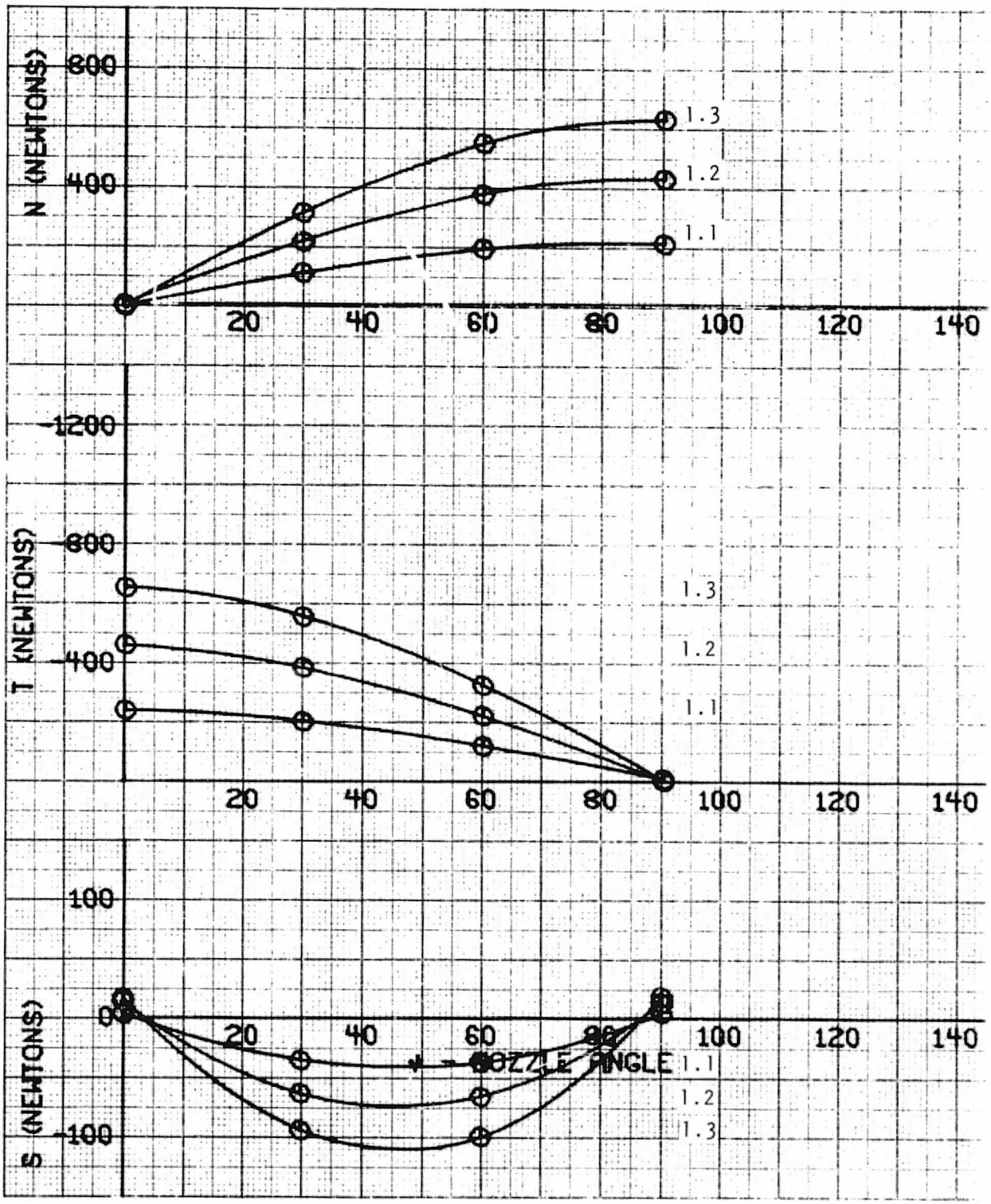

Figure 14. - Nozzle A thrust components at P_{T_5}/P_A = 1.3, 1.2, 1.1 versus nozzle angle.

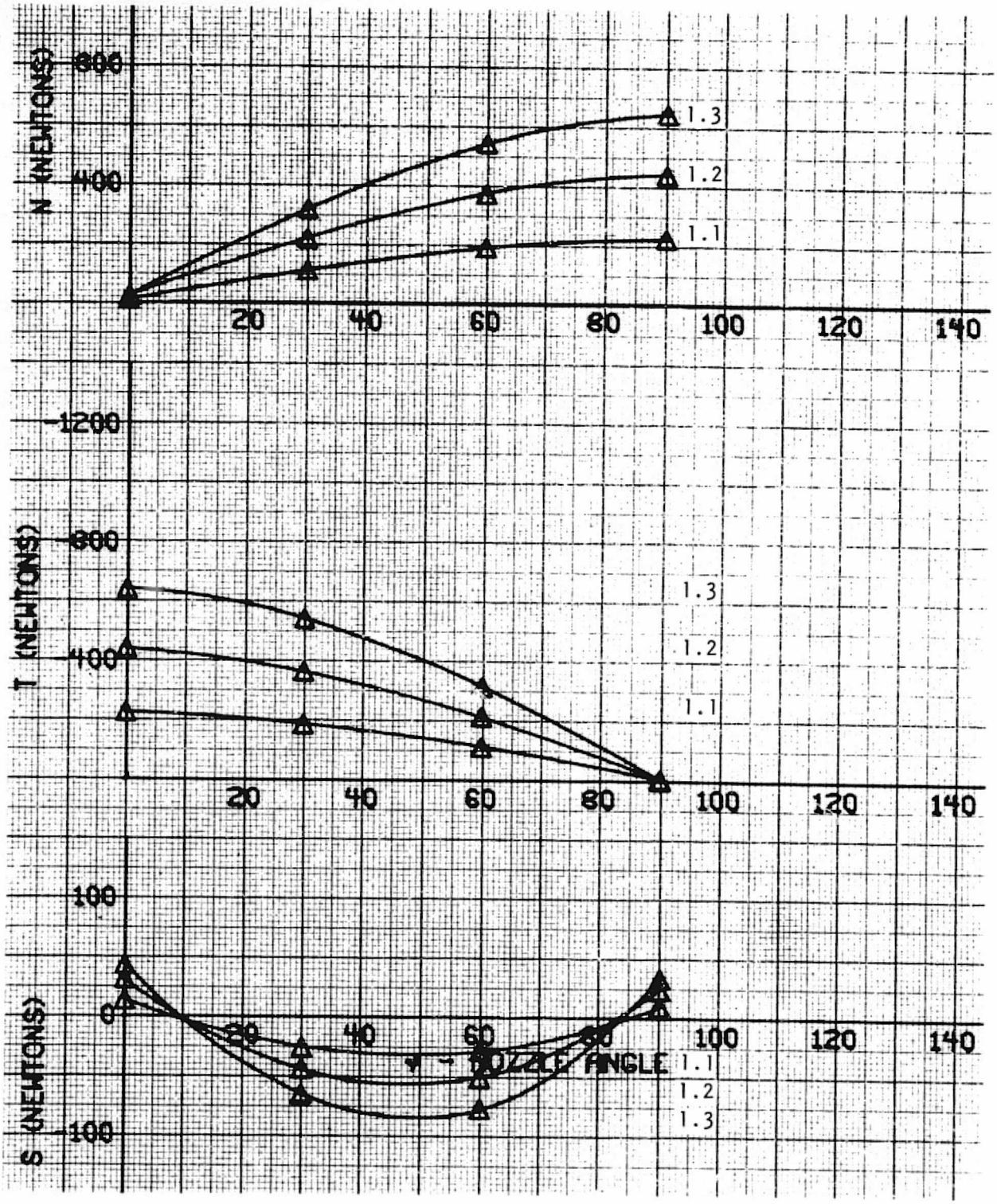

Figure 15. - Nozzle B thrust components at P_T / P_A = 1.3, 1.2, 1.1 versus nozzle angle. 5

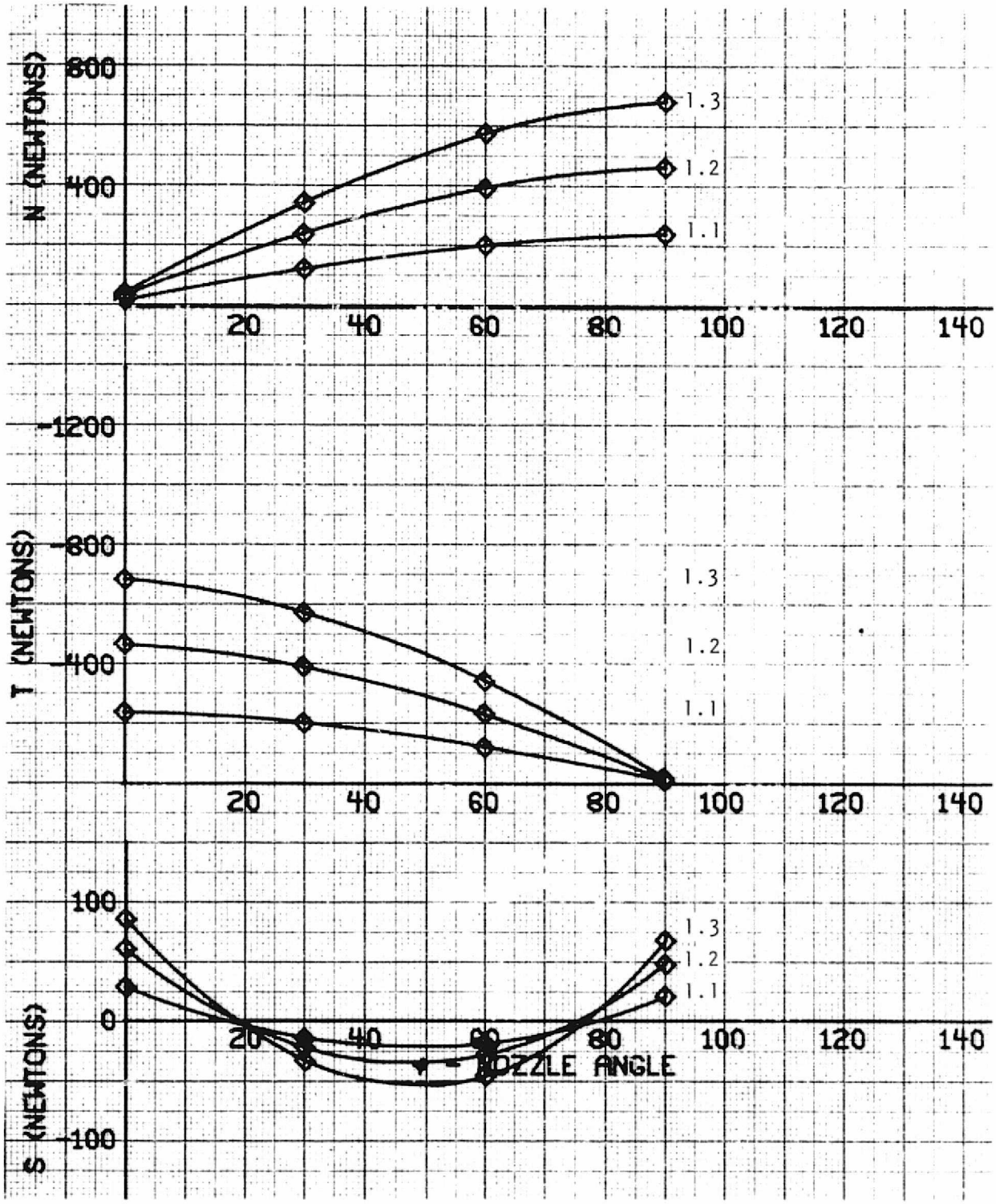

Figure 16. - Nozzle C thrust components at P_{T_5}/P_A = 1.3, 1.2, 1.1 versus nozzle angle.

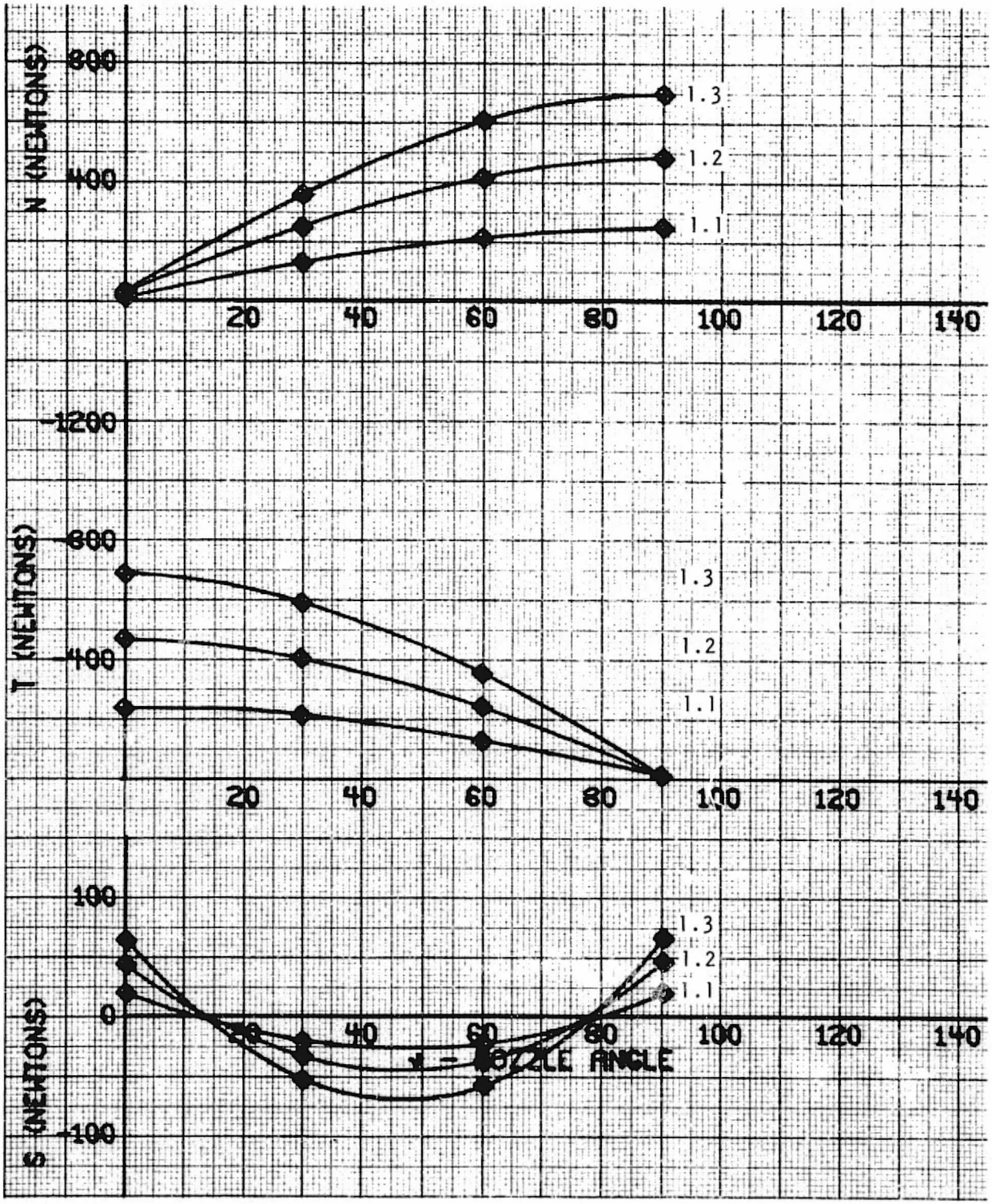

Figure 17. - Nozzle C (with vanes) thrust components at P_{T_5}/P_A = 1.3, 1.2, 1.1 versus nozzle angle.

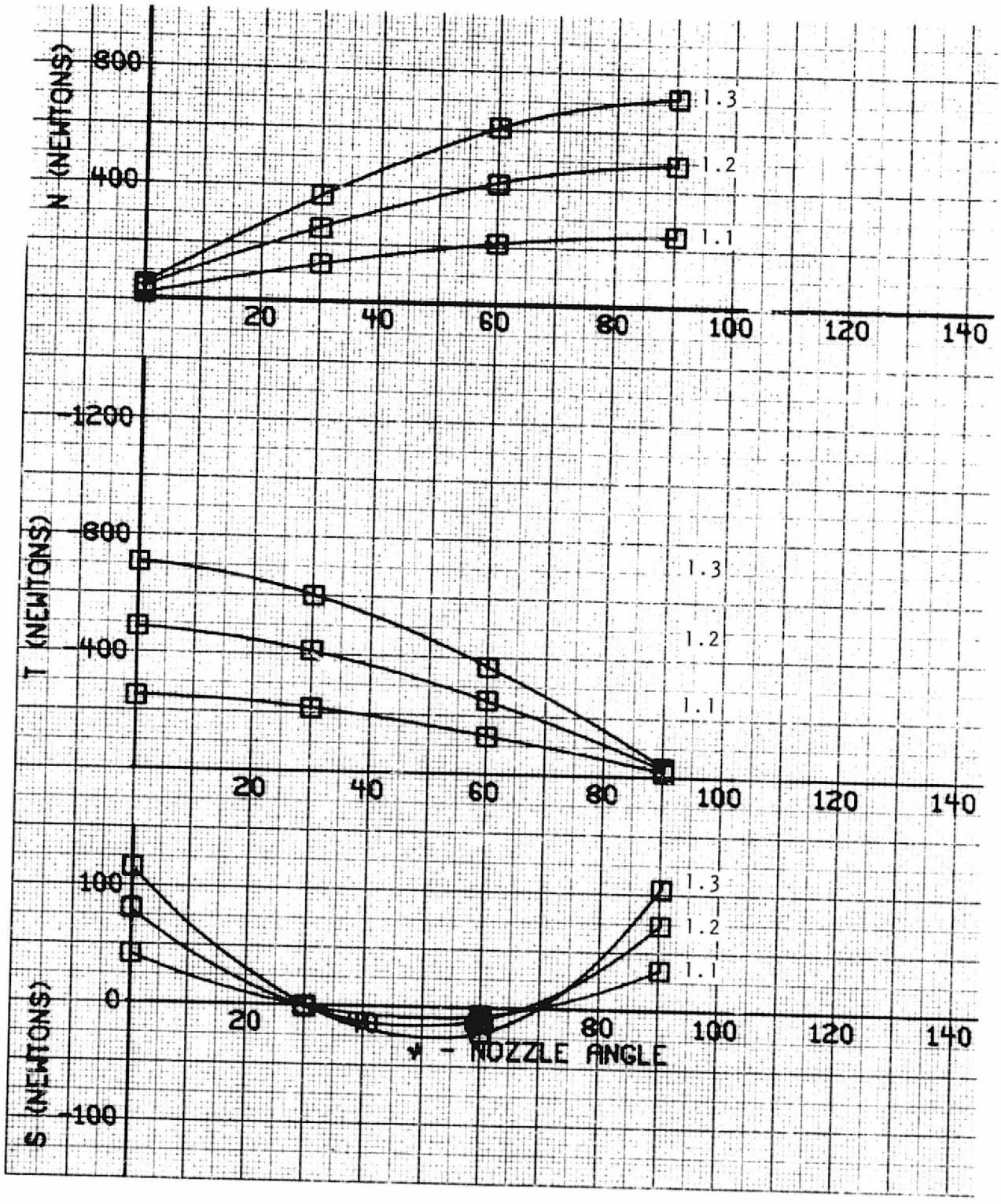

Figure 18. - Nozzle D thrust components at P_{T_5}/P_A = 1.3, 1.2, 1.1 versus nozzle angle.

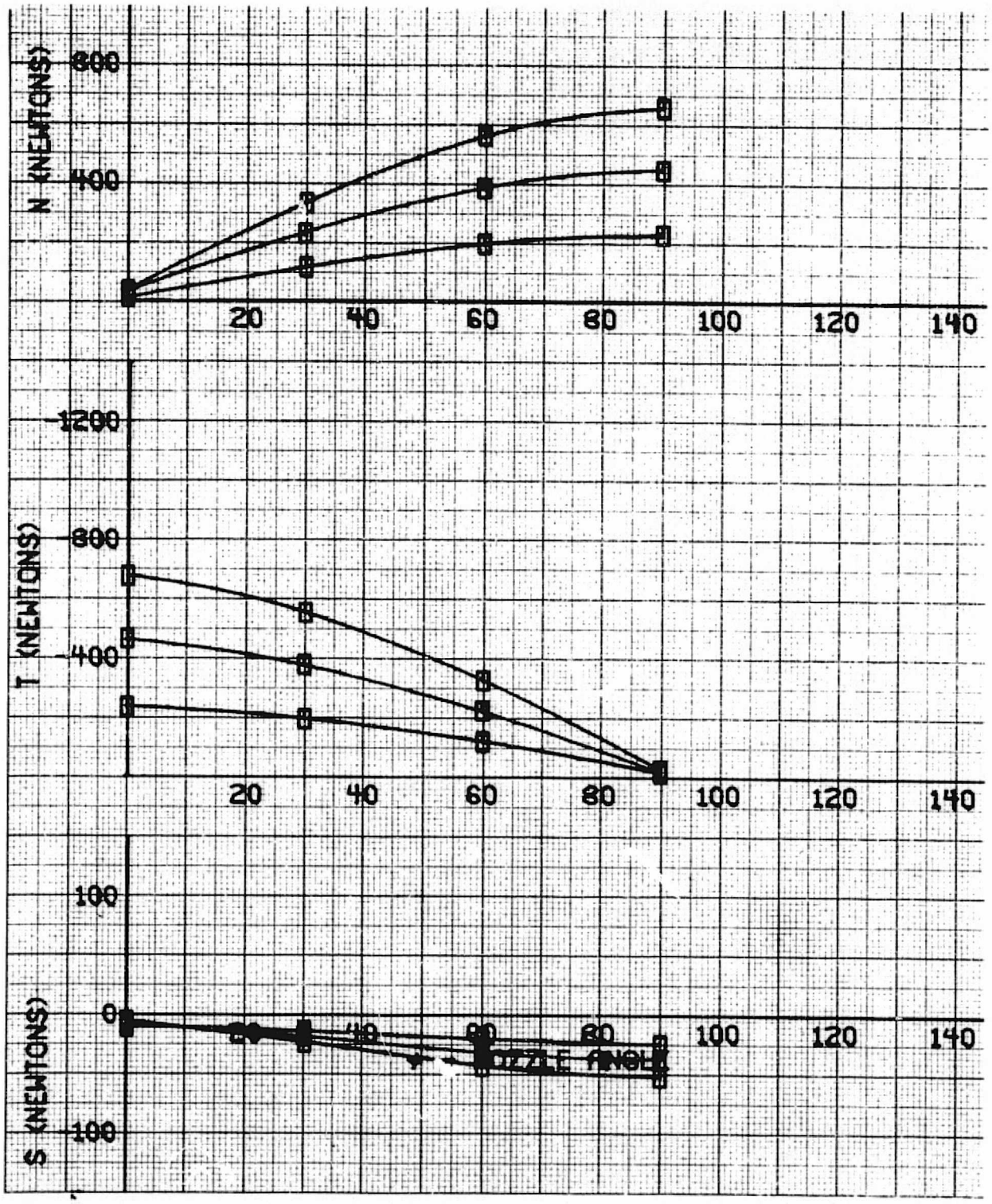

Figure 19. - Twin nozzle thrust components at P_{T_5}/P_A = 1.3, 1.2, 1.1 versus nozzle angle.

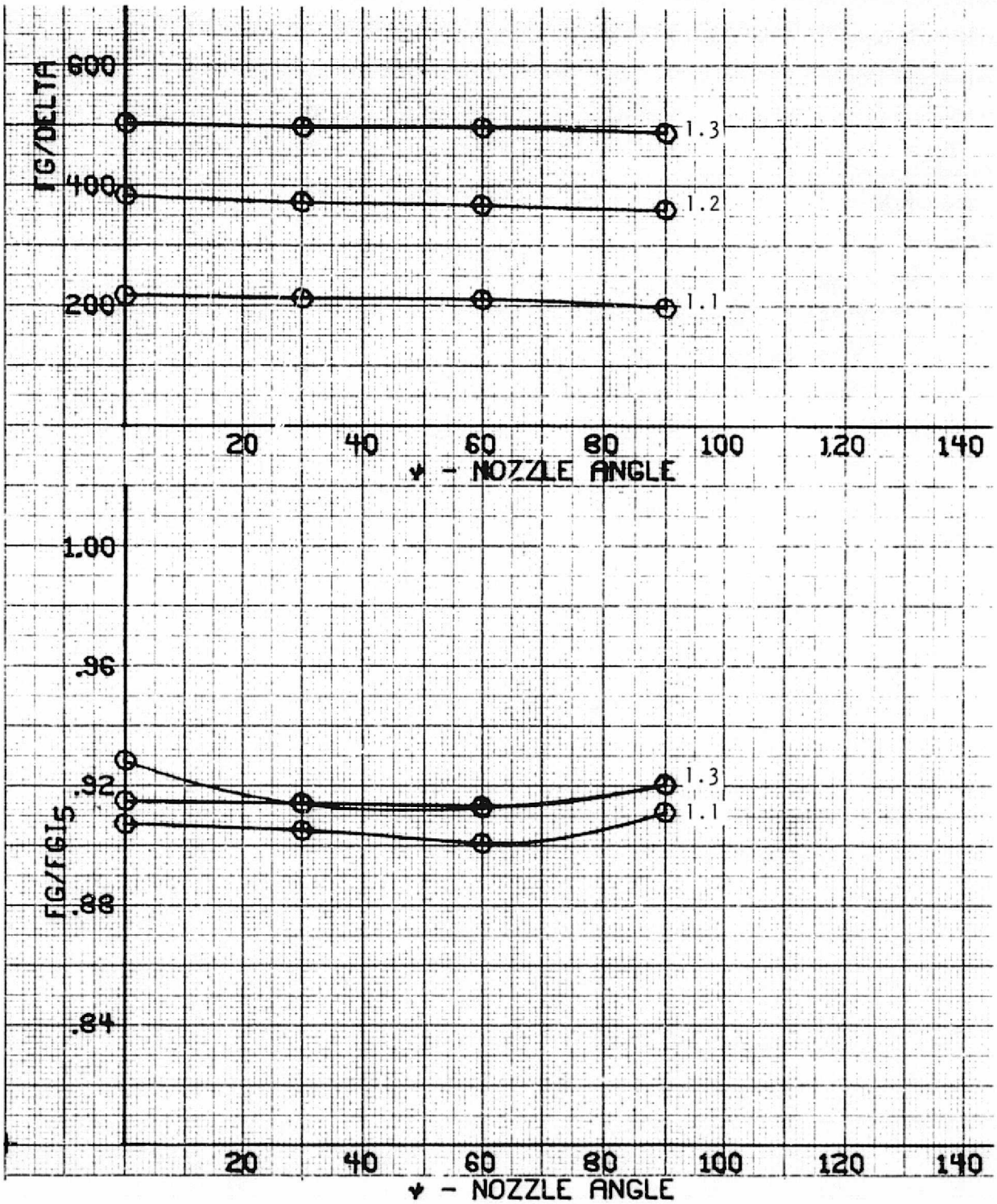

Figure 20. - Nozzle A corrected thrust and thrust coefficient versus nozzle angle.

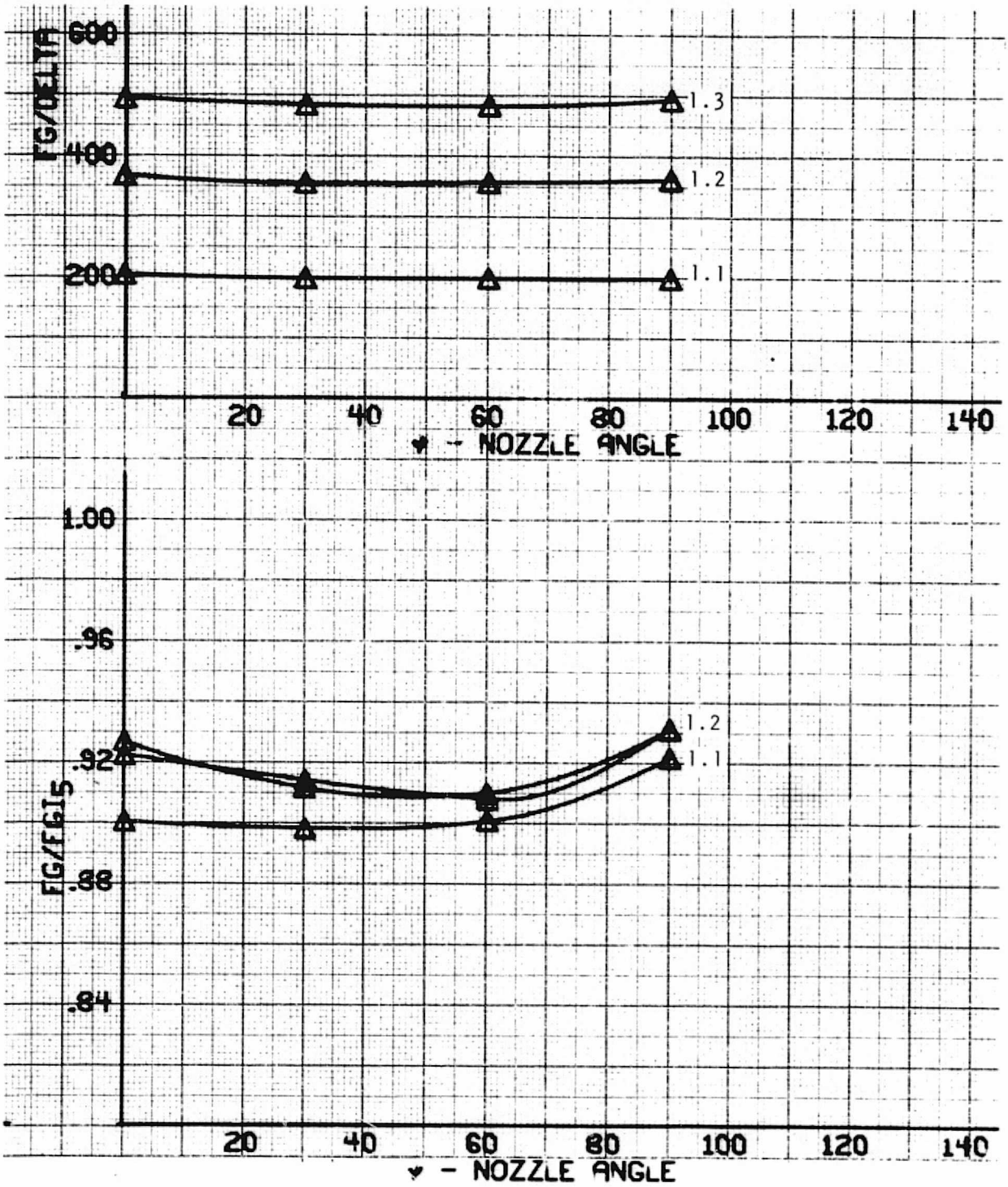

Figure 21. - Nozzle B corrected thrust and thrust coefficient versus nozzle angle.

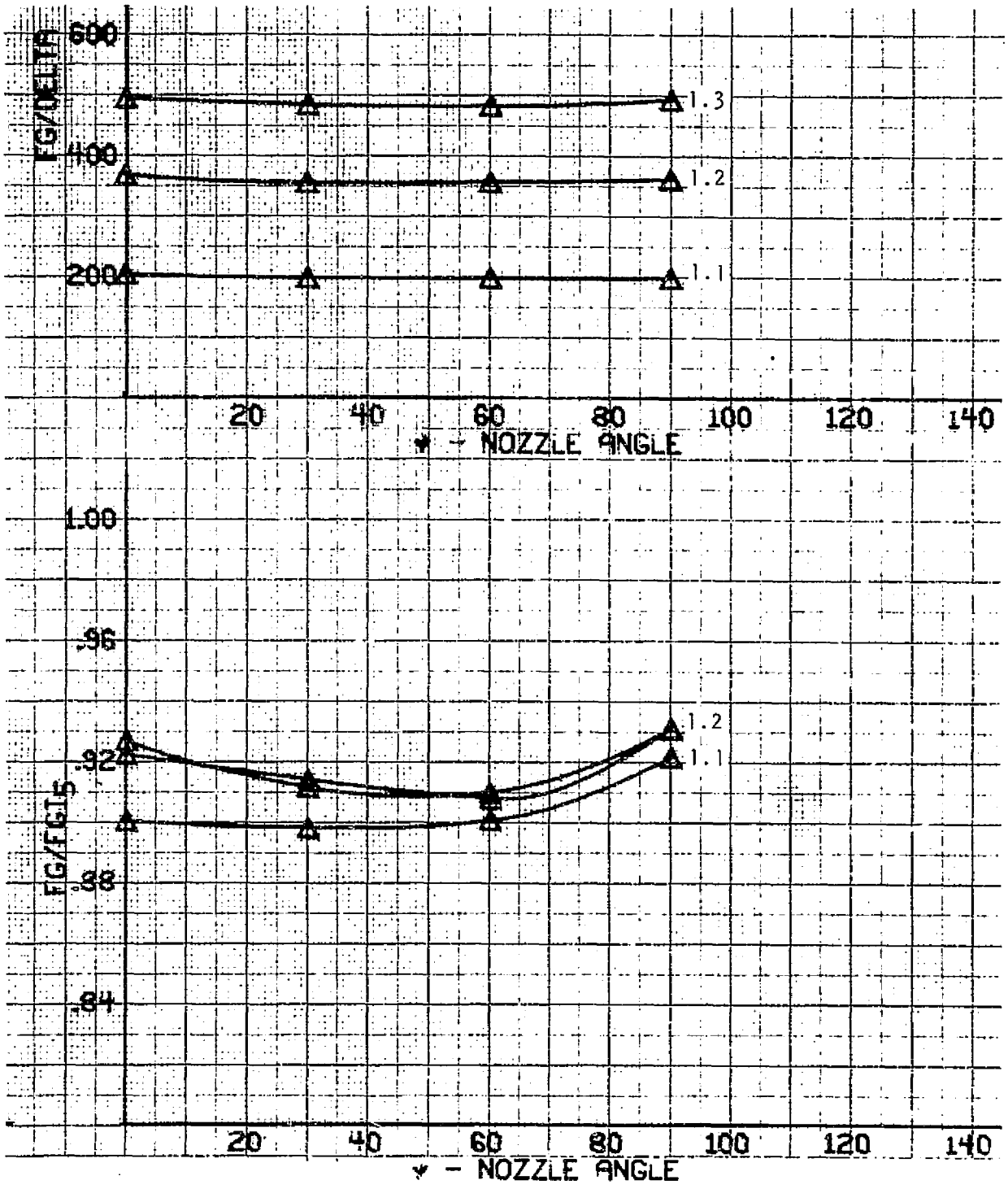

Figure 21. - Nozzle B corrected thrust and thrust coefficient versus nozzle angle.

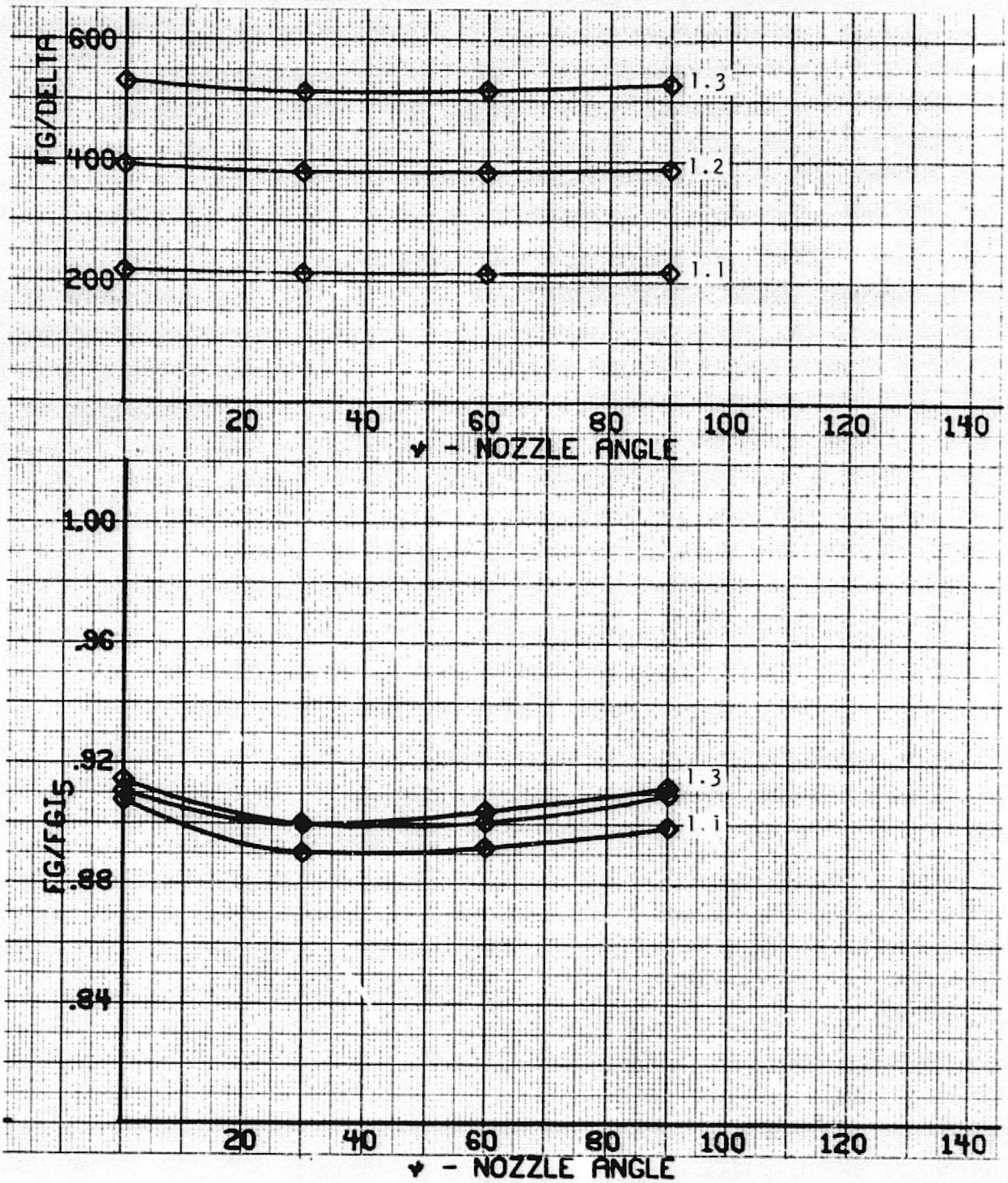

Figure 22. - Nozzle C corrected thrust and thrust coefficient versus nozzle angle.

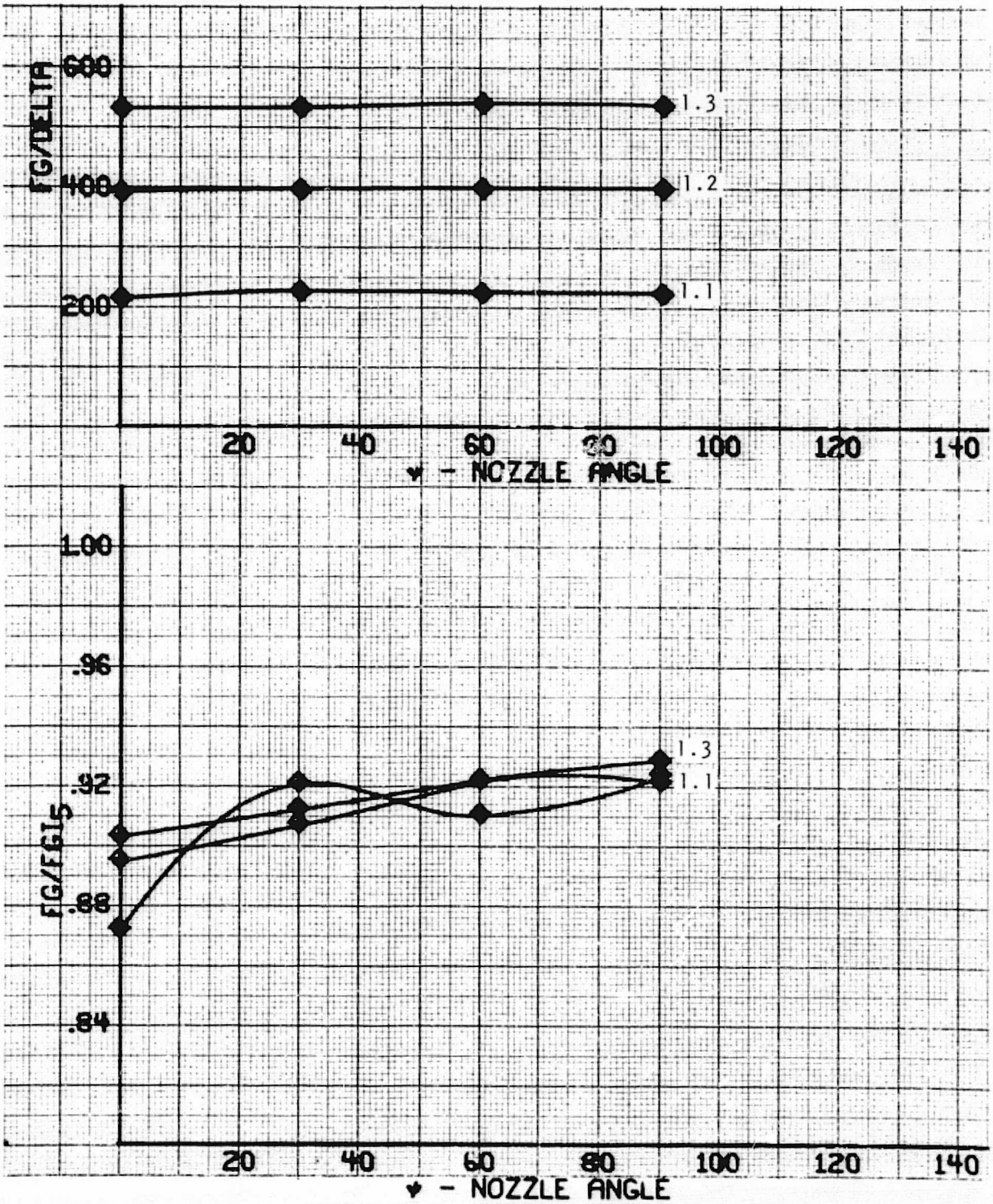

Figure 23. - Nozzle C (with vanes) corrected thrust and thrust coefficient versus nozzle angle.

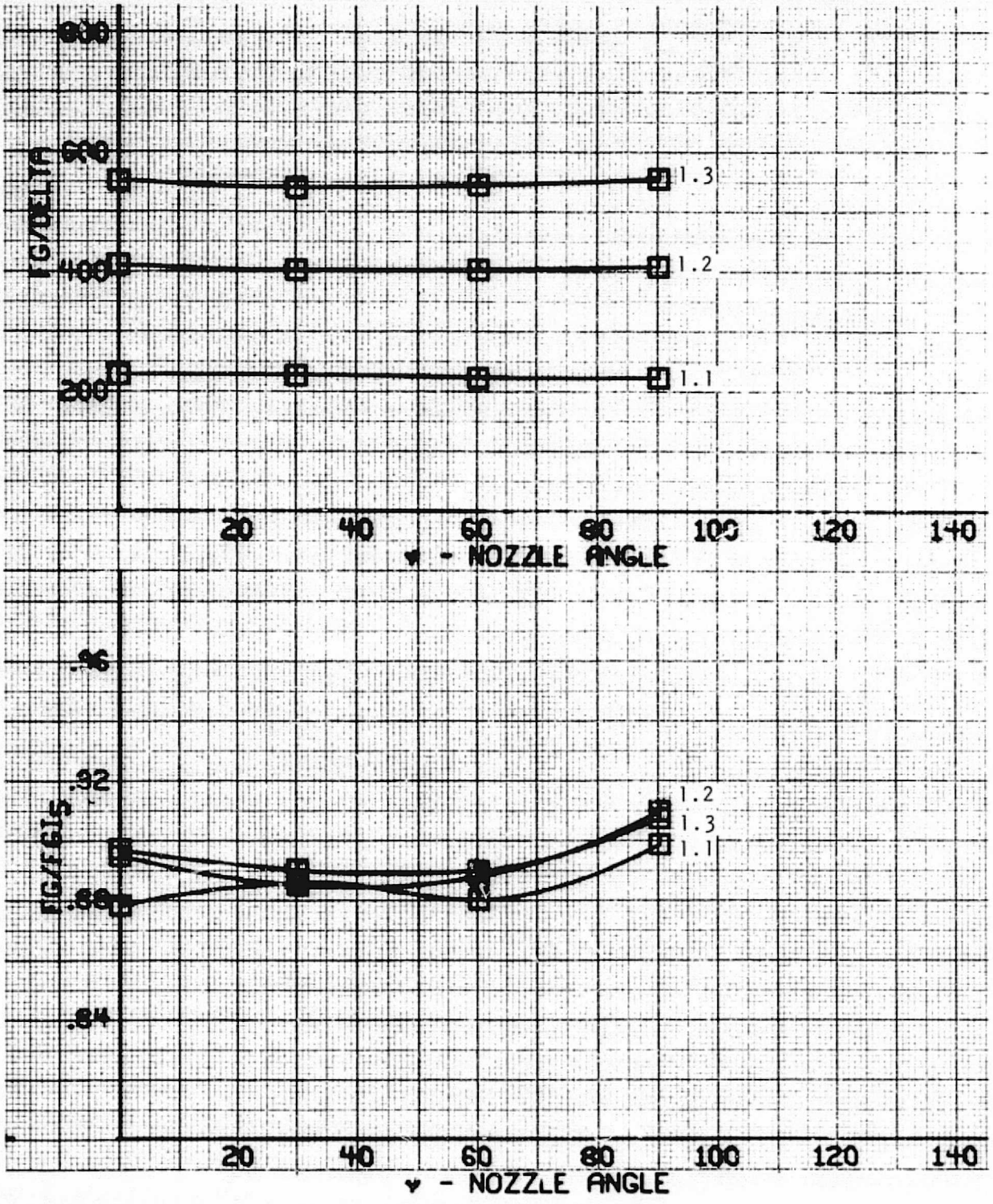

Figure 24. - Nozzle D corrected thrust and thrust coefficient versus nozzle angle.

REPRODUCIBILITY OF THE
ORIGINAL PAGE IS POOR

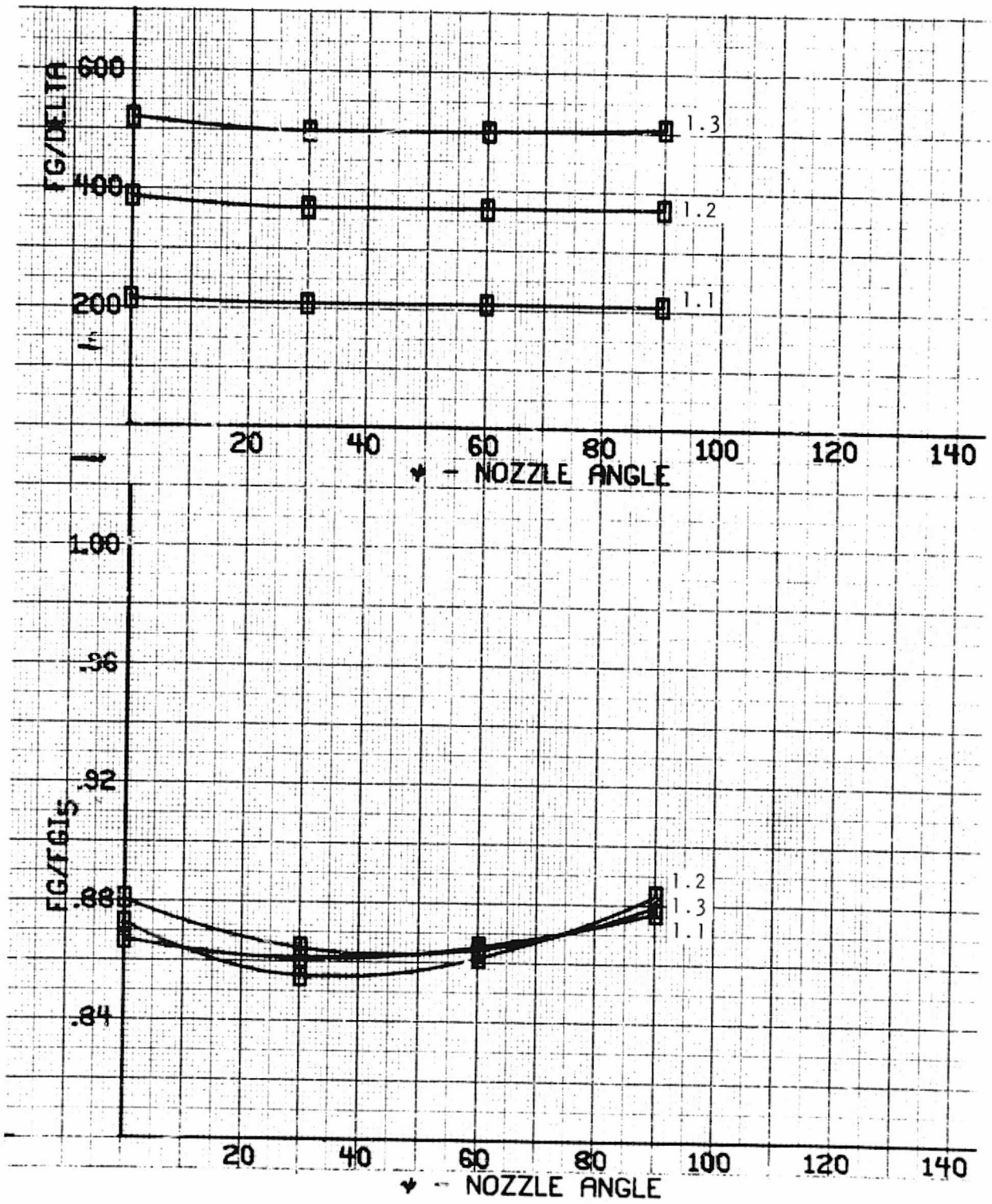

Figure 25. - Twin nozzle corrected thrust and thrust coefficient versus nozzle angle.

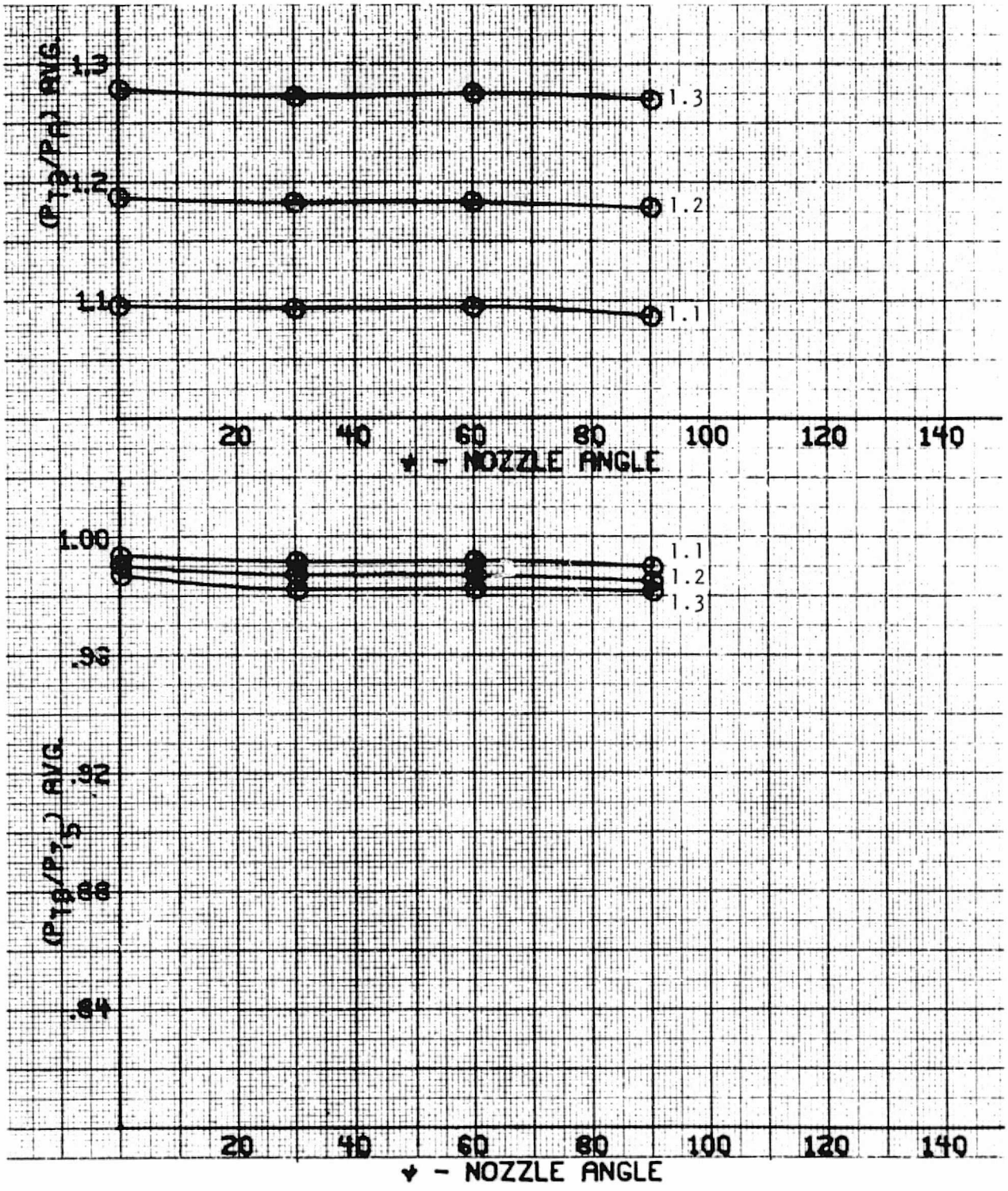

Figure 26. - Nozzle A pressure ratios versus nozzle angle.

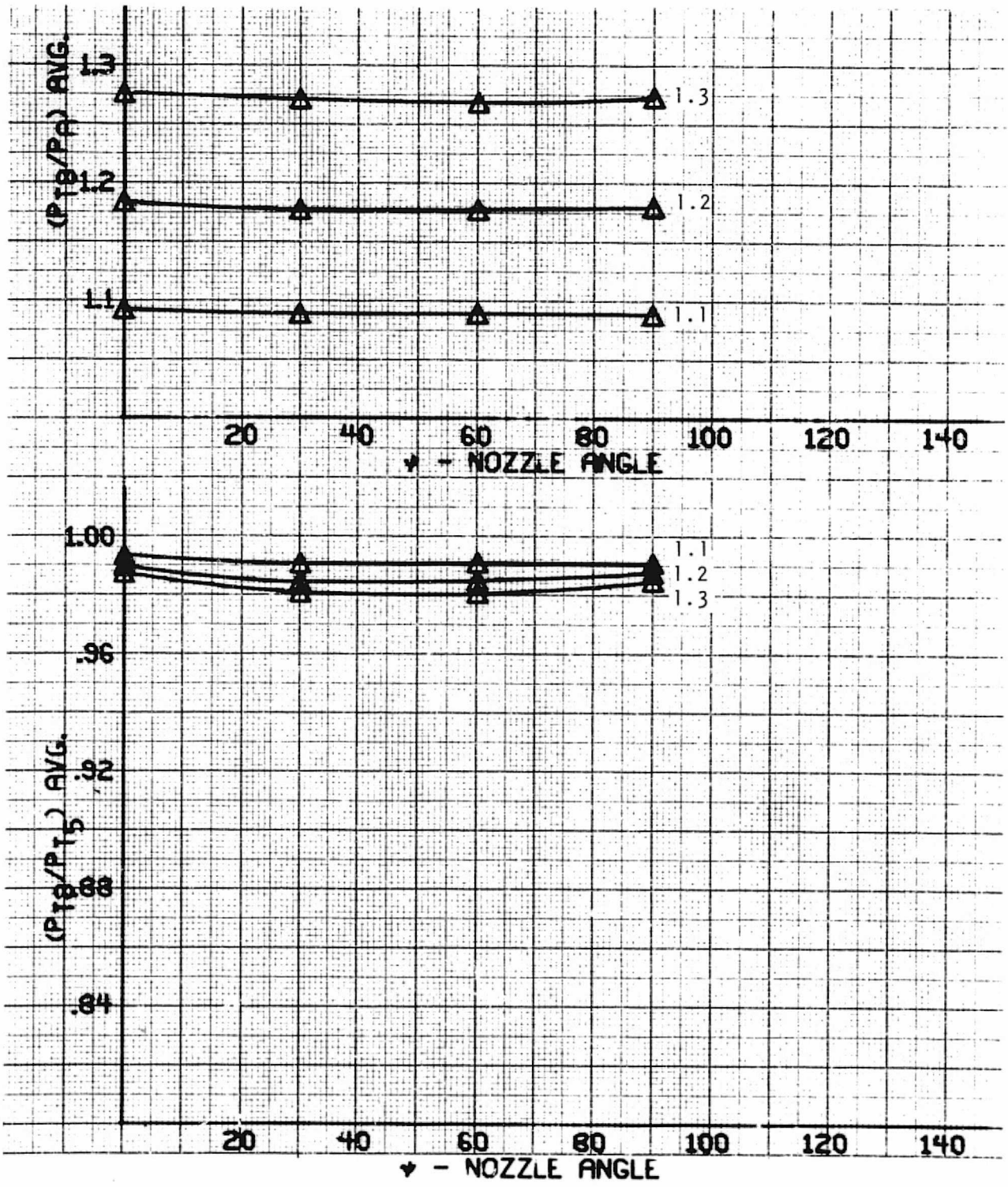

Figure 27. - Nozzle B pressure ratios versus nozzle angle.

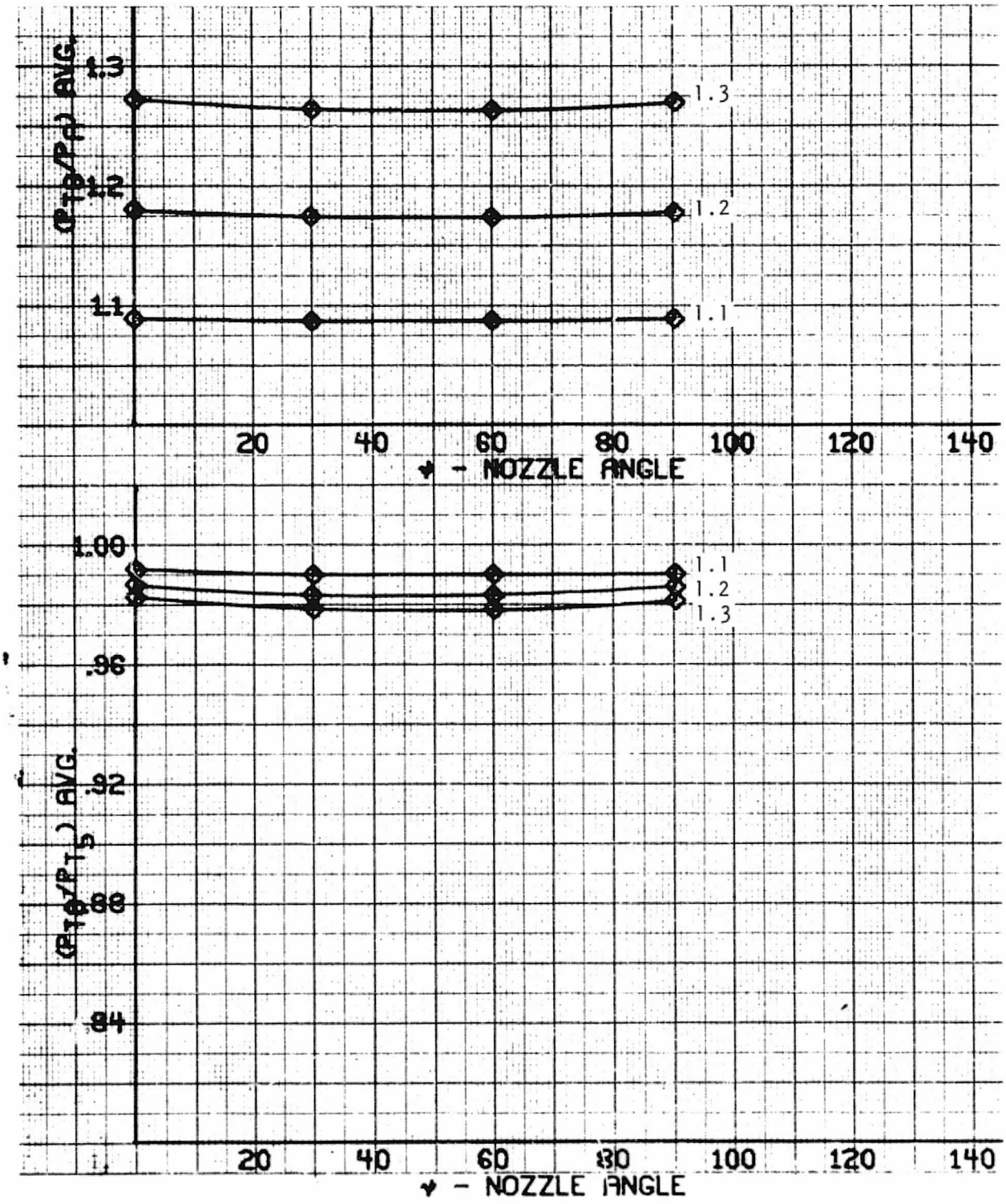

Figure 28. - Nozzle C pressure ratios versus nozzle angle.

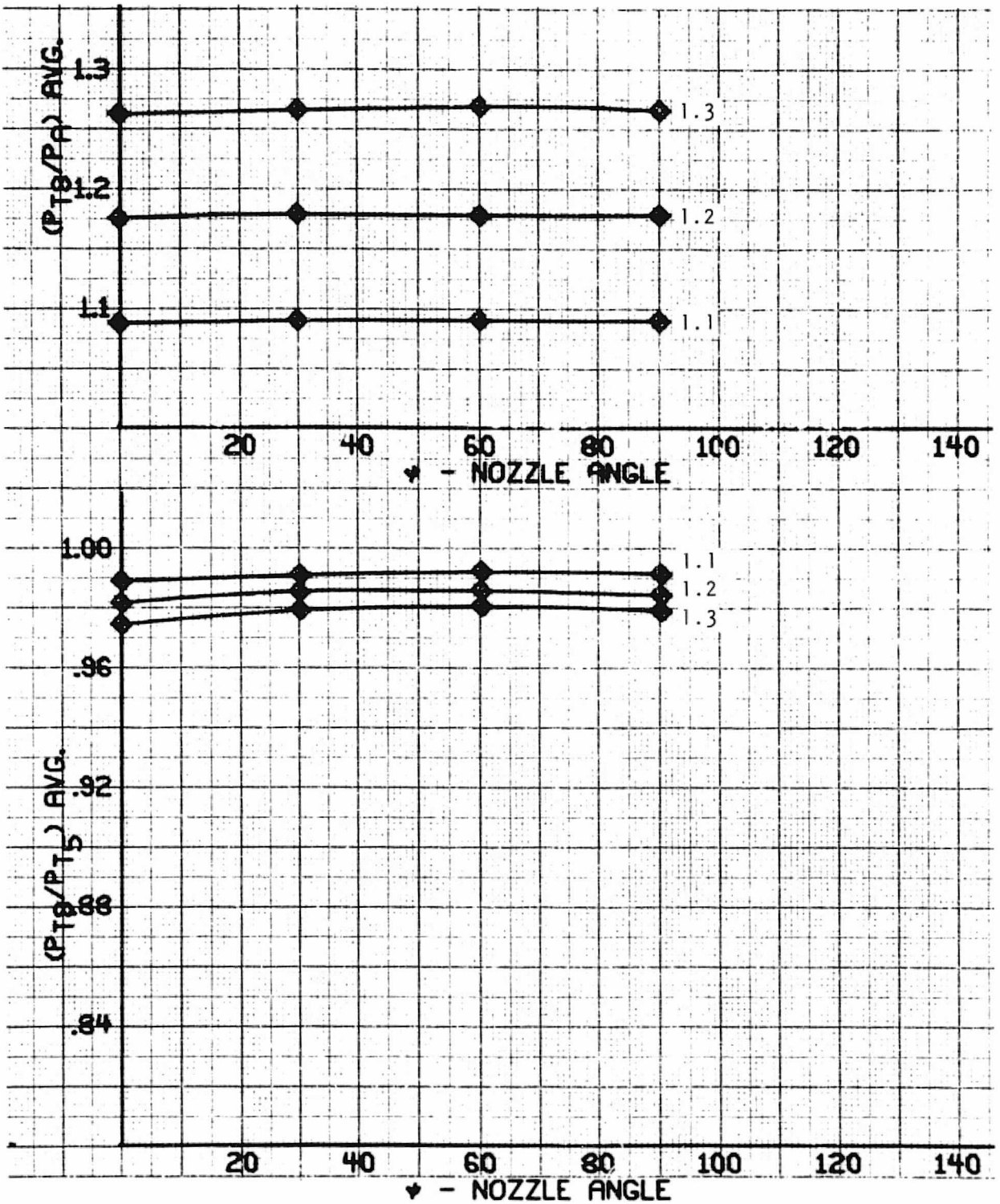

Figure 29. - Nozzle C (with vanes) pressure ratios versus nozzle angle.

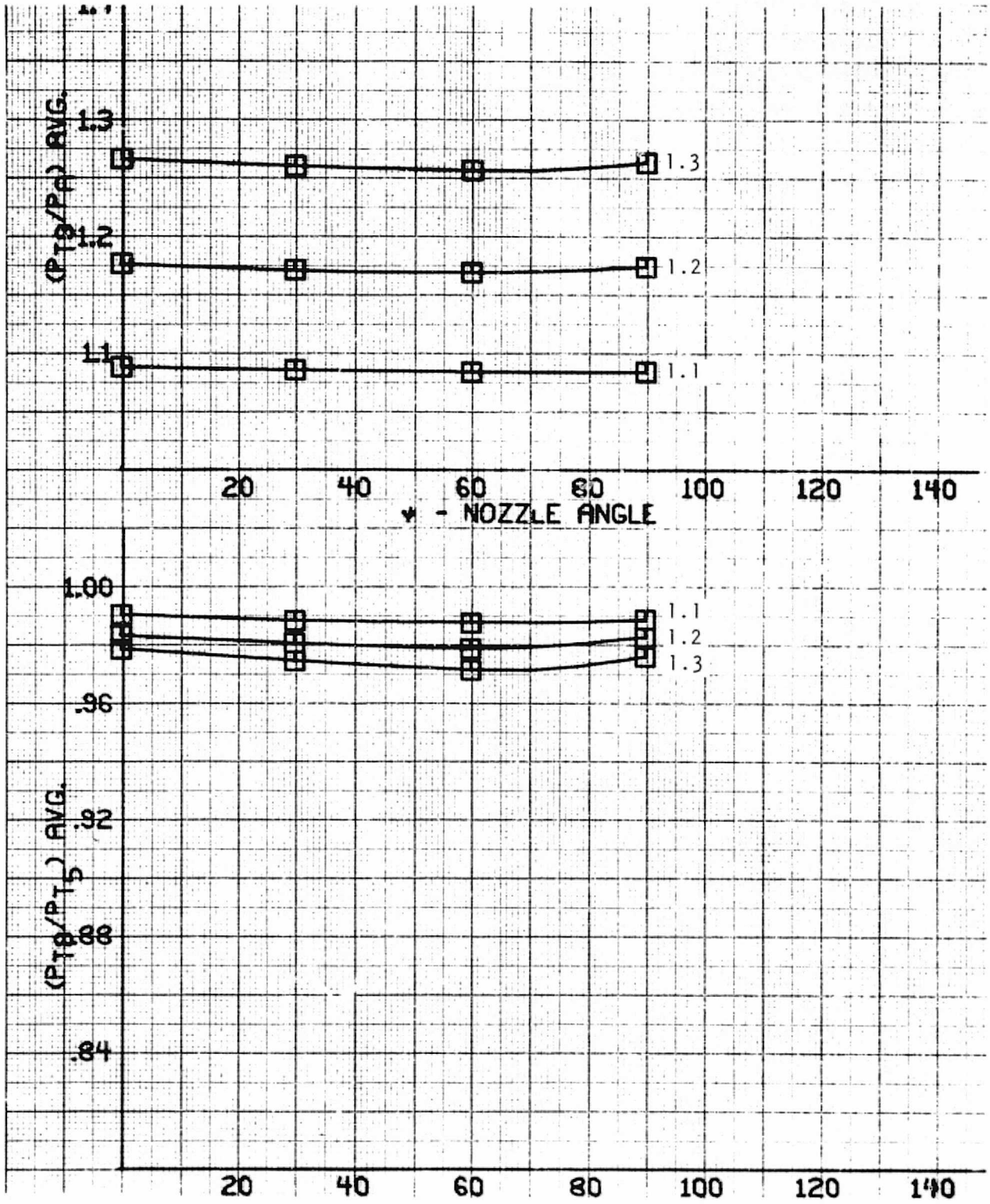

Figure 30. - Nozzle D pressure ratios versus nozzle angle.

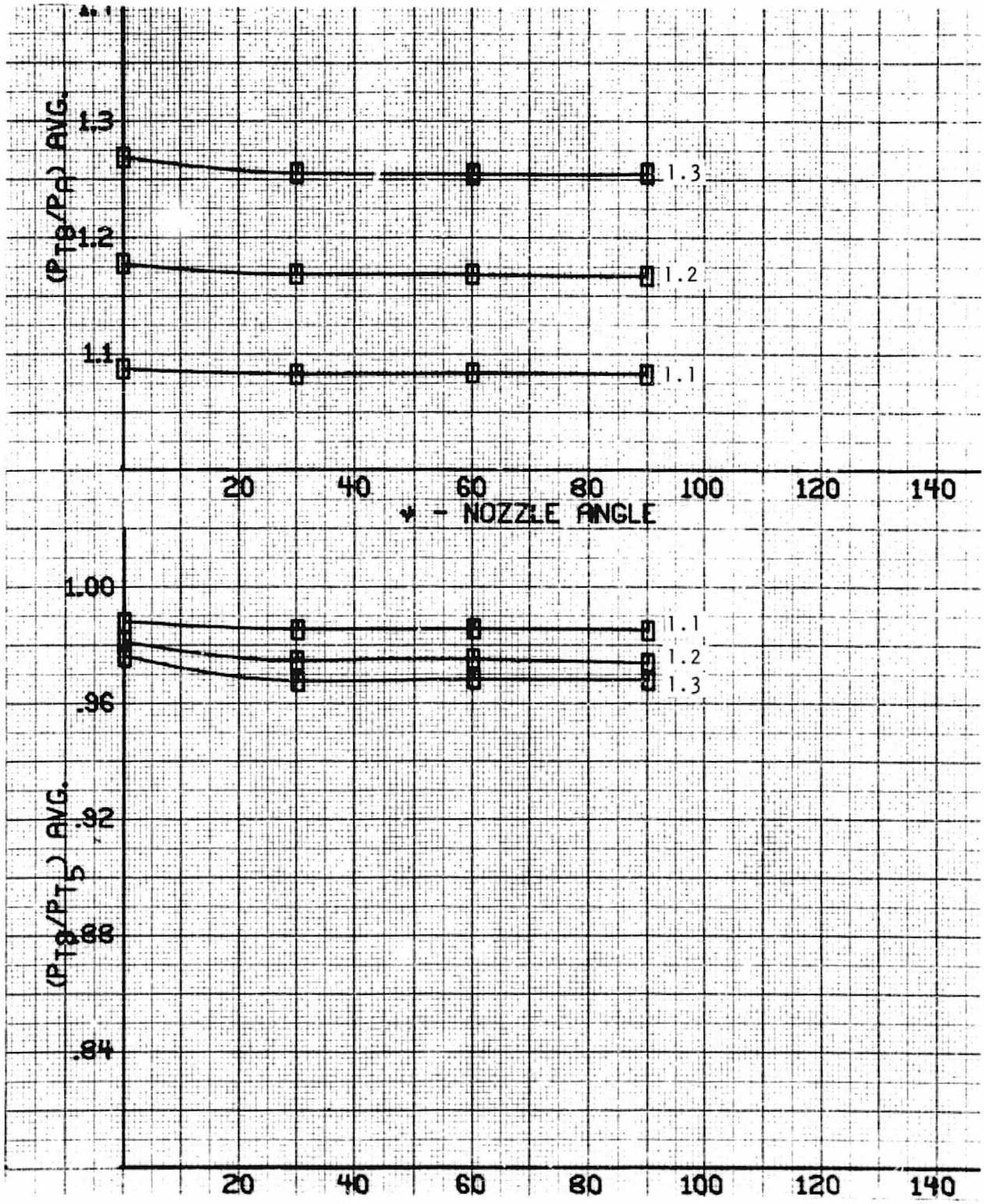

Figure 31. - Twin nozzle pressure ratios versus nozzle angle.

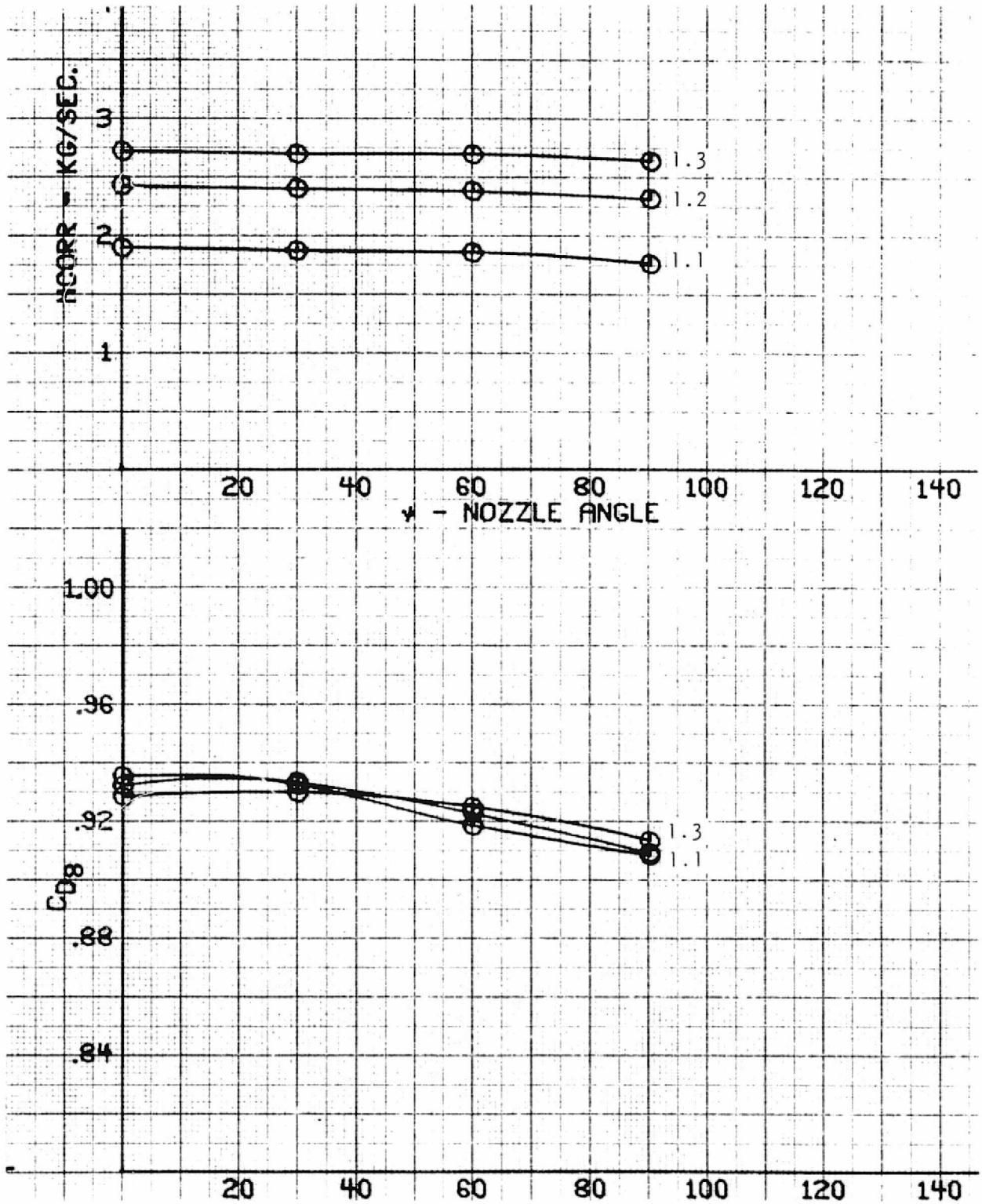

Figure 32. - Nozzle A corrected flow rate and discharge coefficient versus nozzle angle.

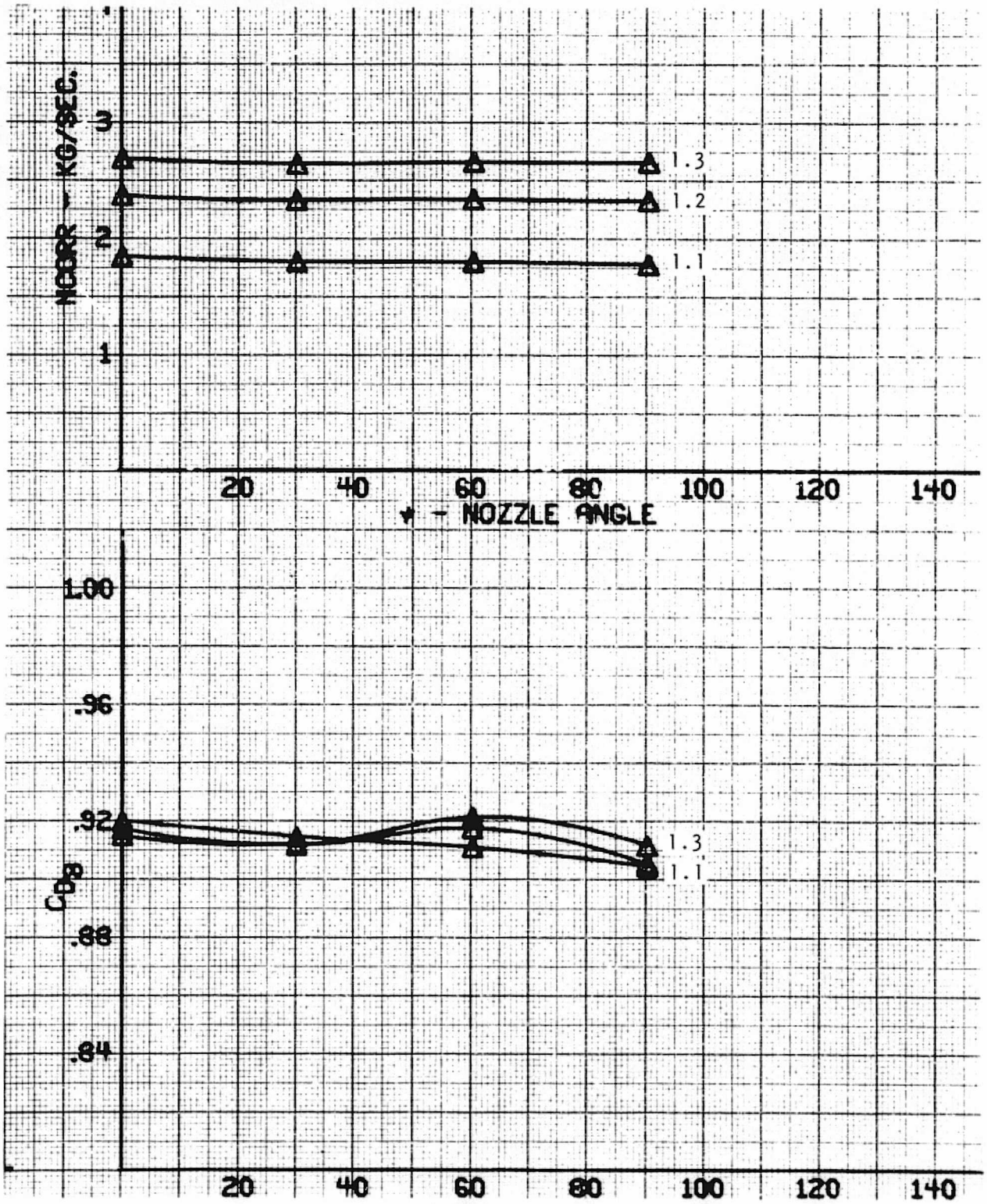

Figure 33. - Nozzle B corrected flow rate and discharge coefficient versus nozzle angle.

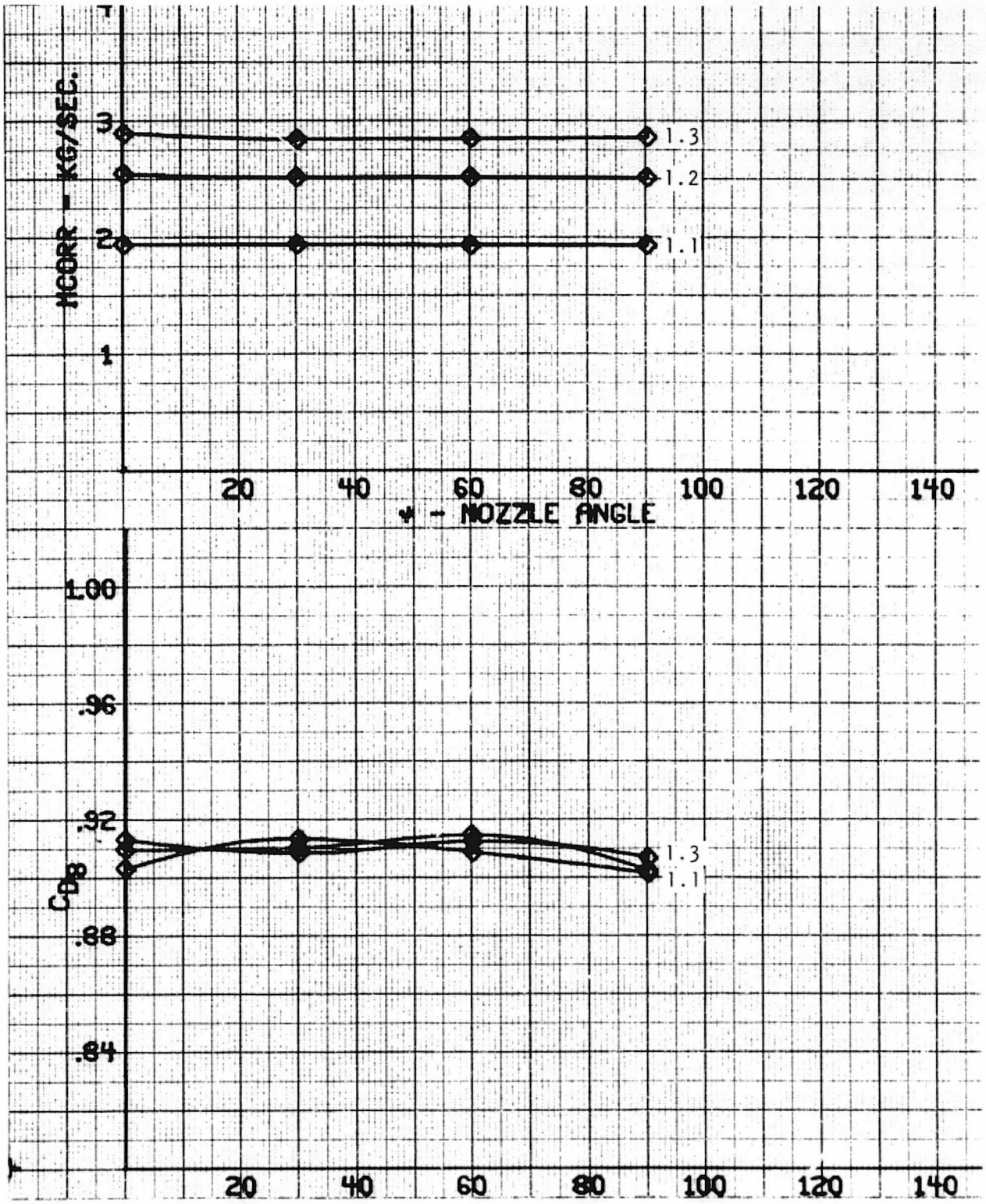

Figure 34. - Nozzle C corrected flow rate and discharge coefficient versus nozzle angle.

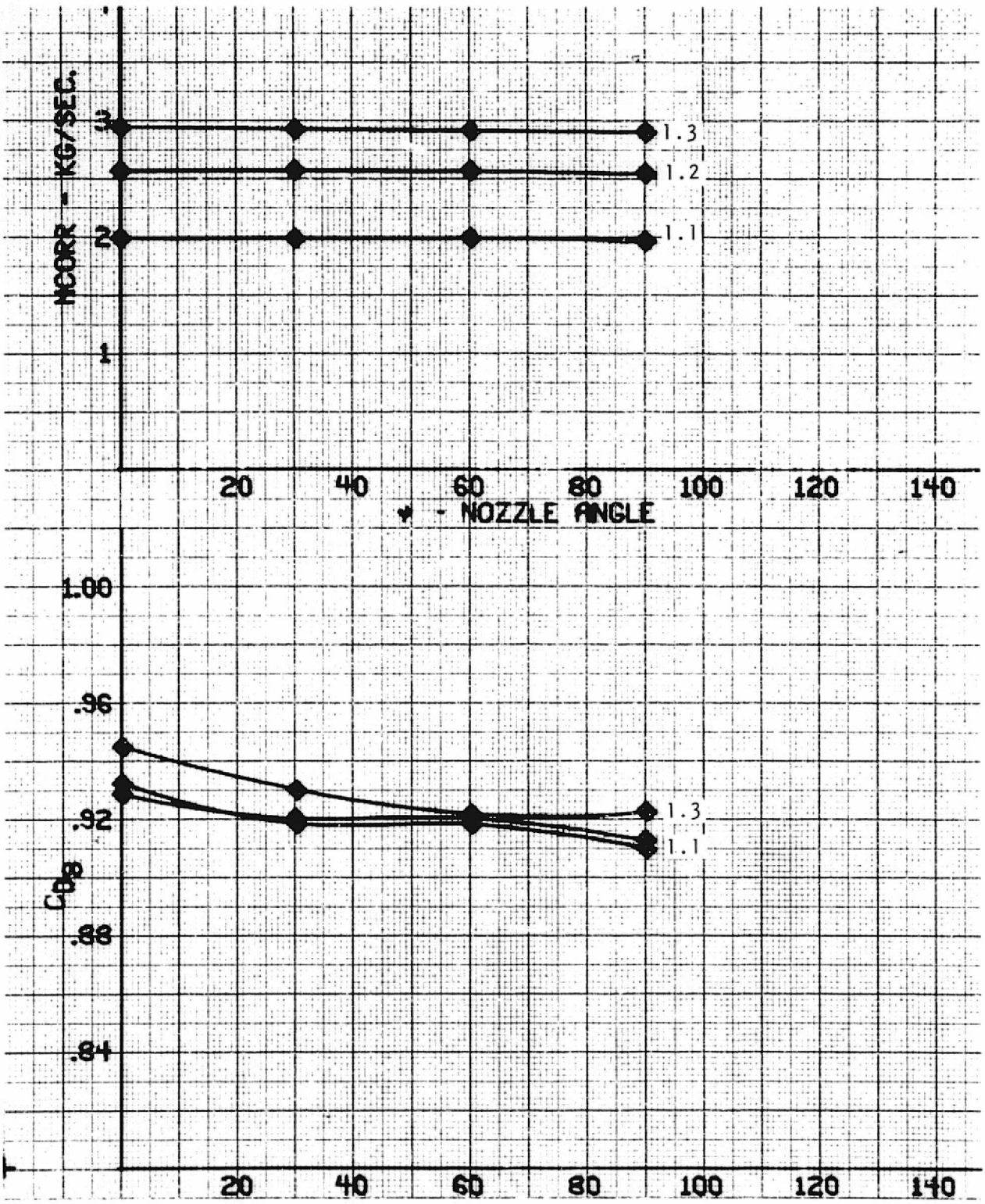

Figure 35. - Nozzle C (with vanes) corrected flow rate and discharge coefficient versus nozzle angle.

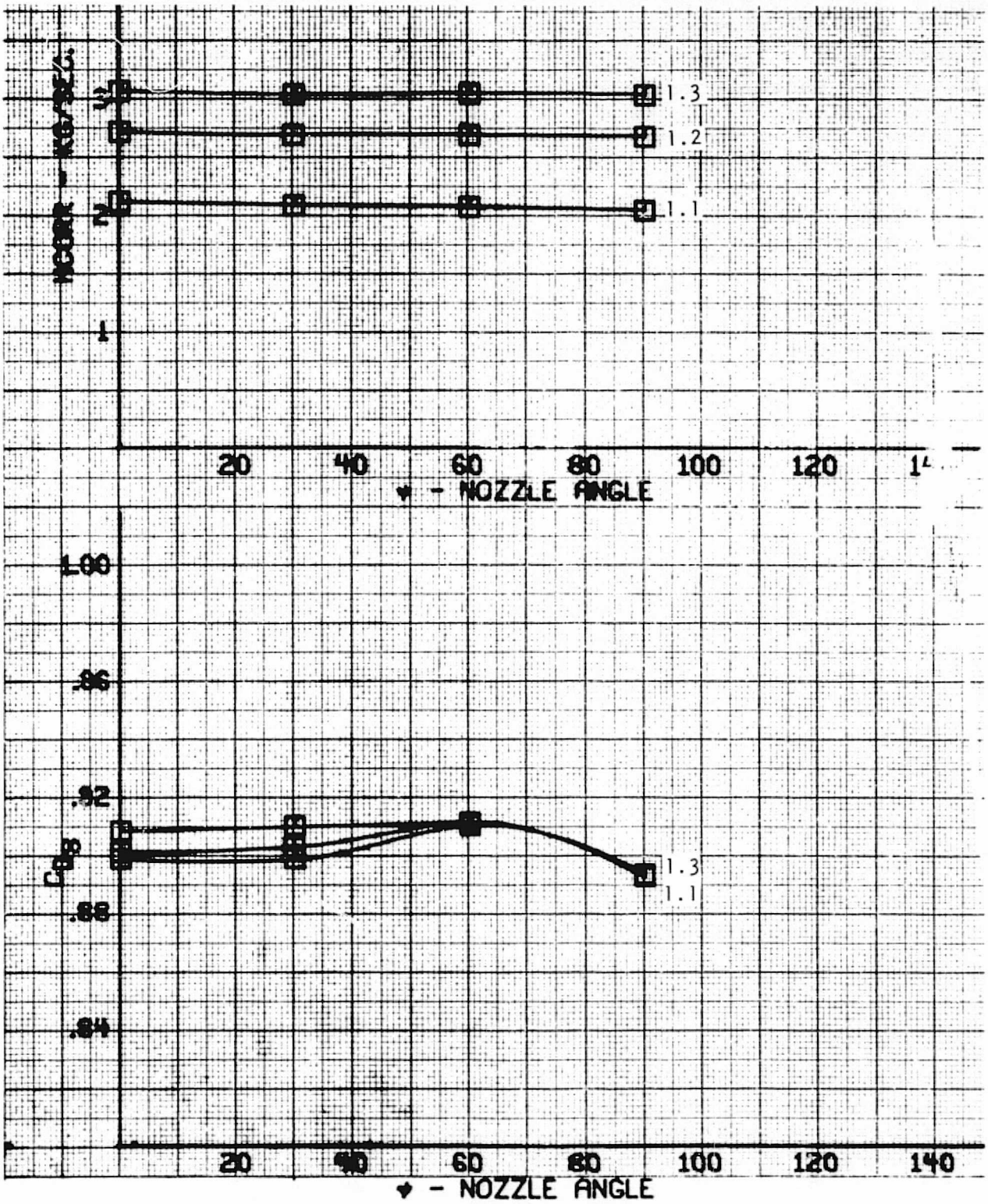

Figure 36. - Nozzle D corrected flow rate and discharge coefficient versus nozzle angle.

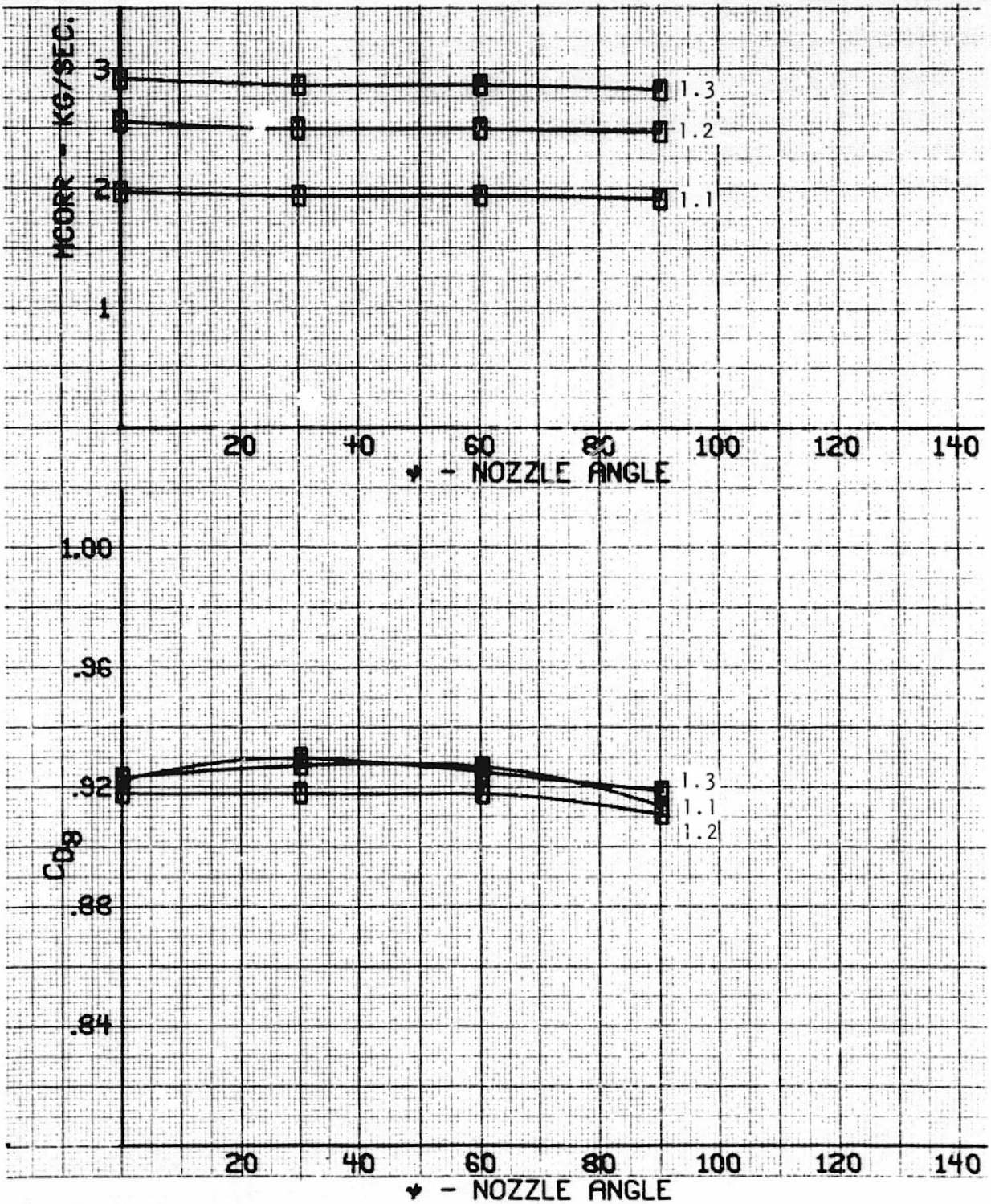

Figure 37. - Twin nozzle corrected flow rate and discharge coefficient versus nozzle angle.

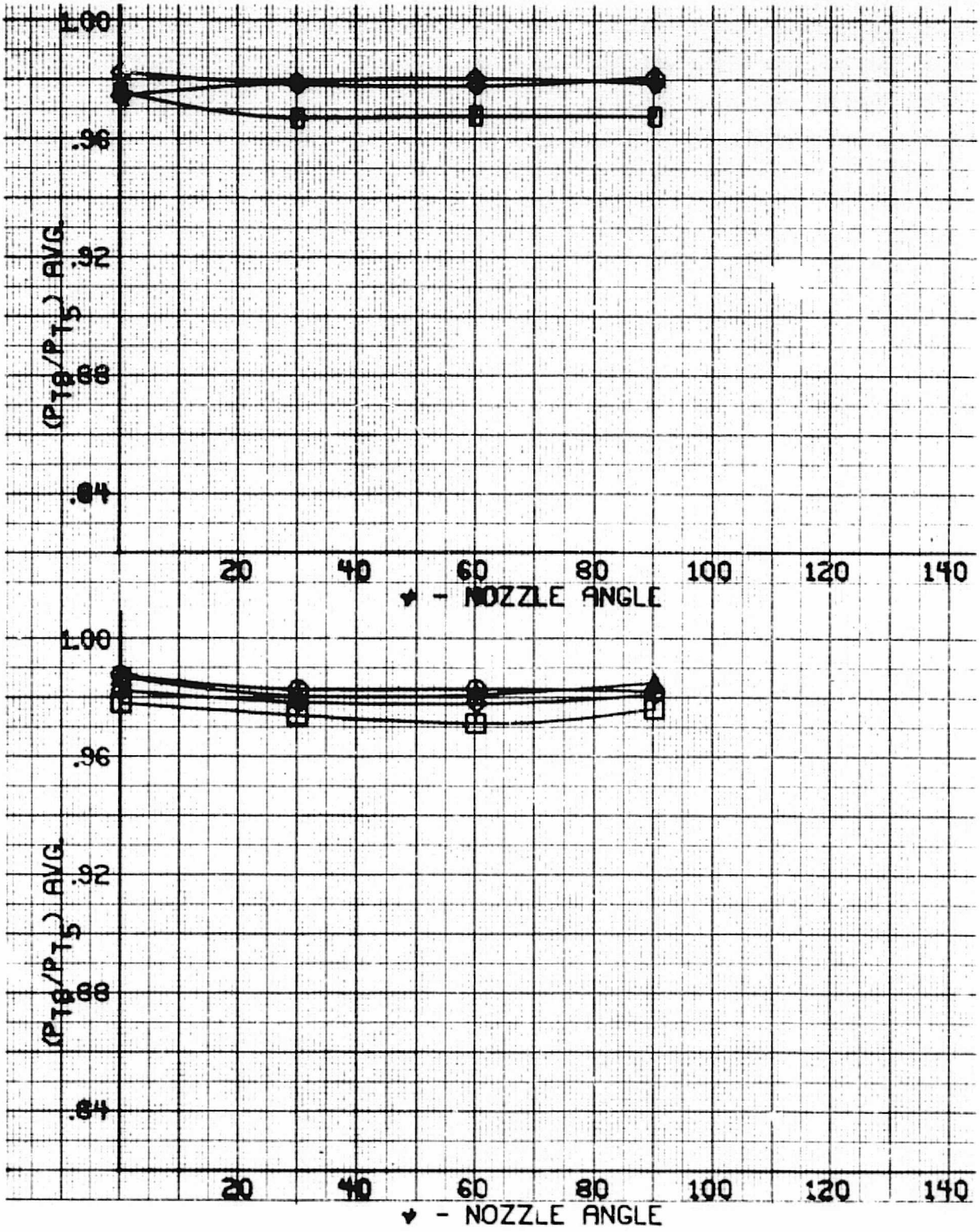

Figure 38. - Exit to inlet total pressure ratio at $P_{T_5}/P_A = 1.3$ versus nozzle angle.

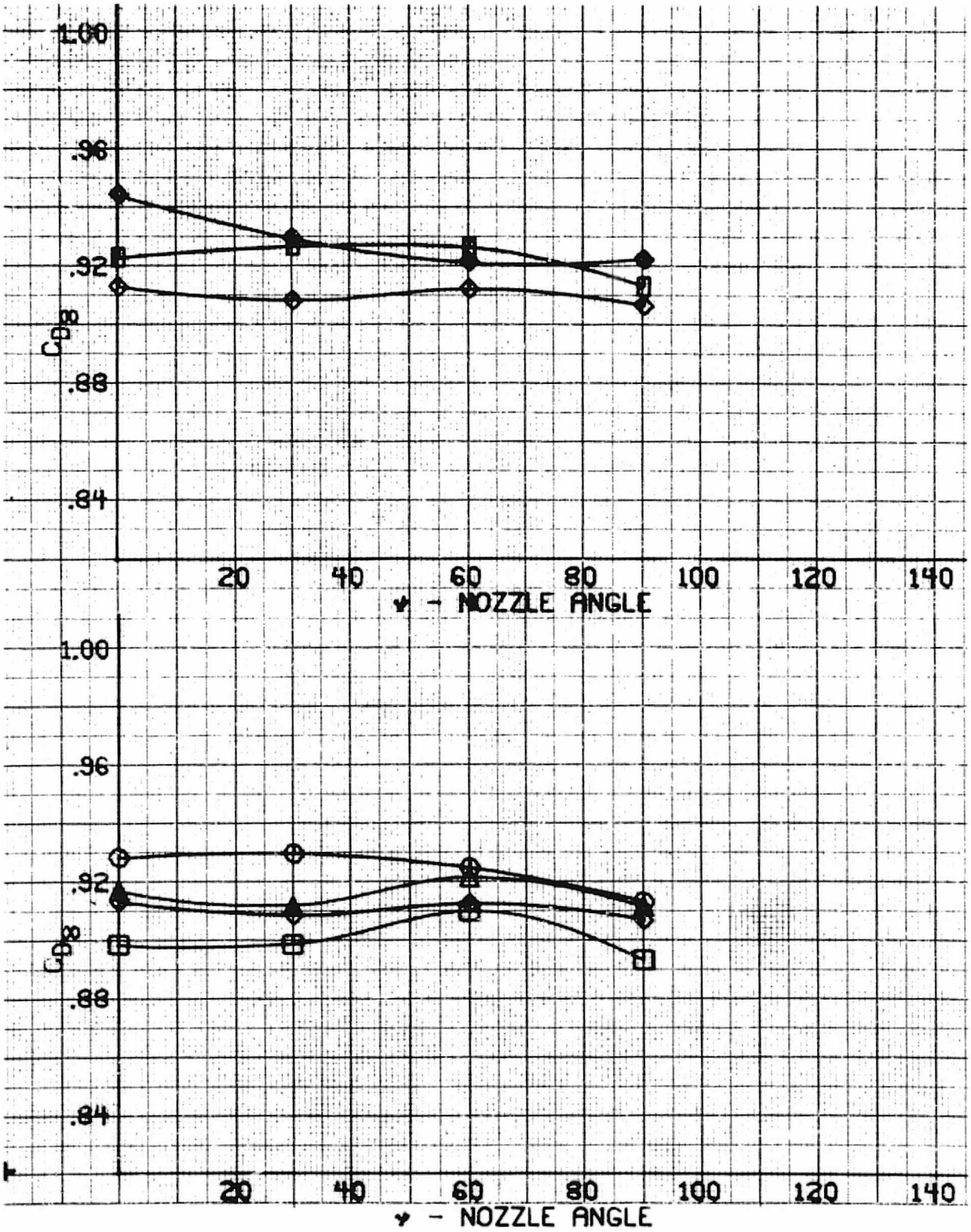

Figure 39. - Exit discharge coefficient at P_{T_5}/P_A = 1.3 versus nozzle angle.

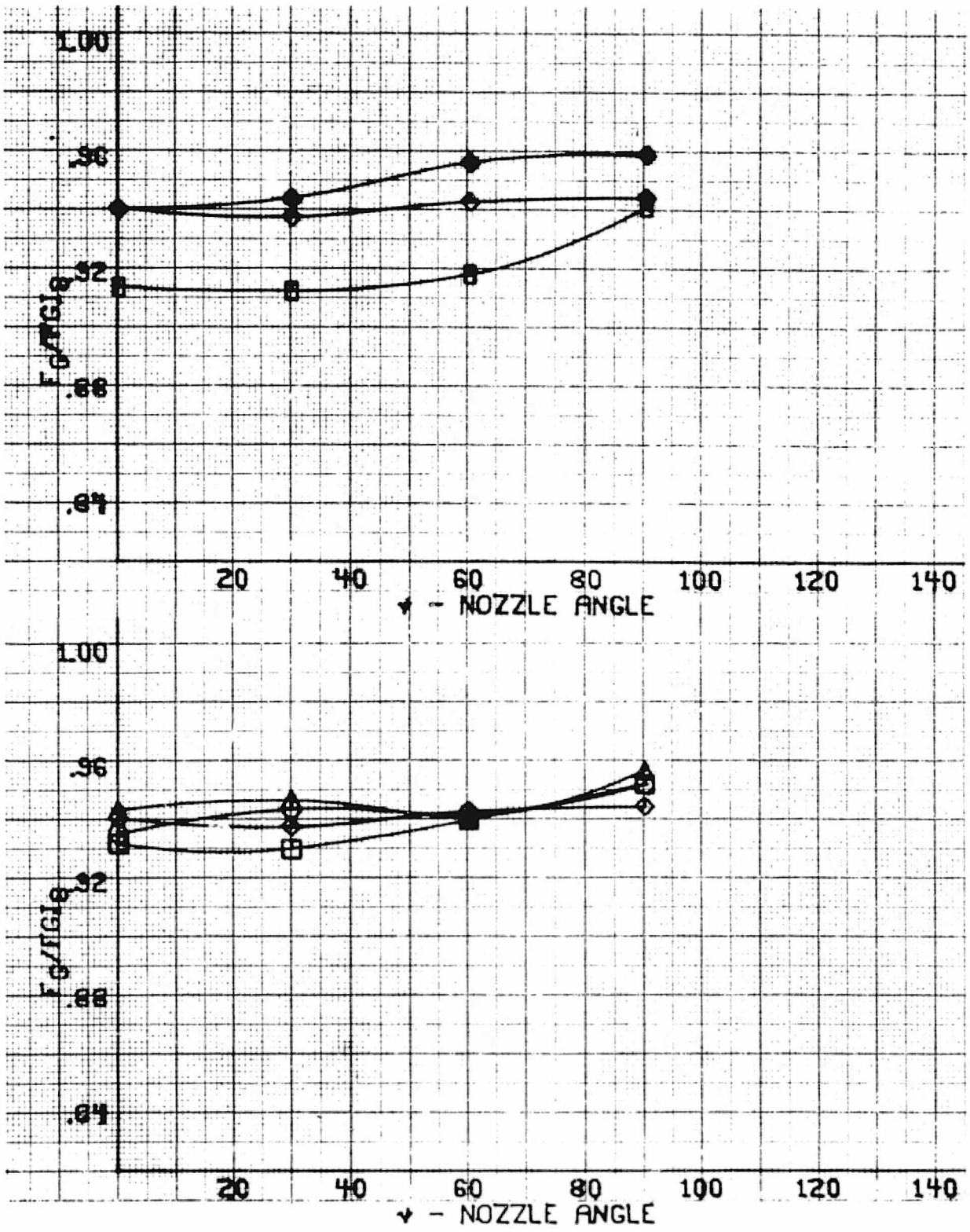

Figure 40. - Exit thrust coefficient at $P_{T_5}/P_A = 1.3$ versus nozzle angle.

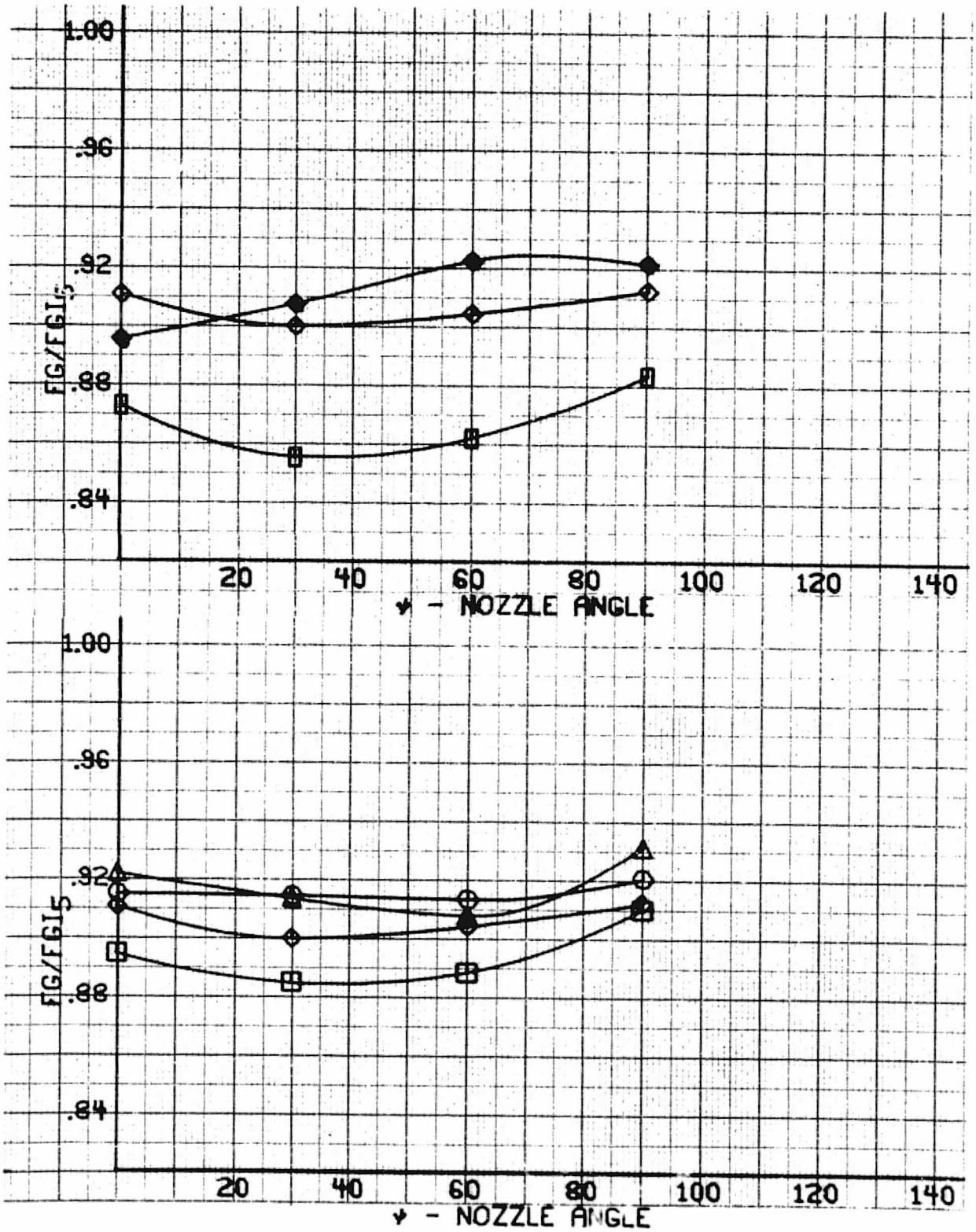

Figure 41. - Diffuser inlet thrust coefficient at $P_{T_5}/P_A = 1.3$ versus nozzle angle.

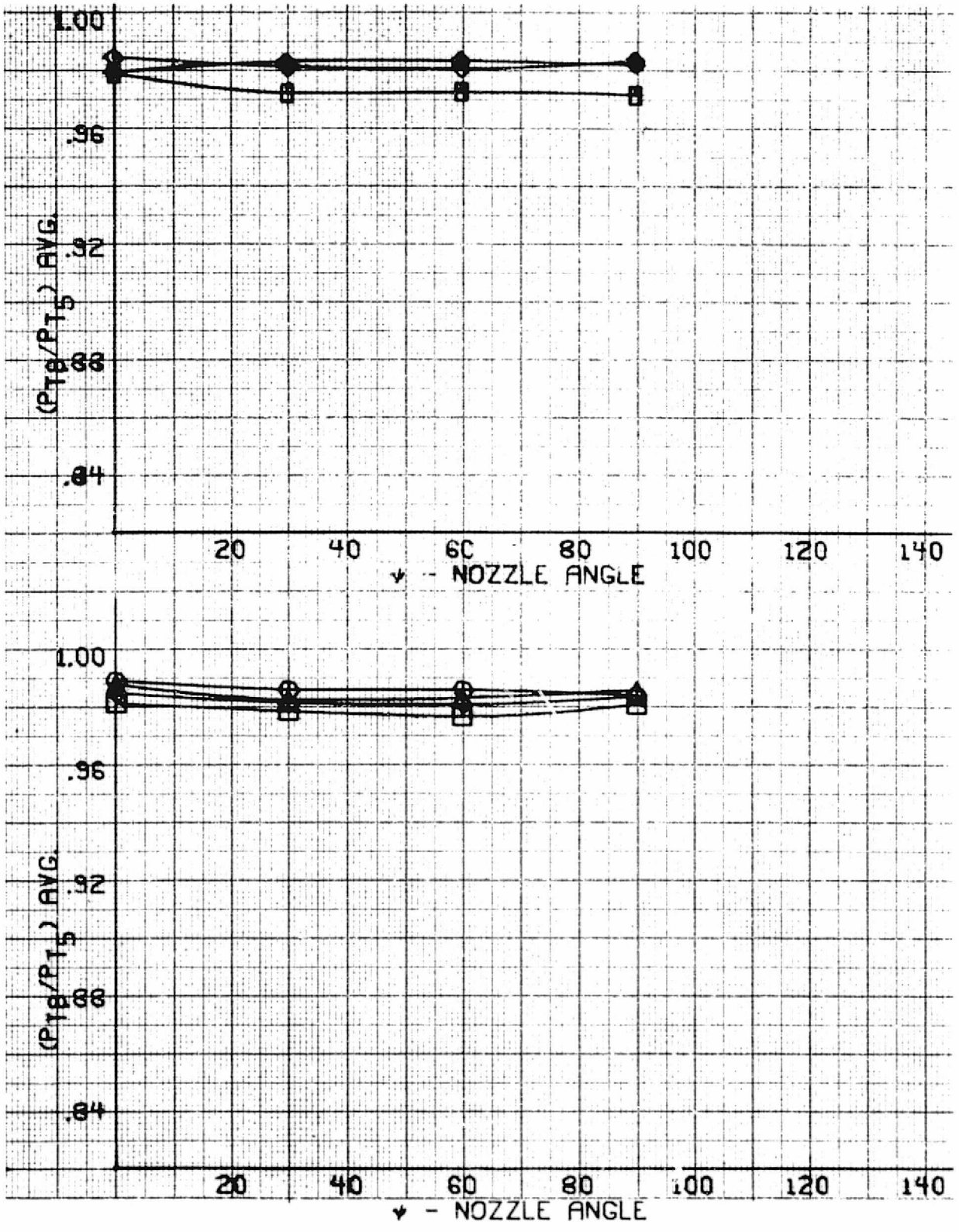

Figure 42. - Exit to inlet total pressure ratio at $P_{T_5}/P_A = 1.2$ versus nozzle angle.

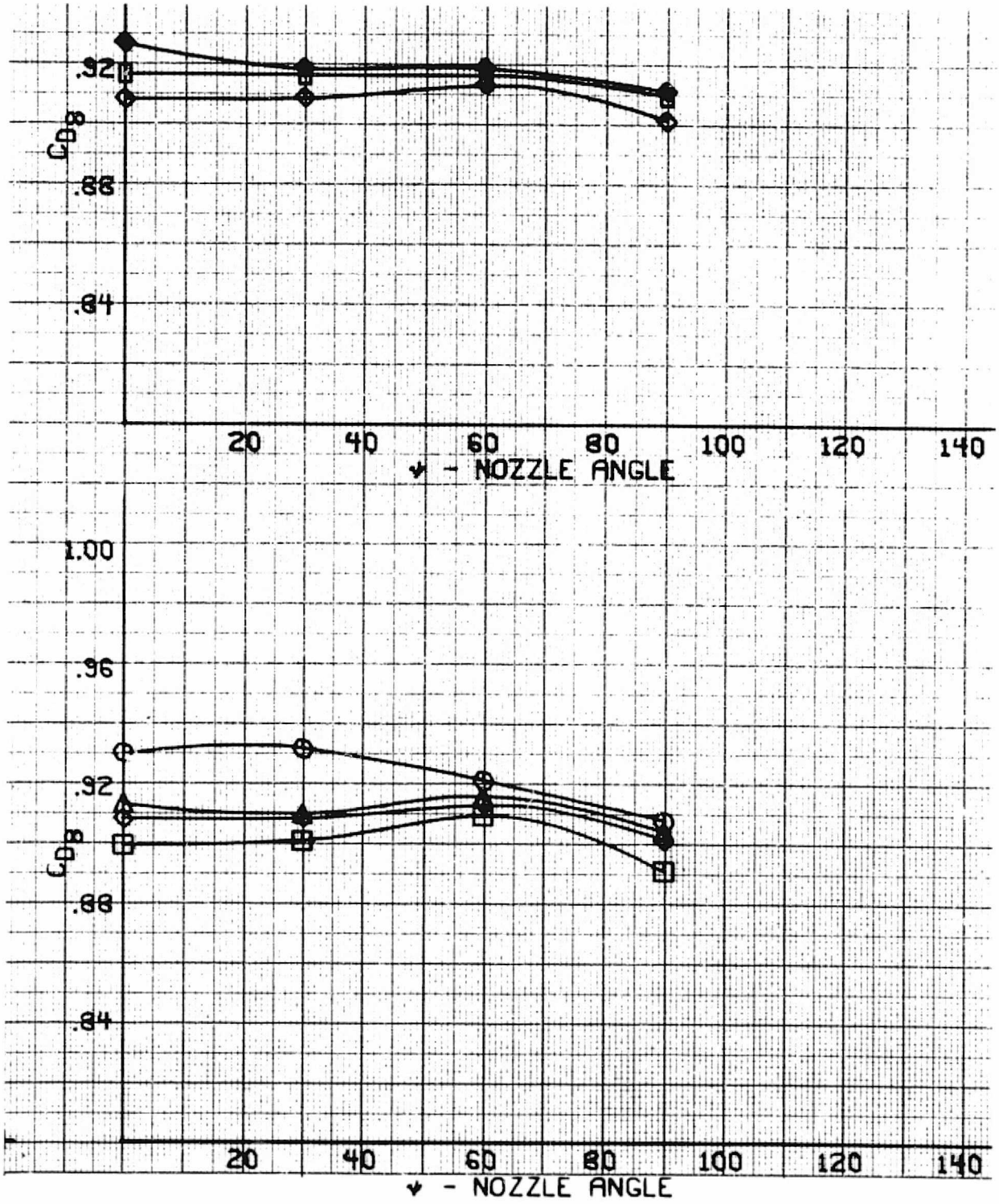

Figure 43. - Exit discharge coefficient at $P_{T_5}/P_A = 1.2$ versus nozzle angle.

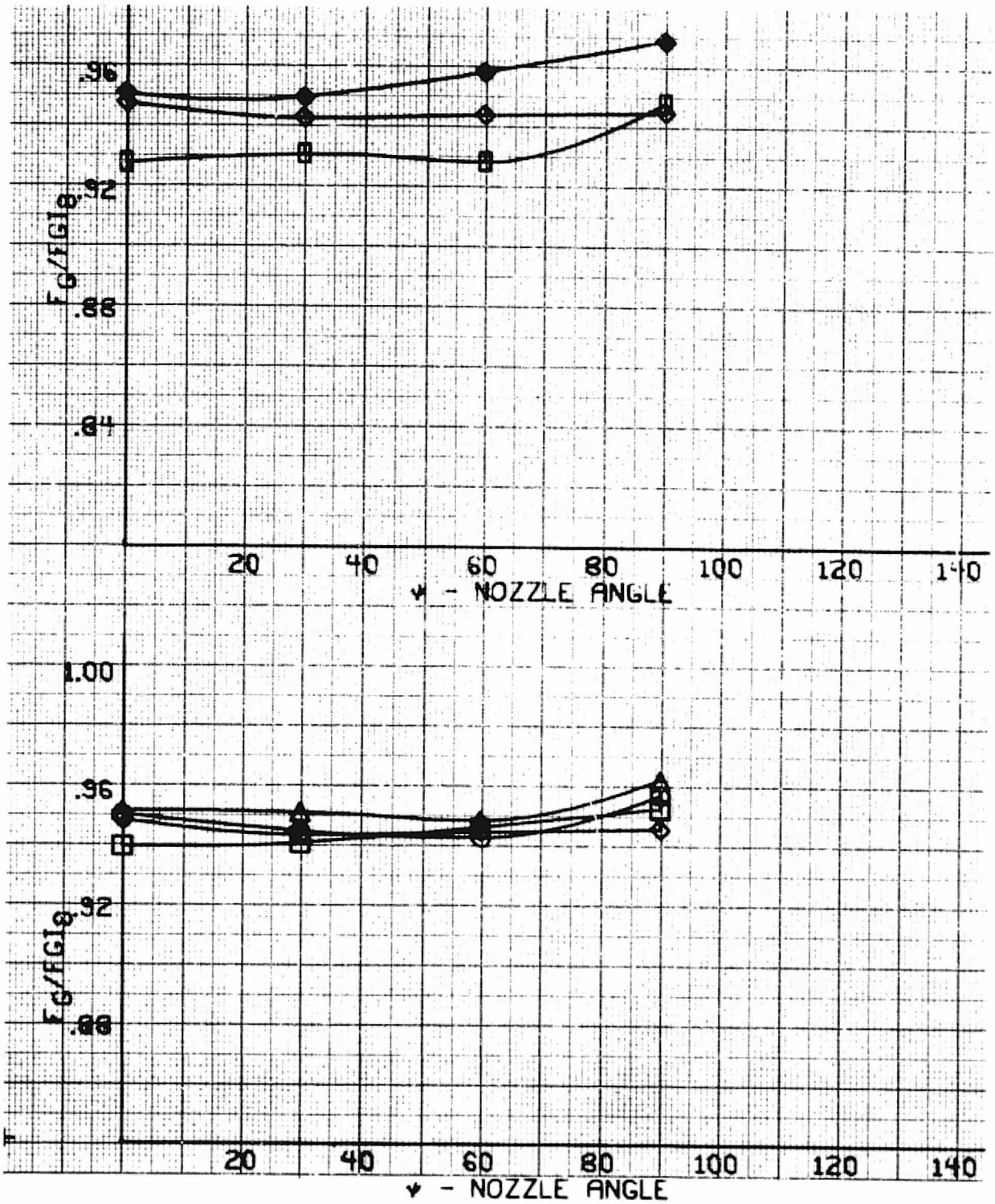

Figure 44. - Exit thrust coefficient at $P_{T_5}/P_A = 1.2$ versus nozzle angle.

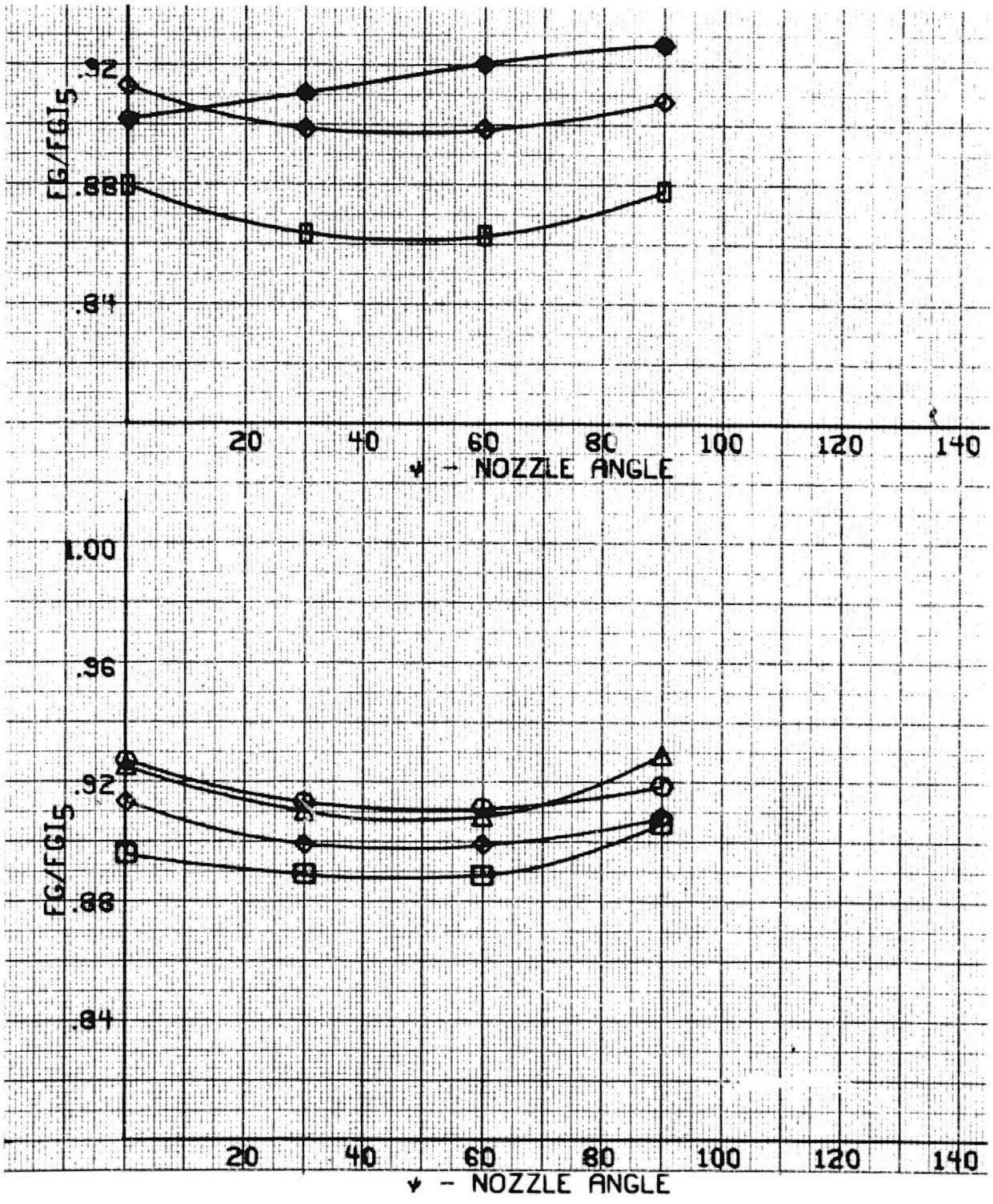

Figure 45. - Diffuser inlet thrust coefficient at $P_{T_5}/P_A = 1.2$ versus nozzle angle.

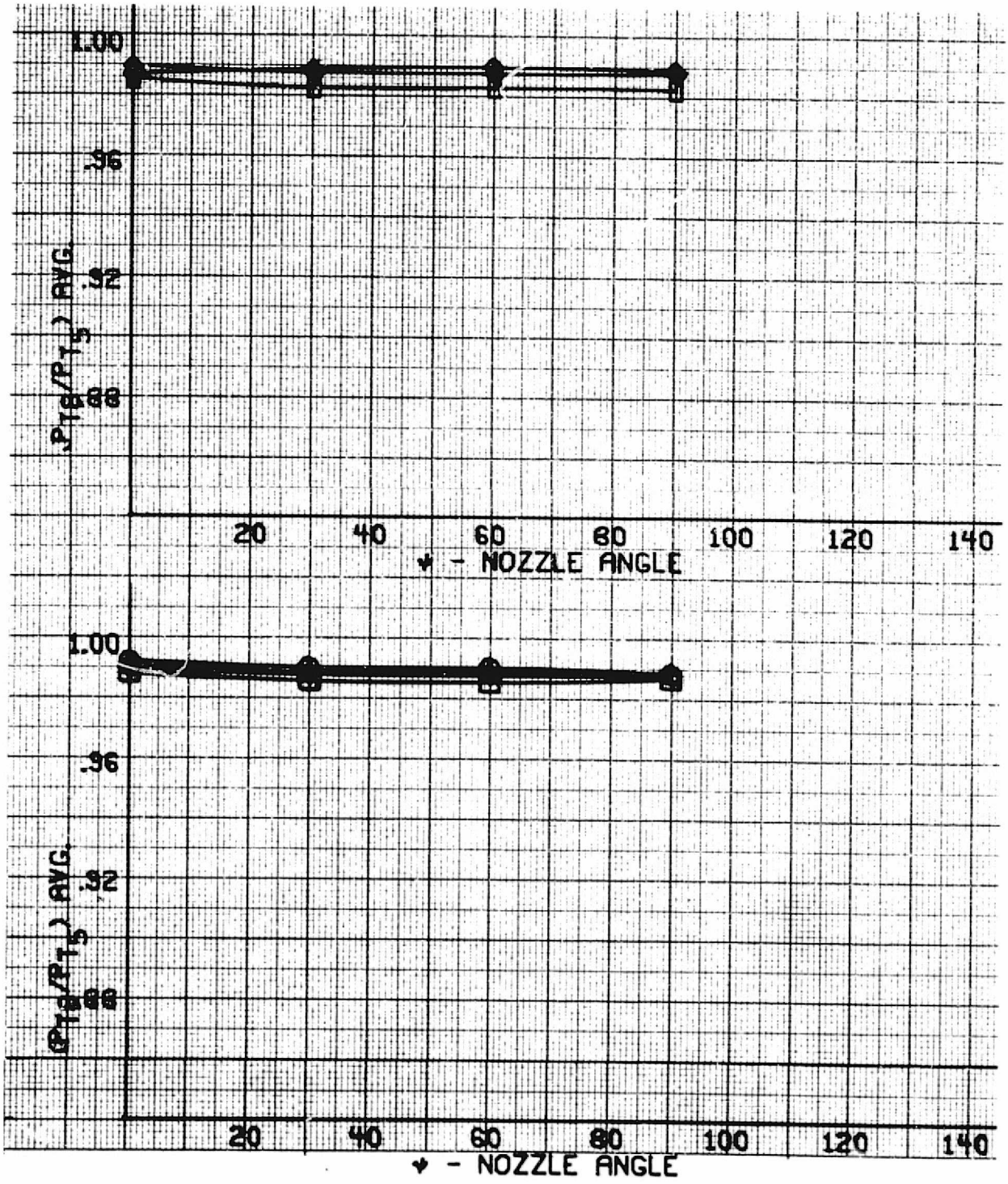

Figure 46. - Exit to inlet total pressure ratio at $P_{T_5}/P_A = 1.1$ versus nozzle angle.

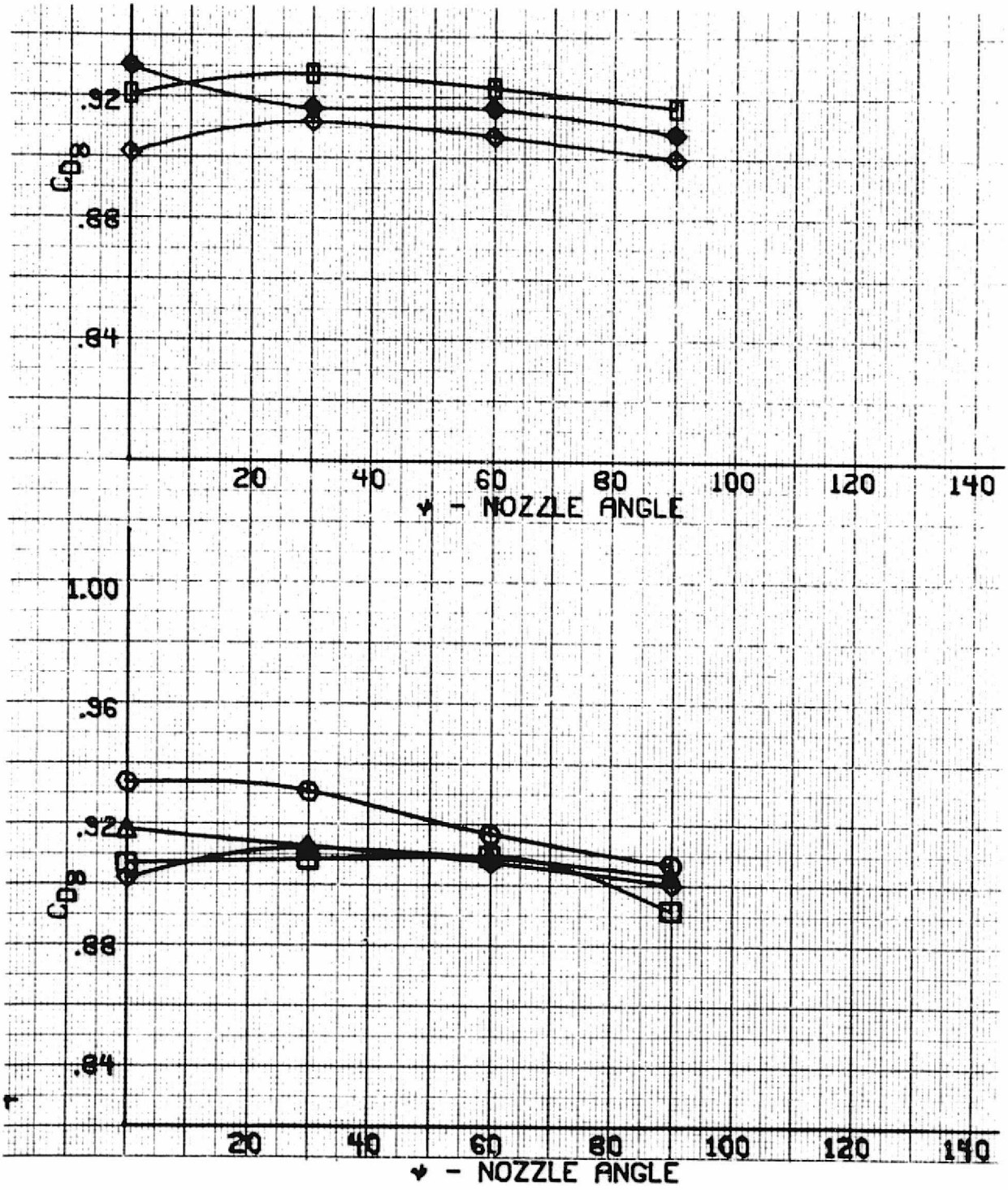

Figure 47. - Exit discharge coefficient at $P_{T_5}/P_A = 1.1$ versus nozzle angle.

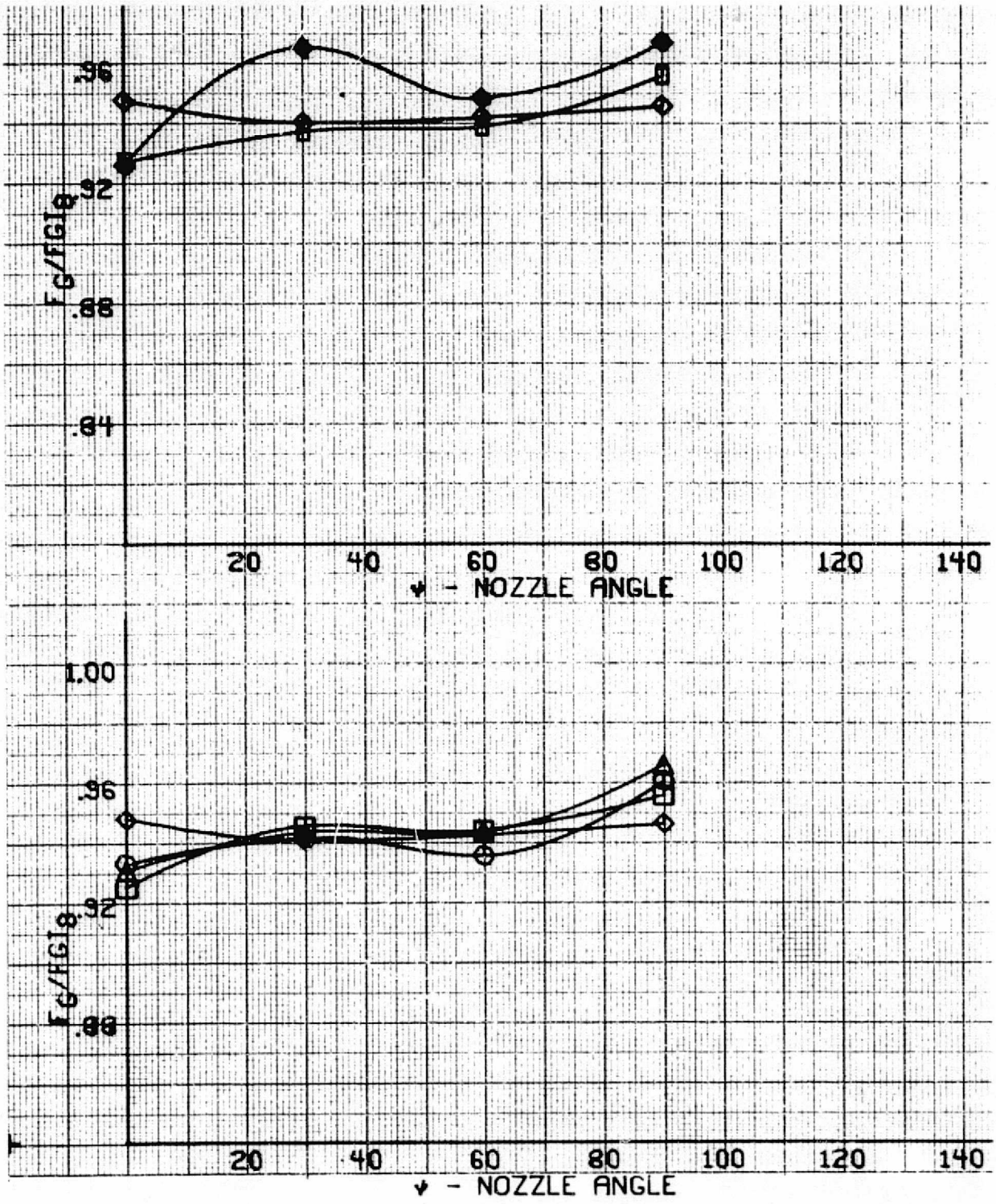

Figure 48. - Exit thrust coefficient at $P_{T_5}/P_A = 1.1$ versus nozzle angle.

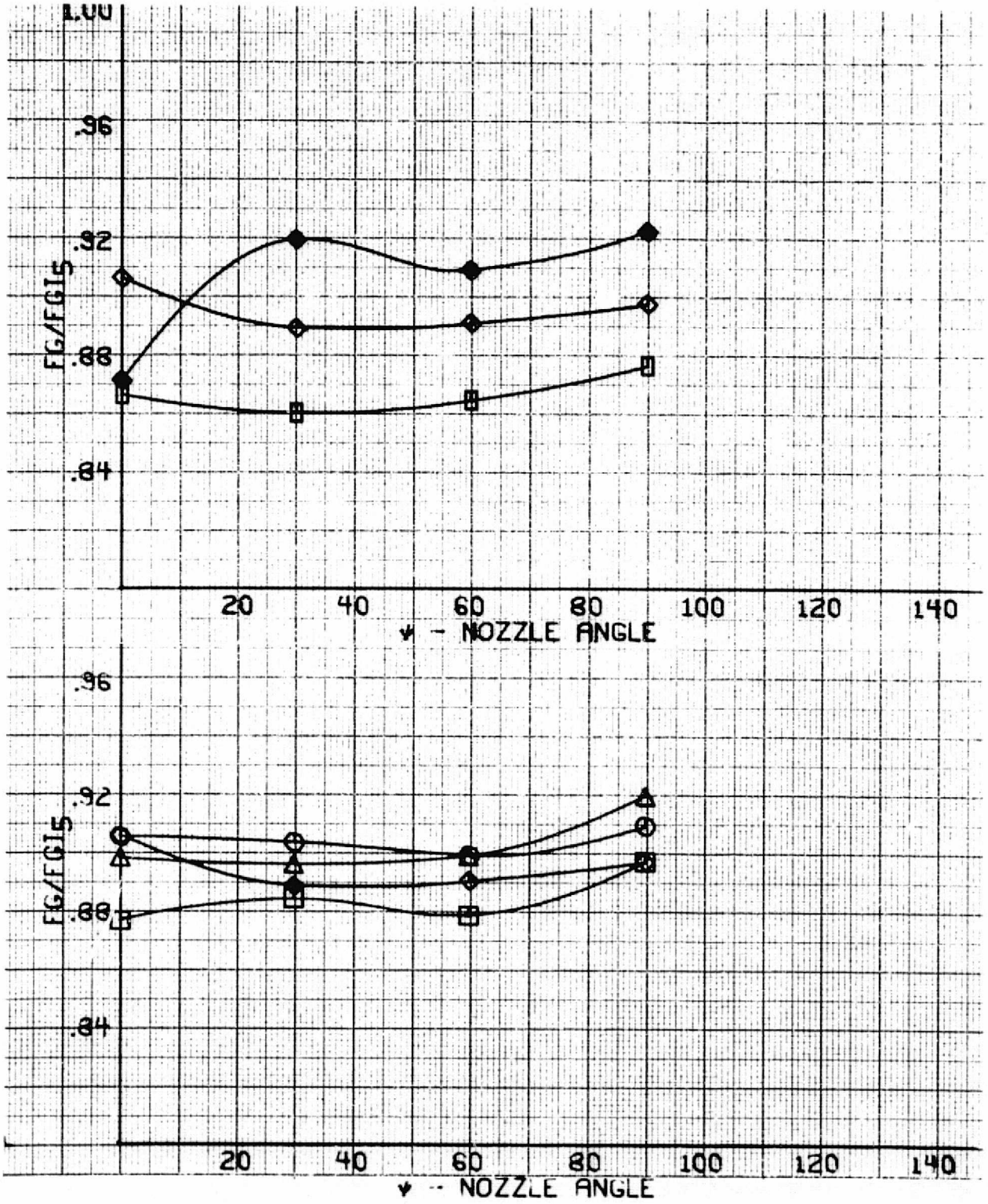

Figure 49. - Diffuser inlet thrust coefficient at $P_{T_5}/P_A = 1.1$ versus nozzle angle.

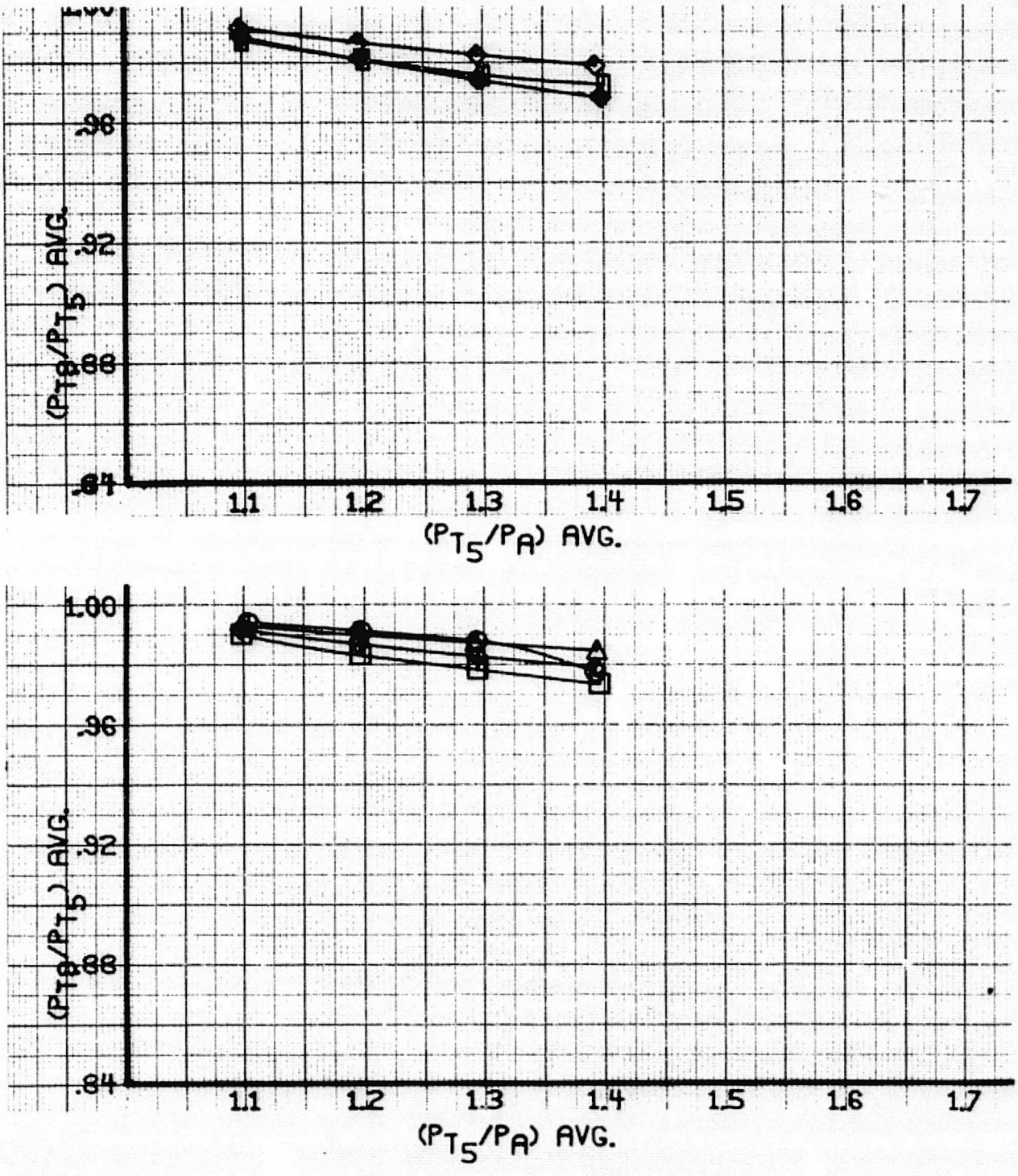

Figure 50. - Exit to inlet pressure ratio at $\psi = 0°$ versus diffuser inlet pressure ratio.

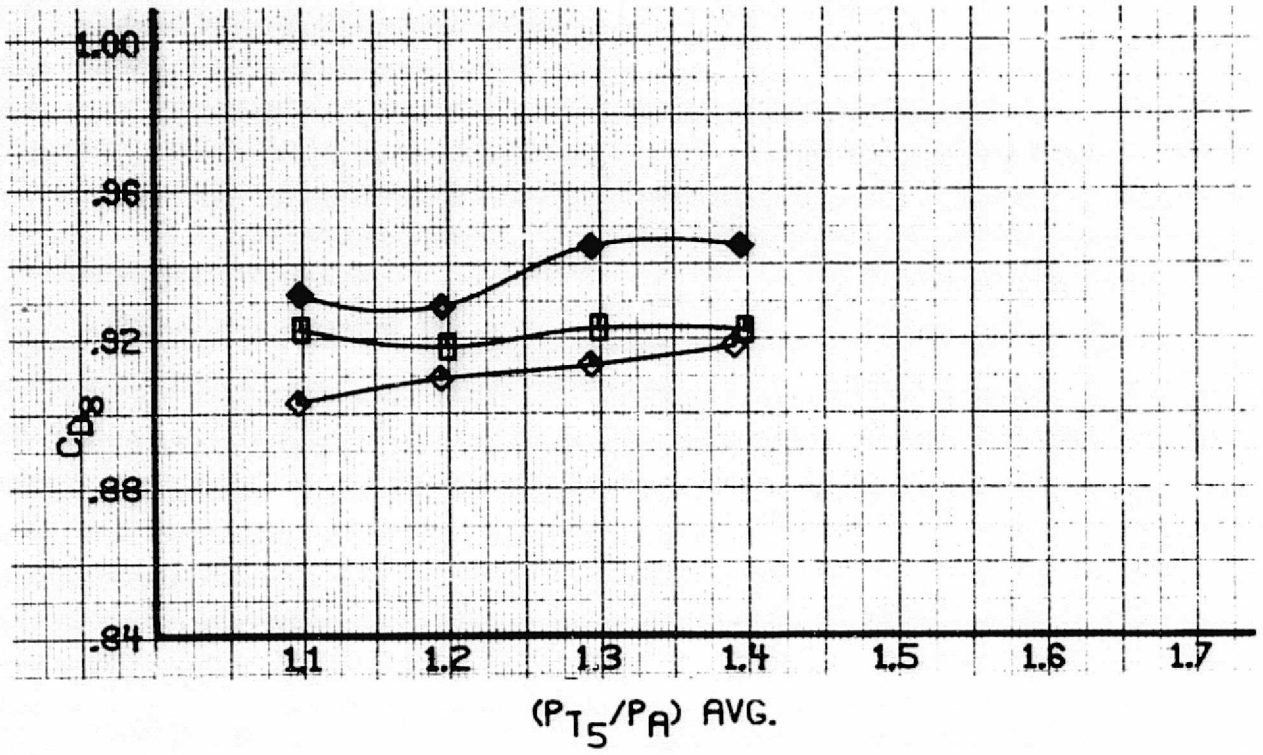

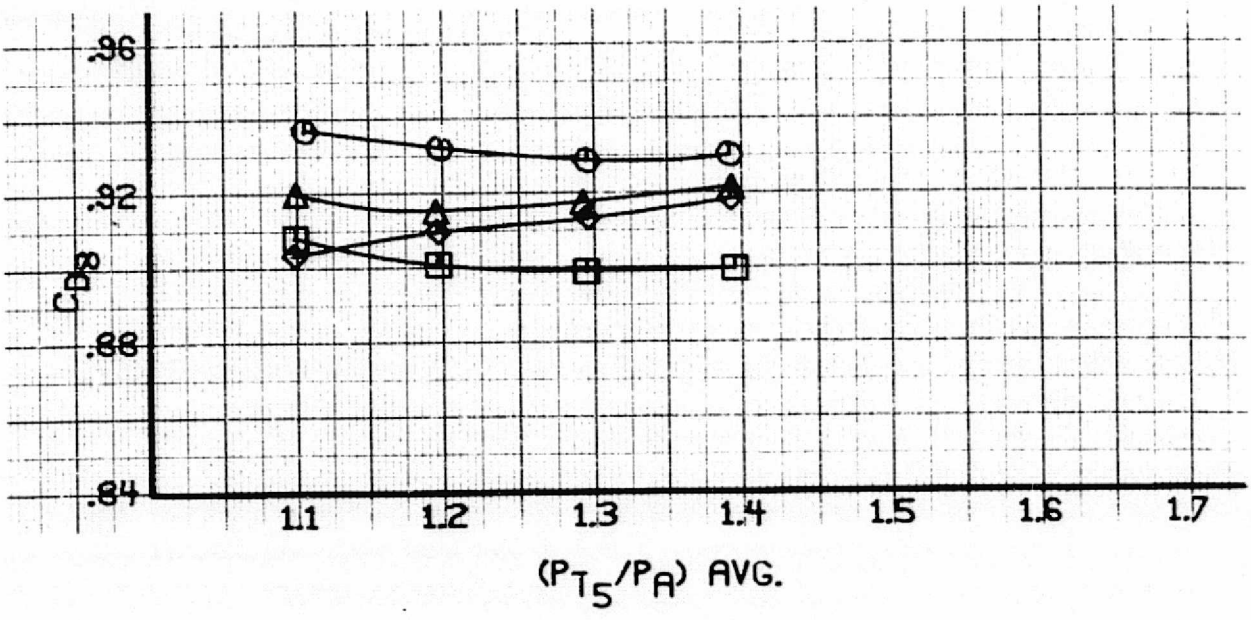

Figure 51. - Exit discharge coefficient at $\psi = 0°$ versus diffuser inlet pressure ratio.

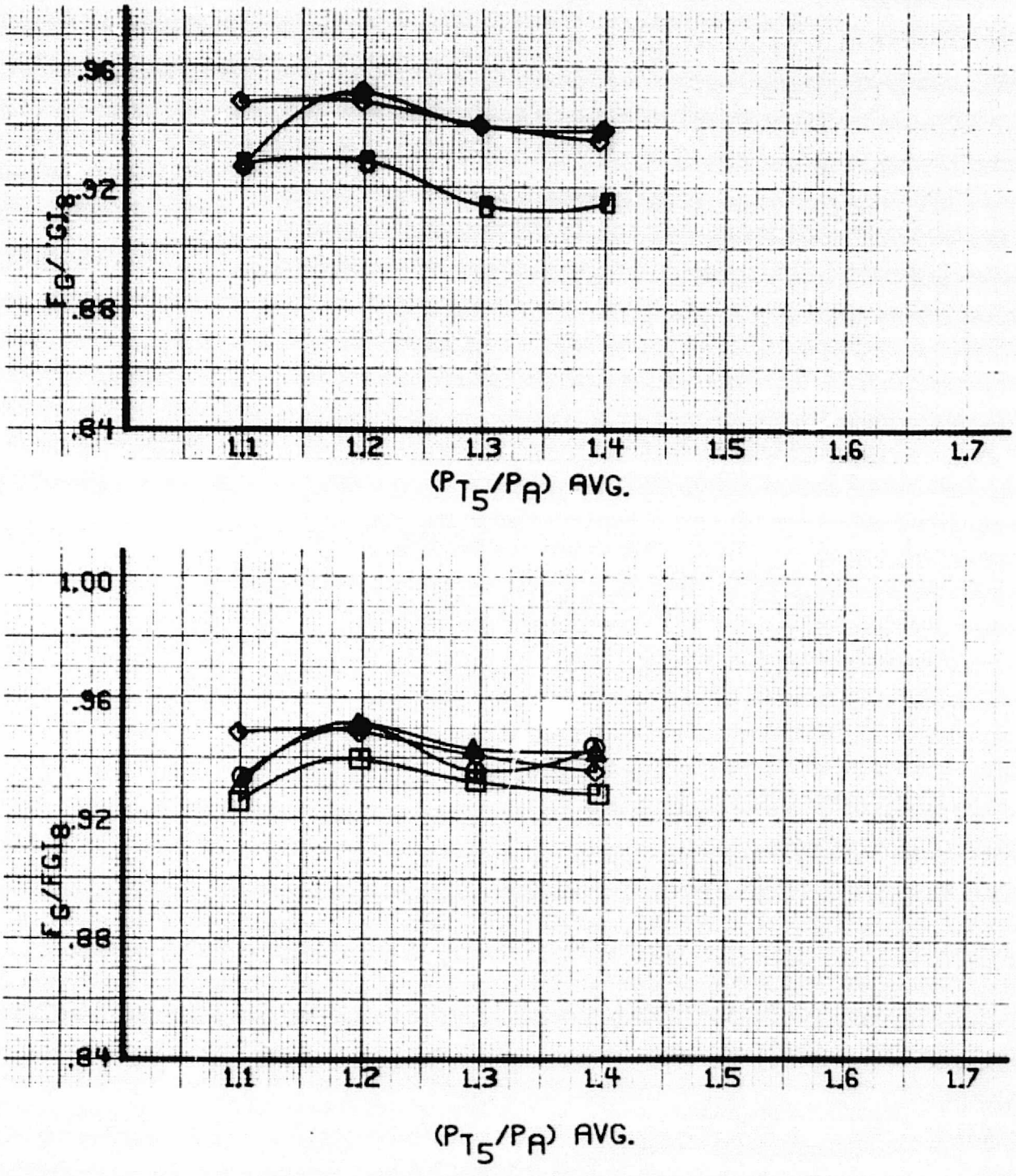

Figure 52. - Exit thrust coefficient at $\psi = 0°$ versus diffuser inlet pressure ratio.

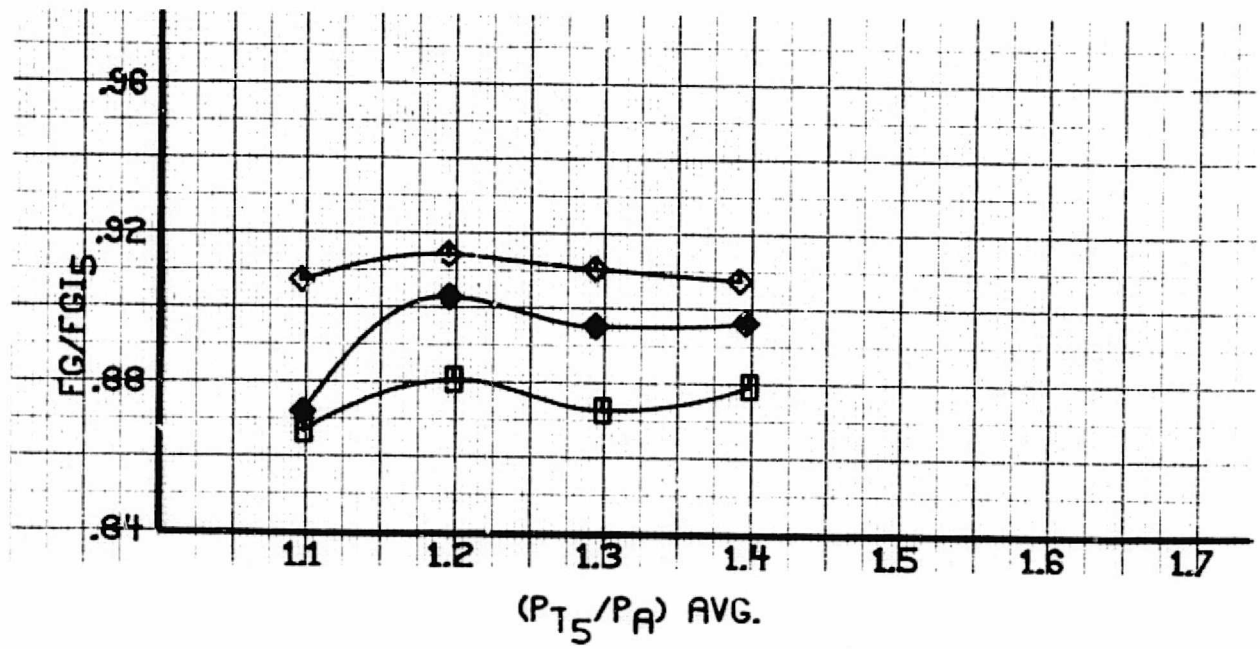

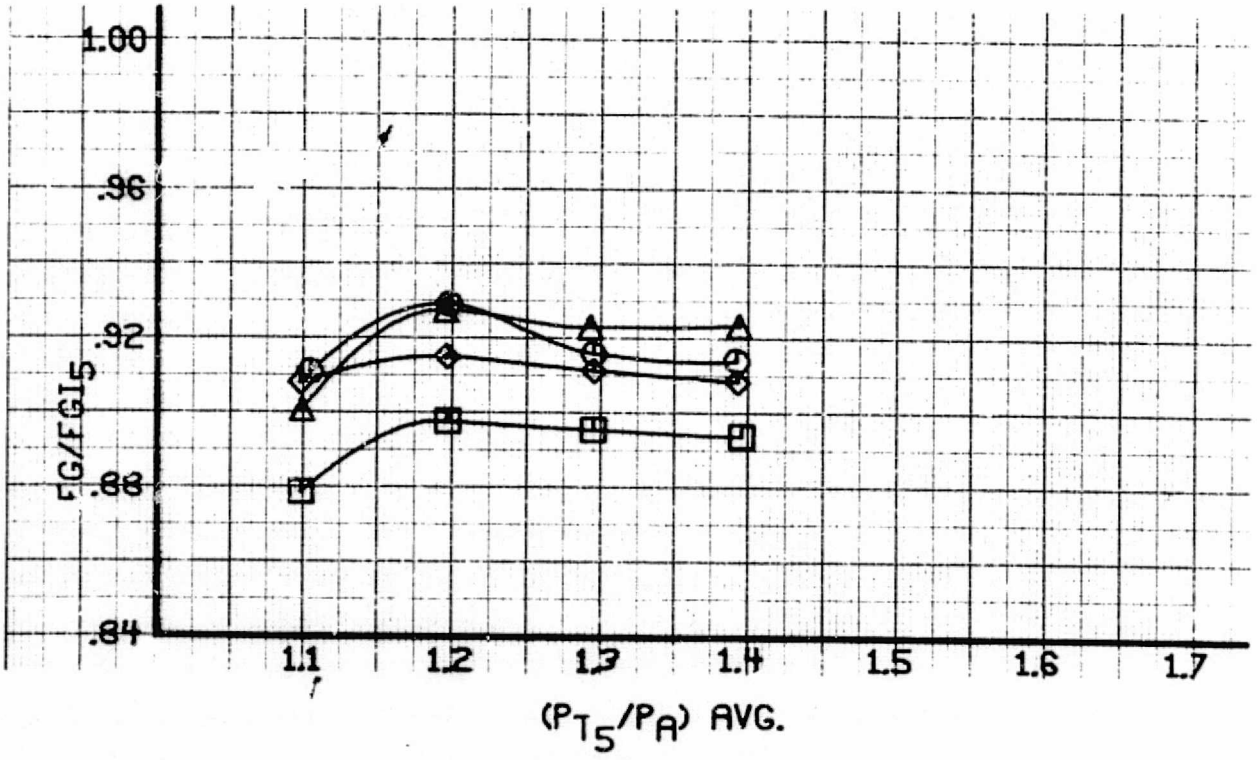

Figure 53. - Diffuser inlet thrust coefficient at $\psi = 0°$ versus diffuser inlet pressure ratio.

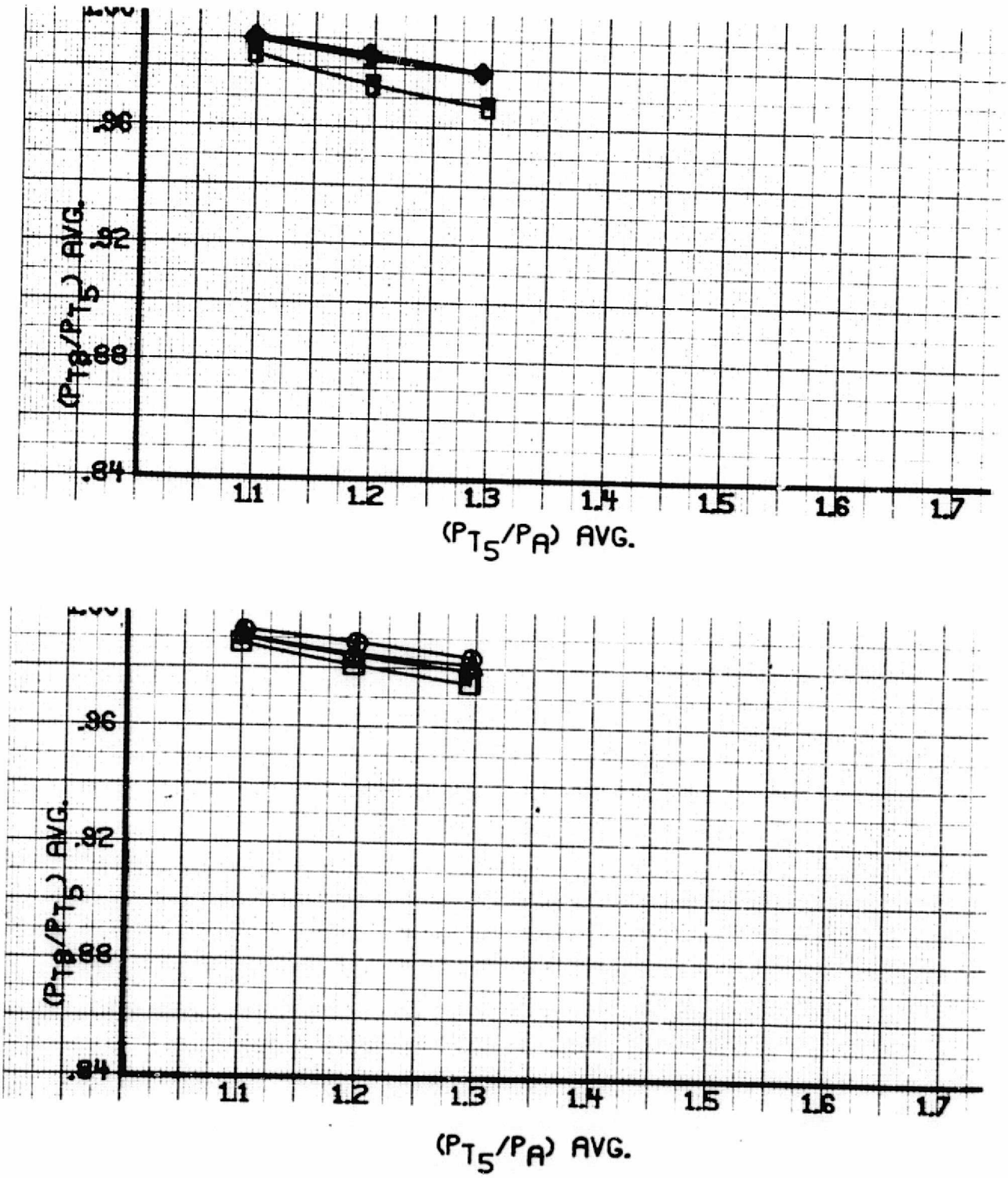

Figure 54. - Exit to inlet pressure ratio at ψ = 30° versus diffuser inlet pressure ratio.

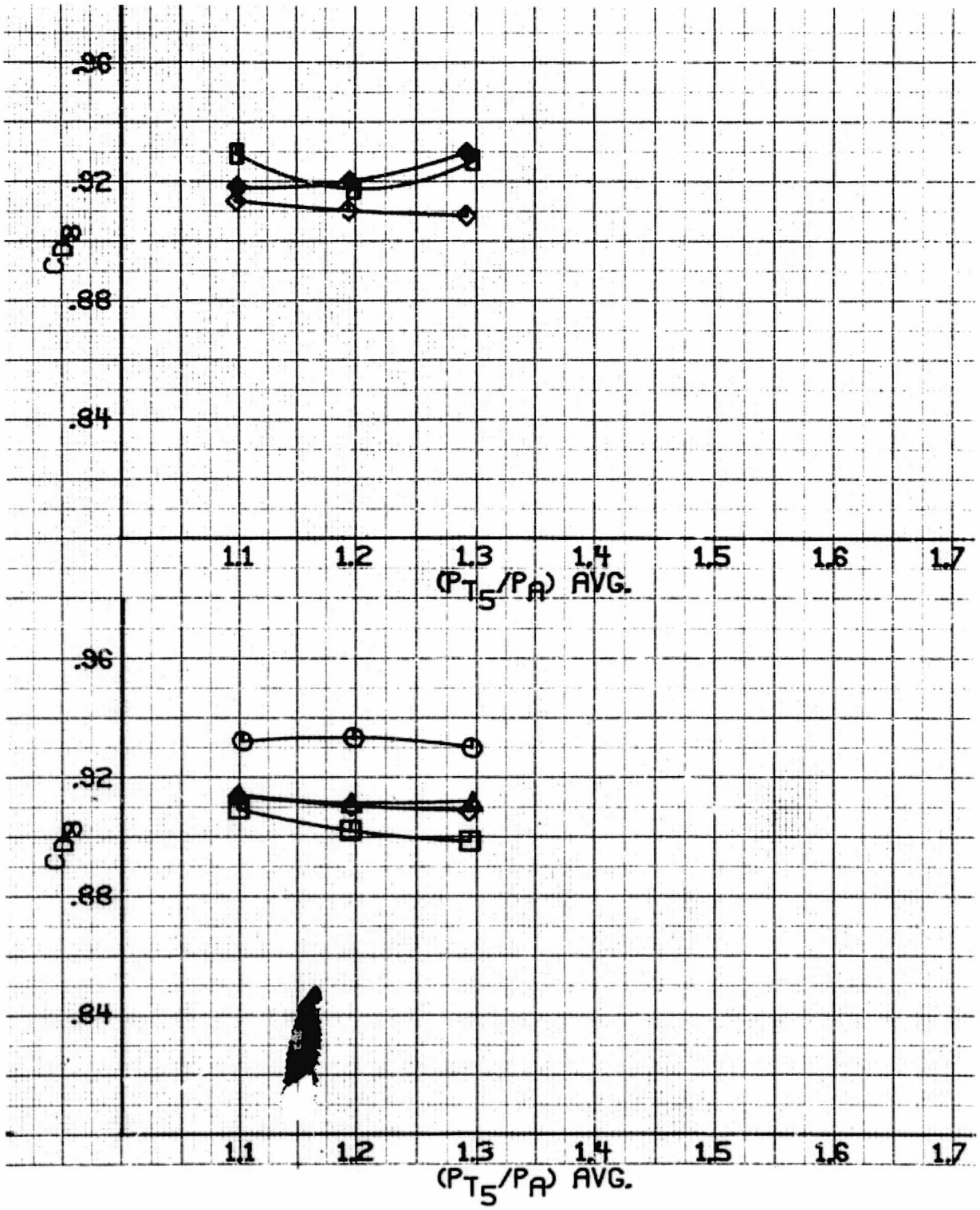

Figure 55. - Exit discharge coefficient at $\psi = 30°$ versus diffuser inlet pressure ratio.

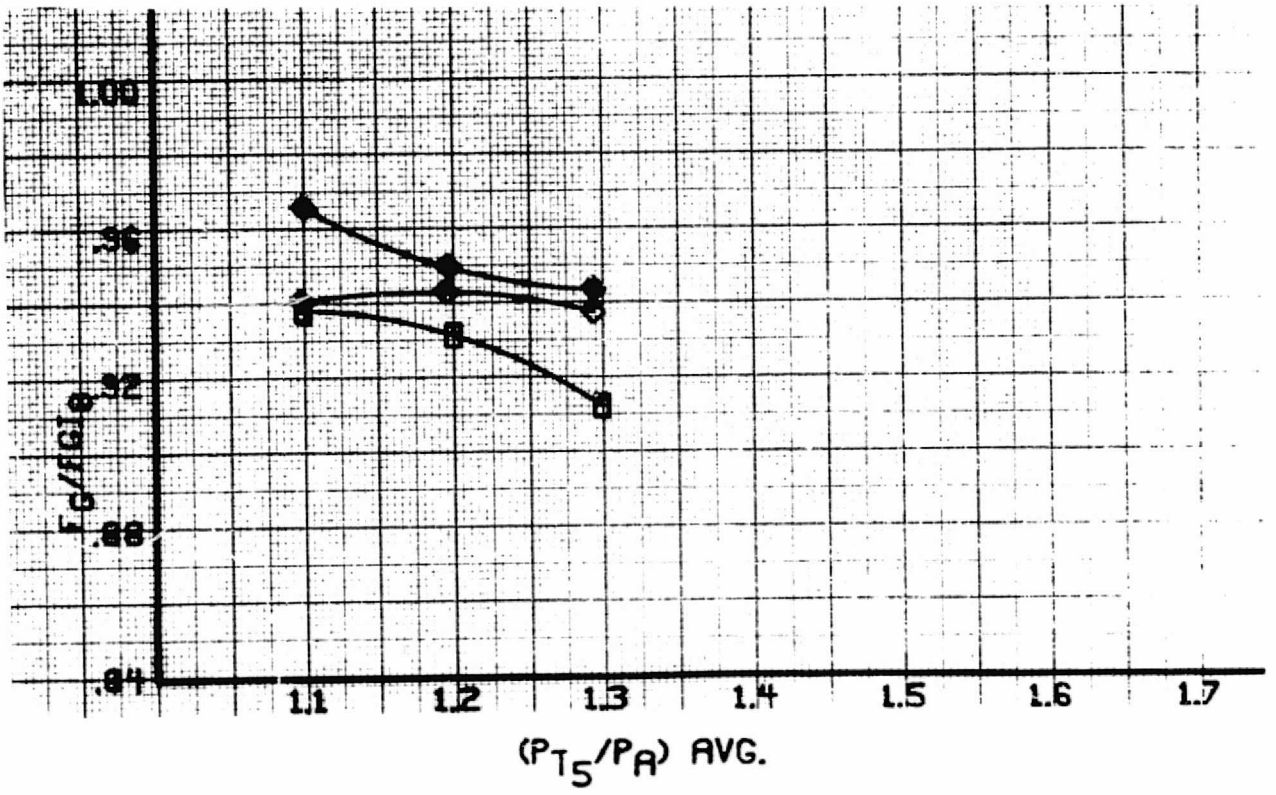

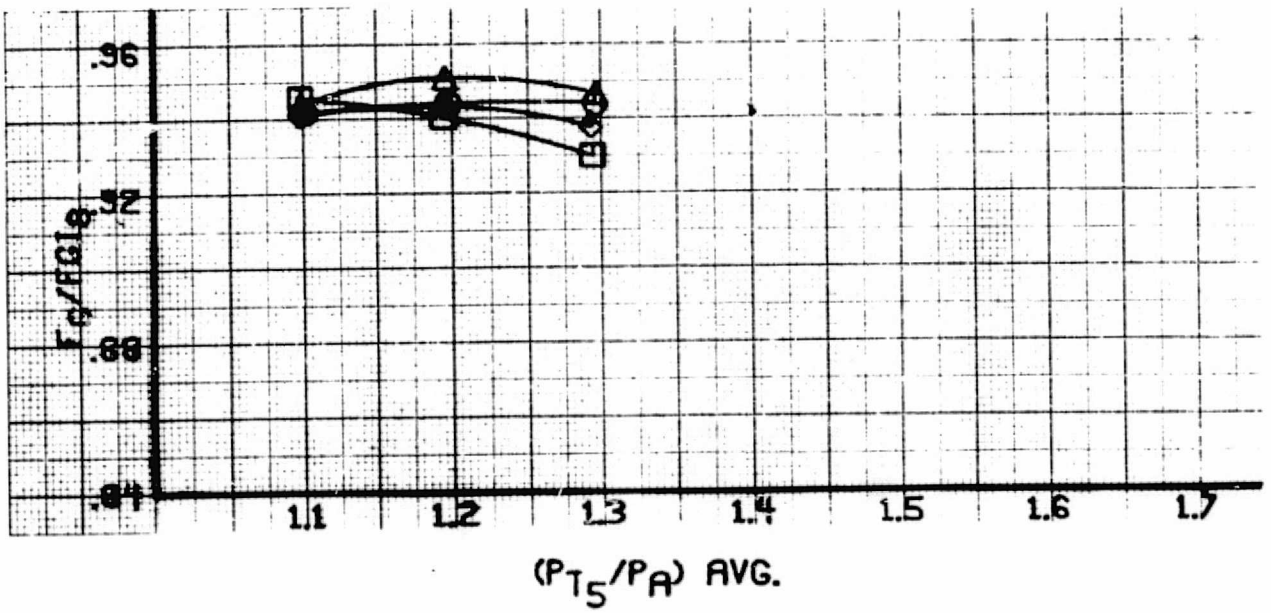

Figure 56. - Exit thrust coefficient at $\Psi = 30°$ versus diffuser inlet pressure ratio.

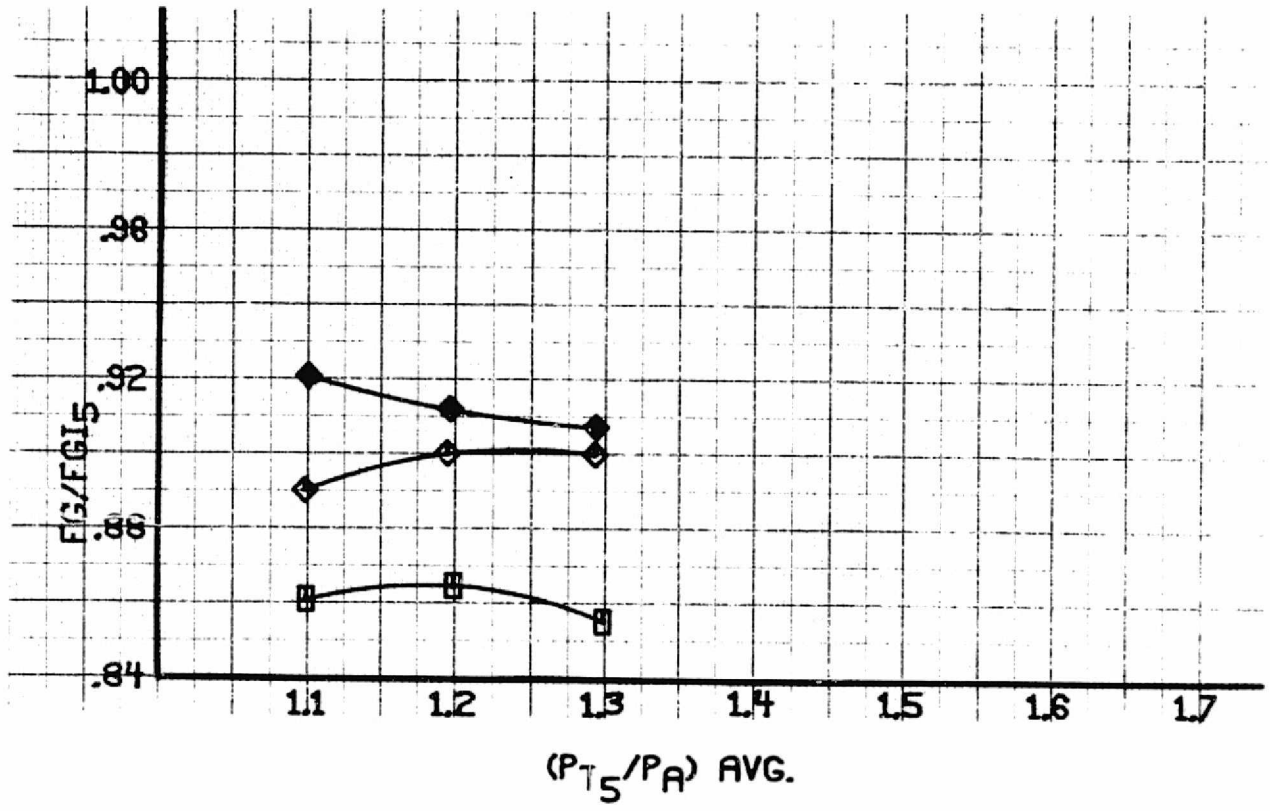

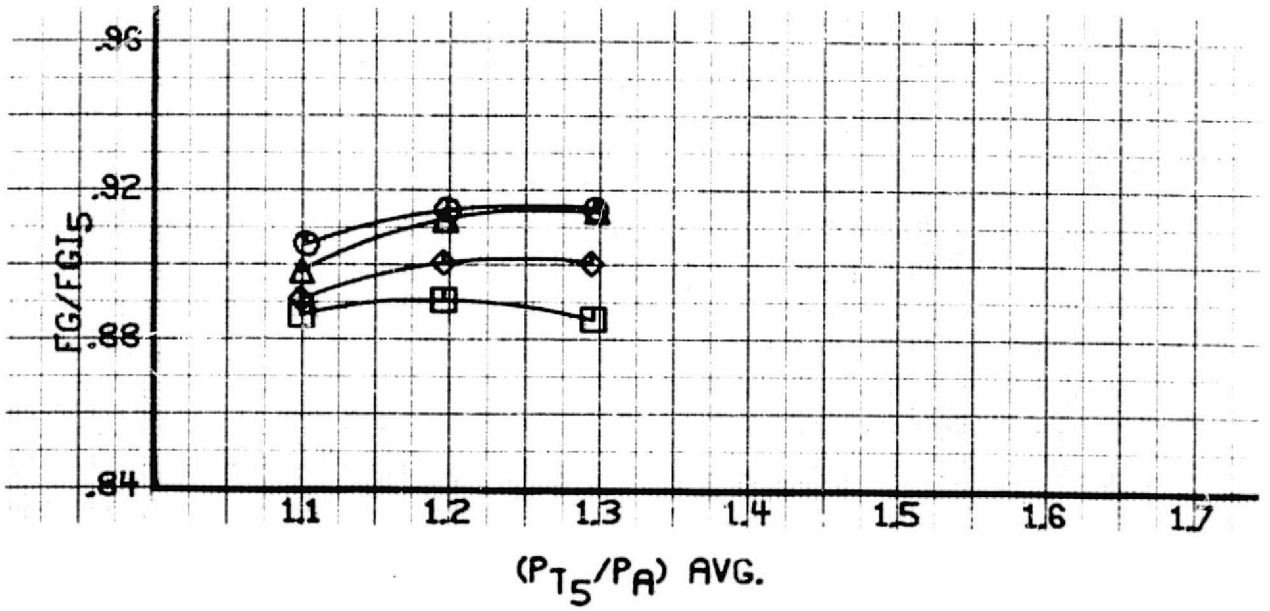

Figure 57. - Diffuser inlet thrust coefficient at $\psi = 30°$ versus diffuser inlet pressure ratio.

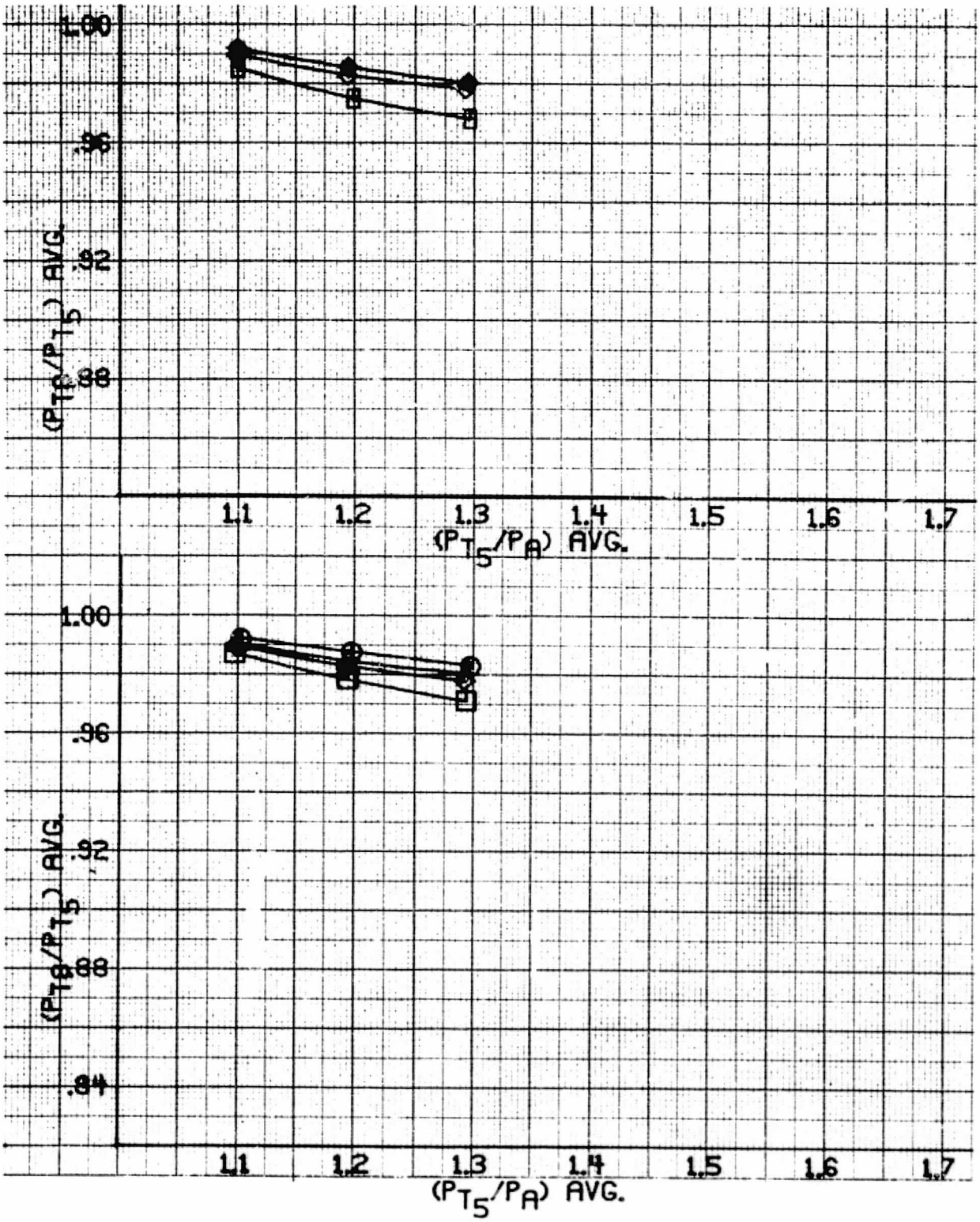

Figure 58. - Exit to inlet pressure ratio at $\psi = 60°$ versus diffuser inlet pressure ratio.

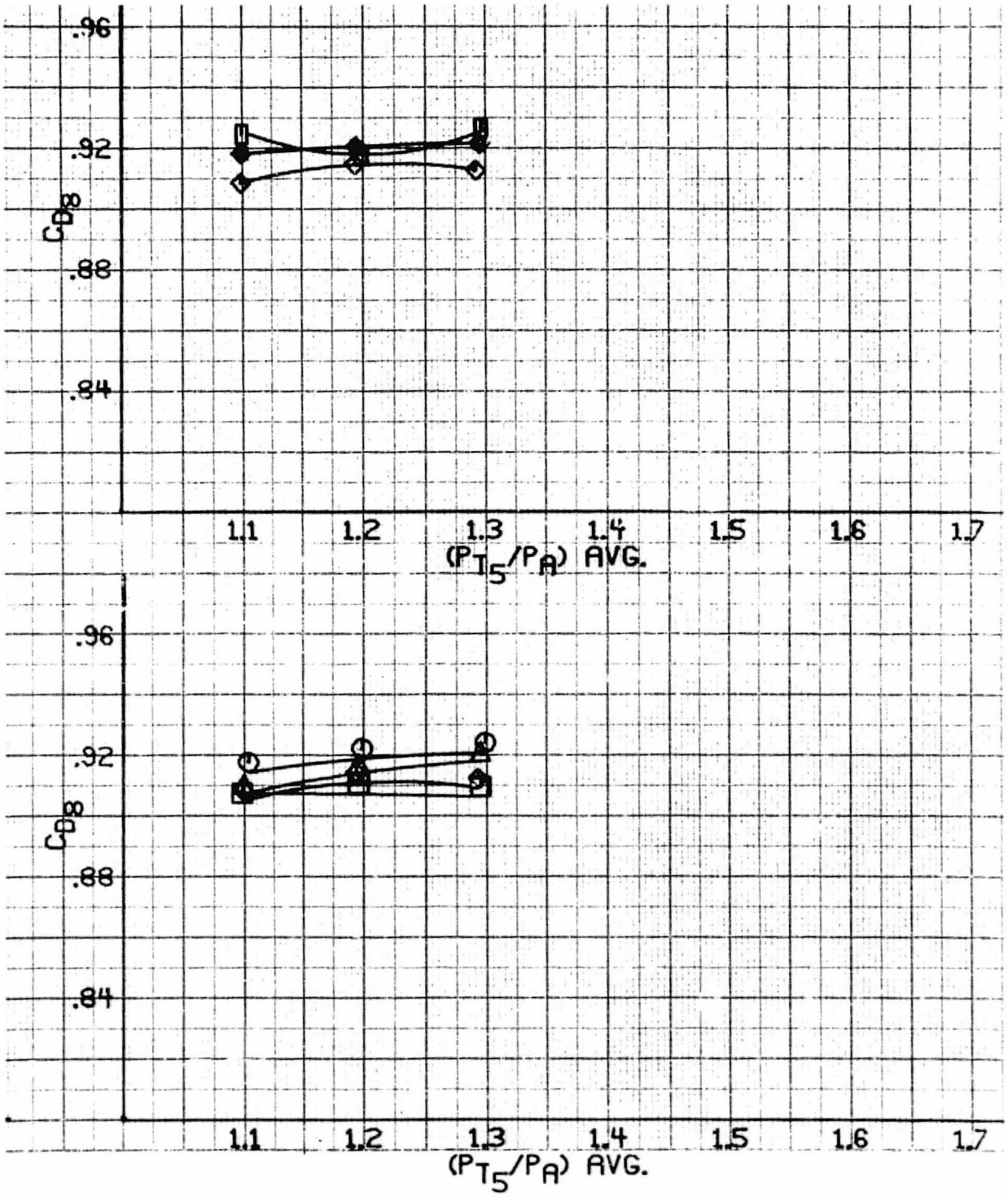

Figure 59. - Exit discharge coefficient at $\psi = 60°$ versus diffuser inlet pressure ratio.

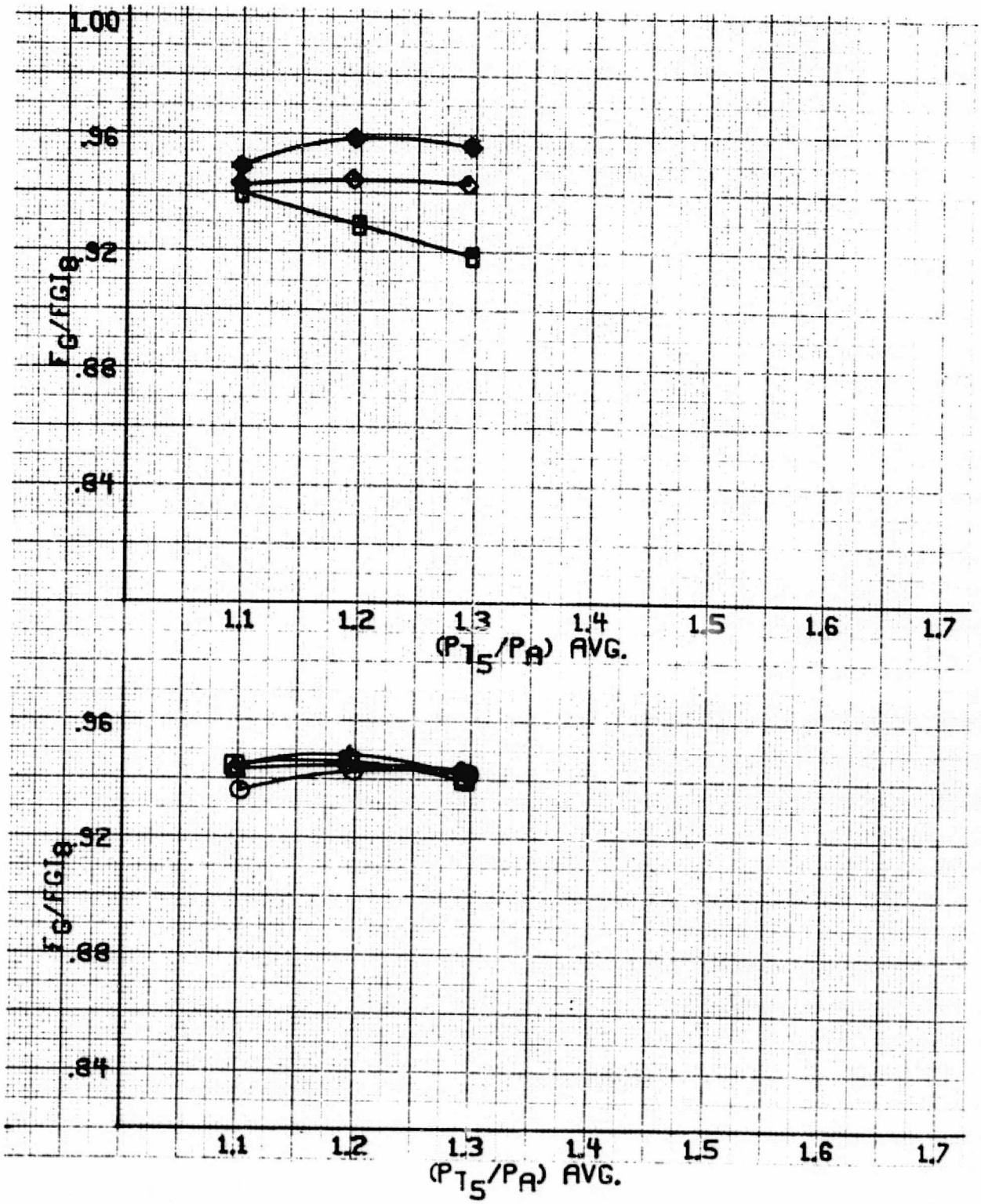

Figure 60. - Exit thrust coefficient at $\psi = 60°$ versus diffuser inlet pressure ratio.

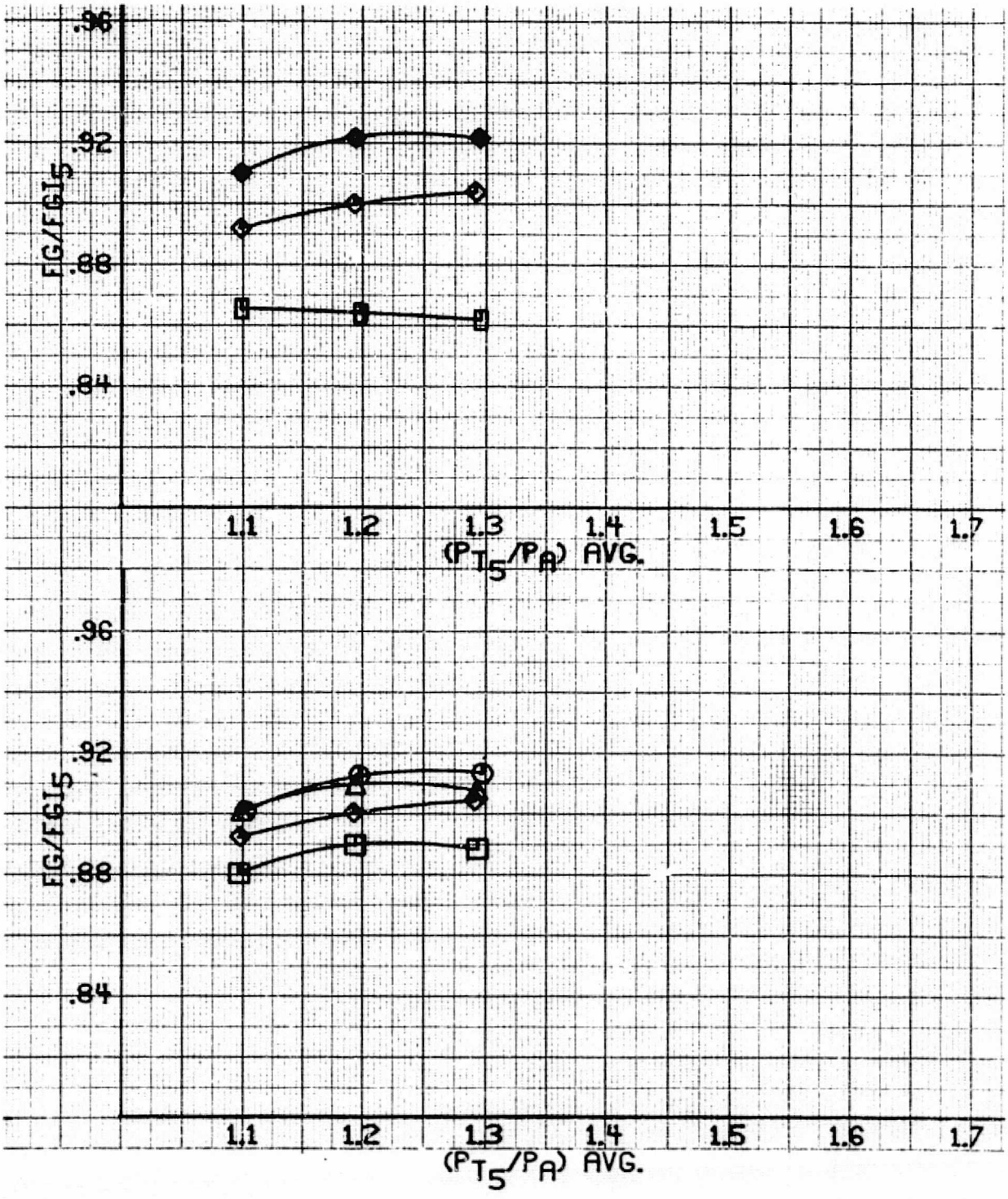

Figure 61. - Diffuser inlet thrust coefficient at $\psi = 60°$ versus diffuser inlet pressure ratio.

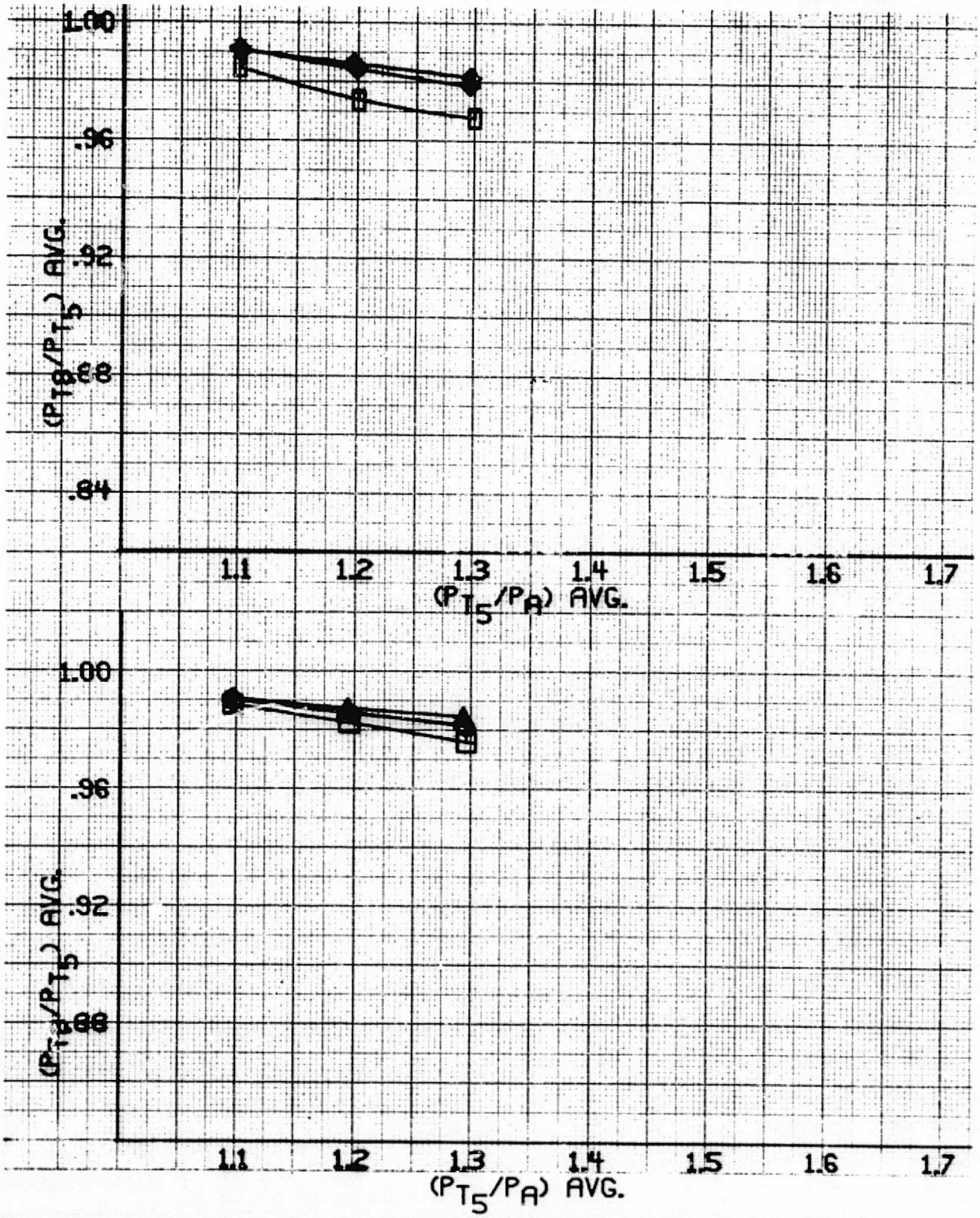

Figure 62. - Exit to inlet total pressure ratio at $\psi = 90°$ versus diffuser inlet pressure ratio.

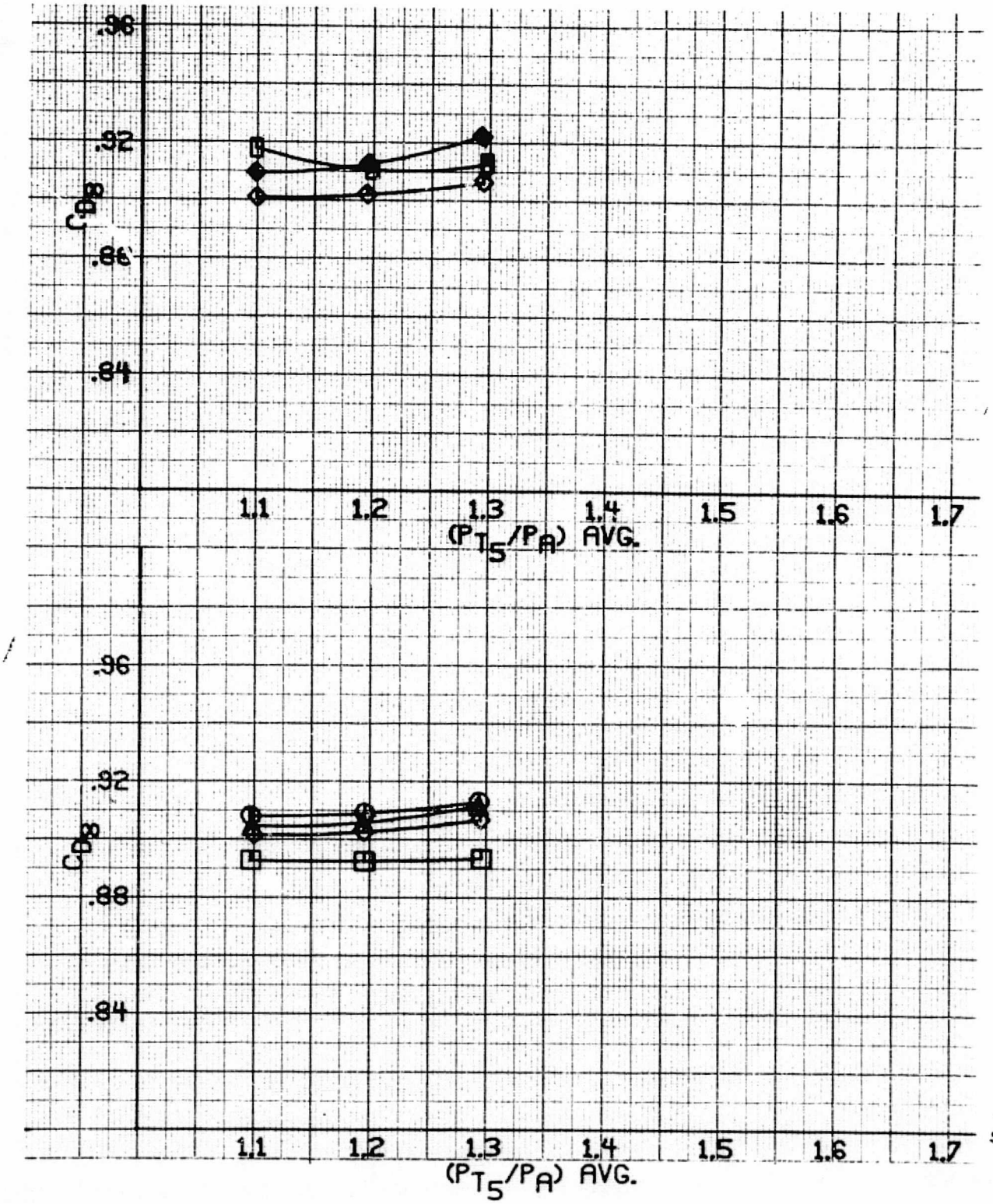

Figure 63. - Exit discharge coefficient at $\psi = 90°$ versus diffuser inlet pressure ratio.

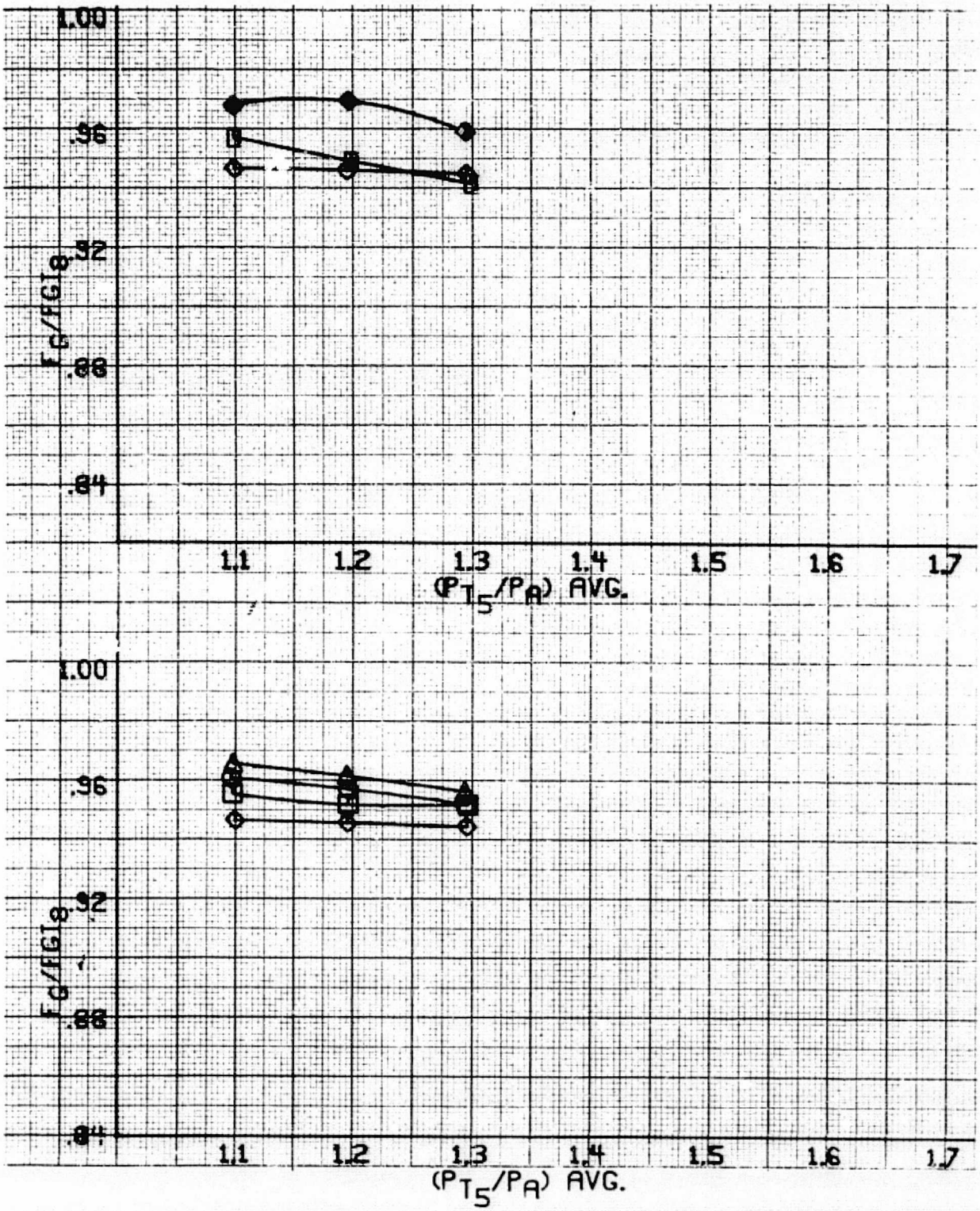

Figure 64. - Exit thrust coefficient at $\psi = 90°$ versus diffuser inlet pressure ratio.

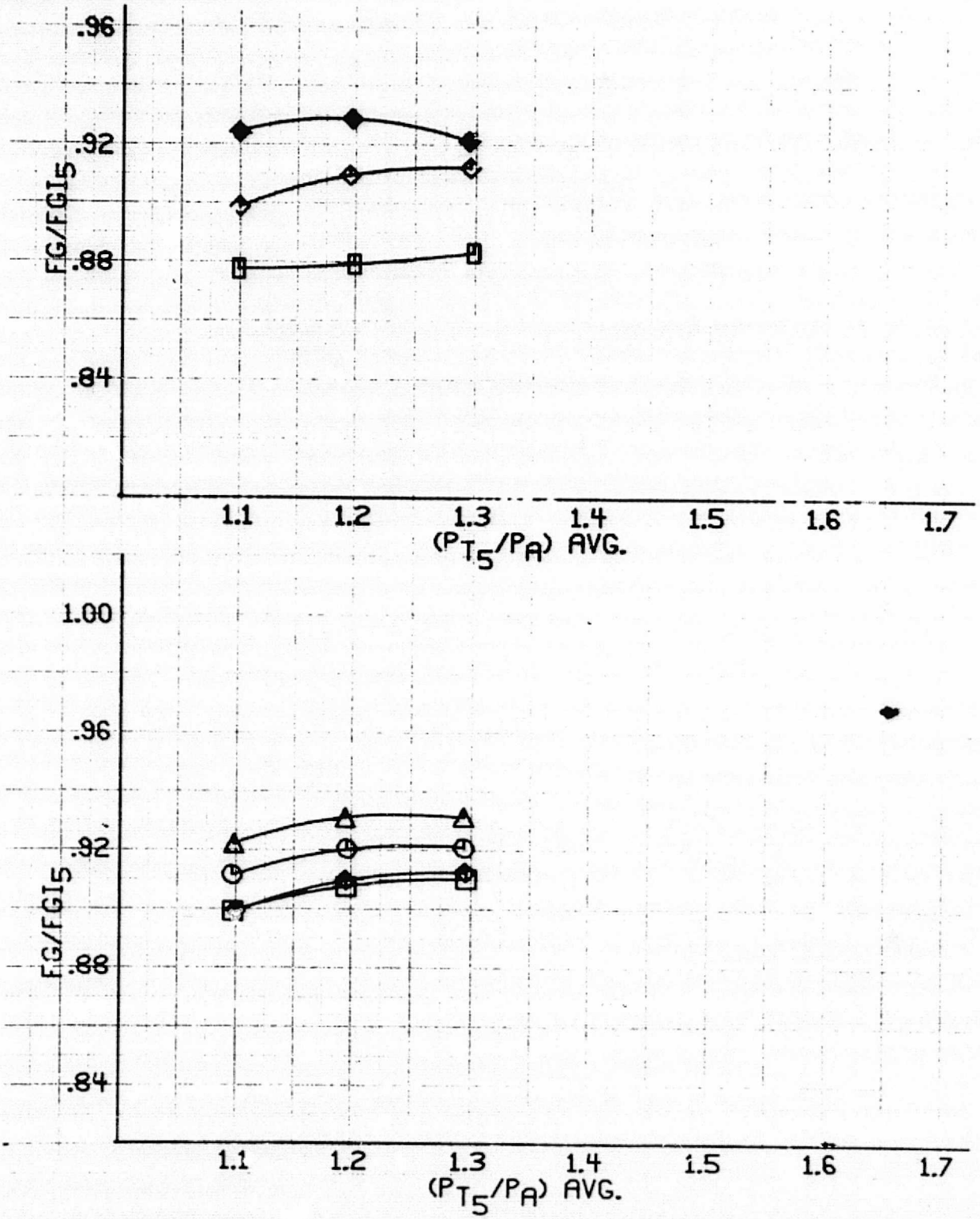

Figure 65. - Diffuser inlet thrust coefficient at $\psi = 90°$ versus diffuser inlet pressure ratio.

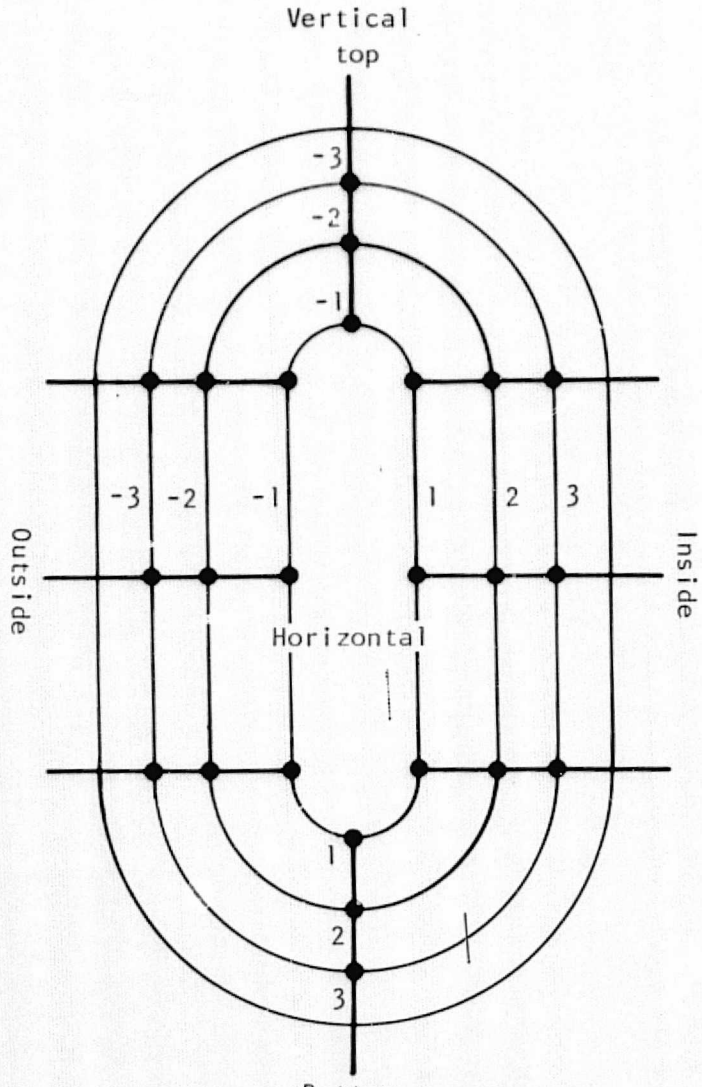

Single swivel

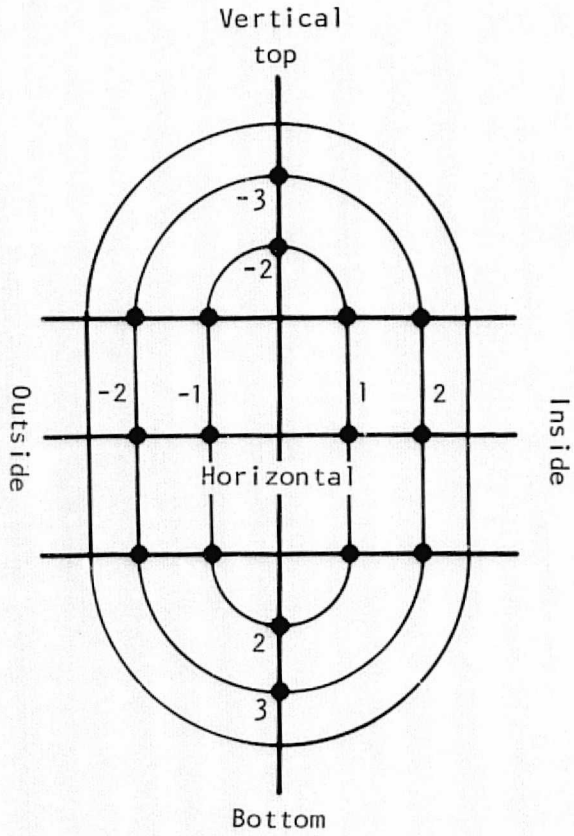

Twin swivel

(View aft looking forward)

Figure 66. - Exit total pressure rake schematics.

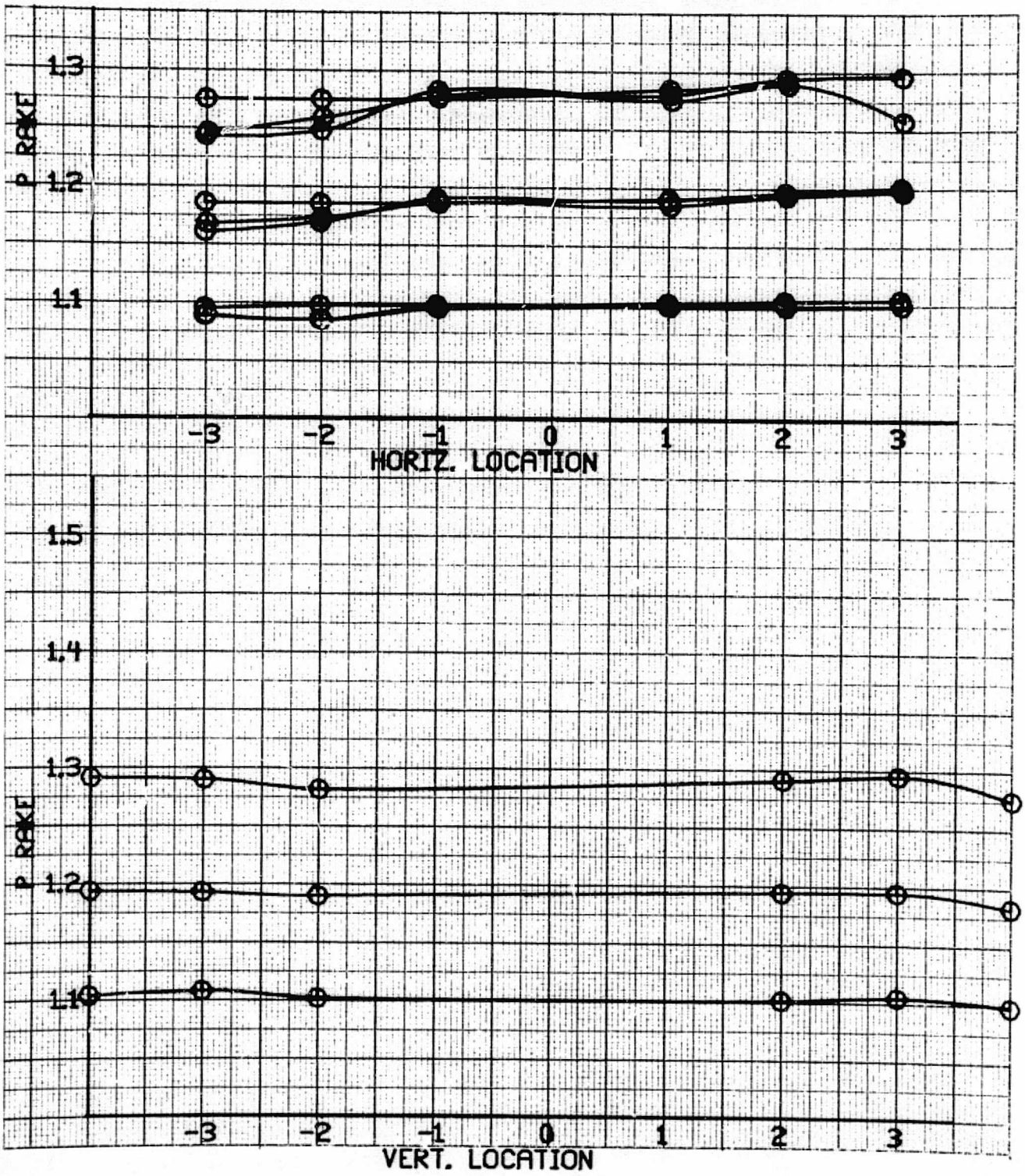

Figure 67. - Nozzle A exit total pressure ratio versus probe location for 0° nozzle angle.

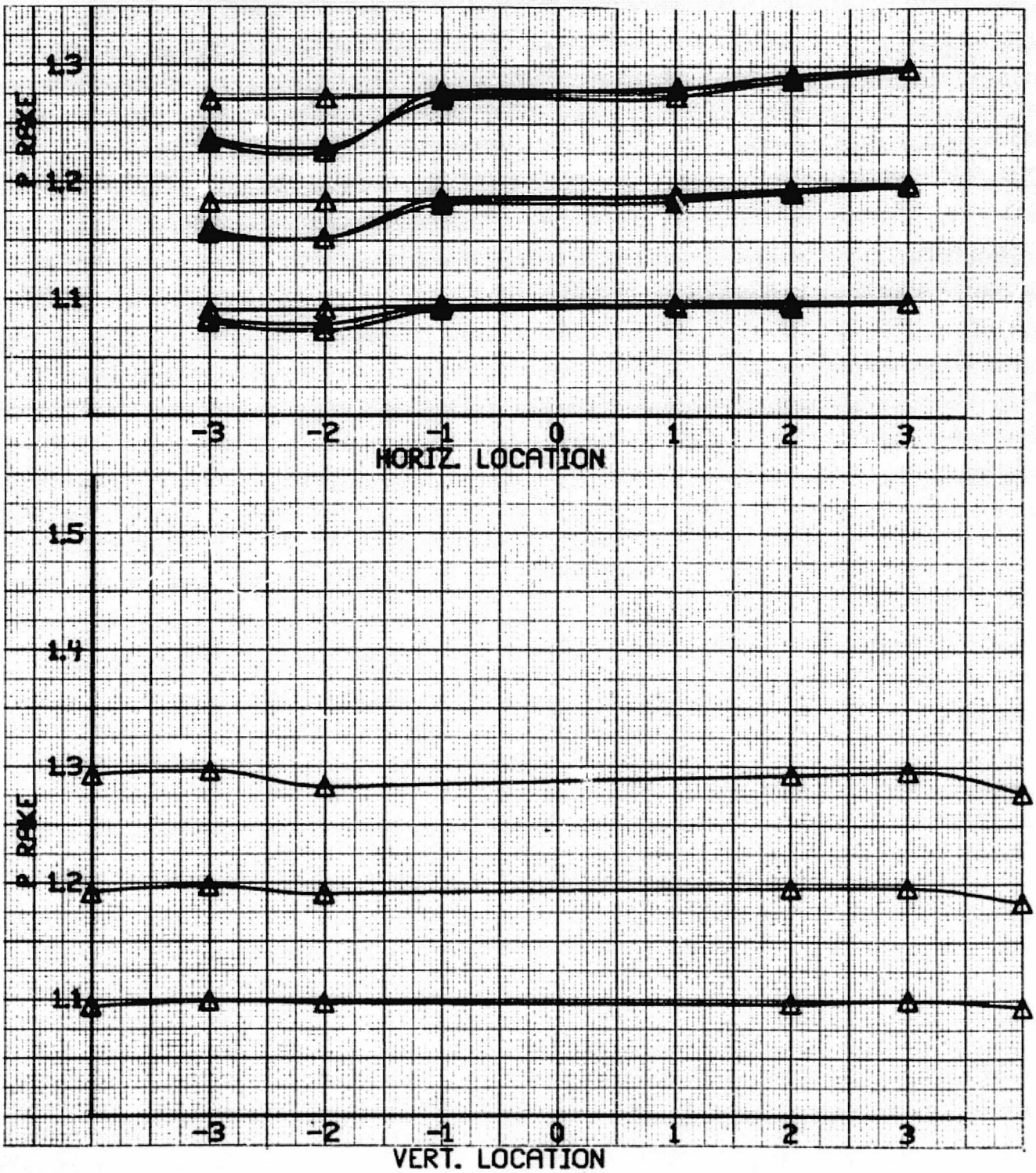

Figure 68. - Nozzle B exit total pressure ratio versus probe location for 0° nozzle angle.

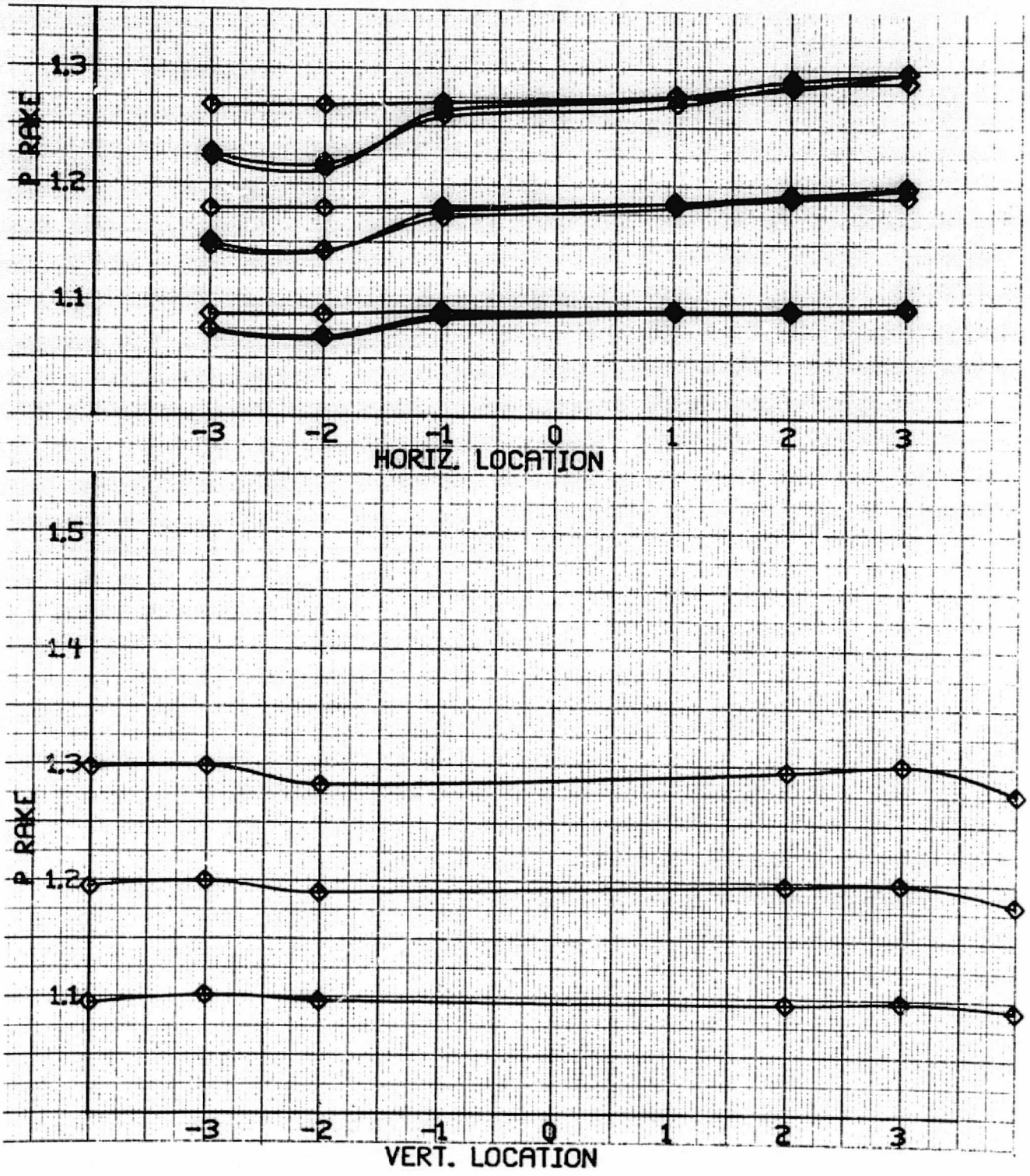

Figure 69. - Nozzle C exit total pressure ratio versus probe location for 0° nozzle angle.

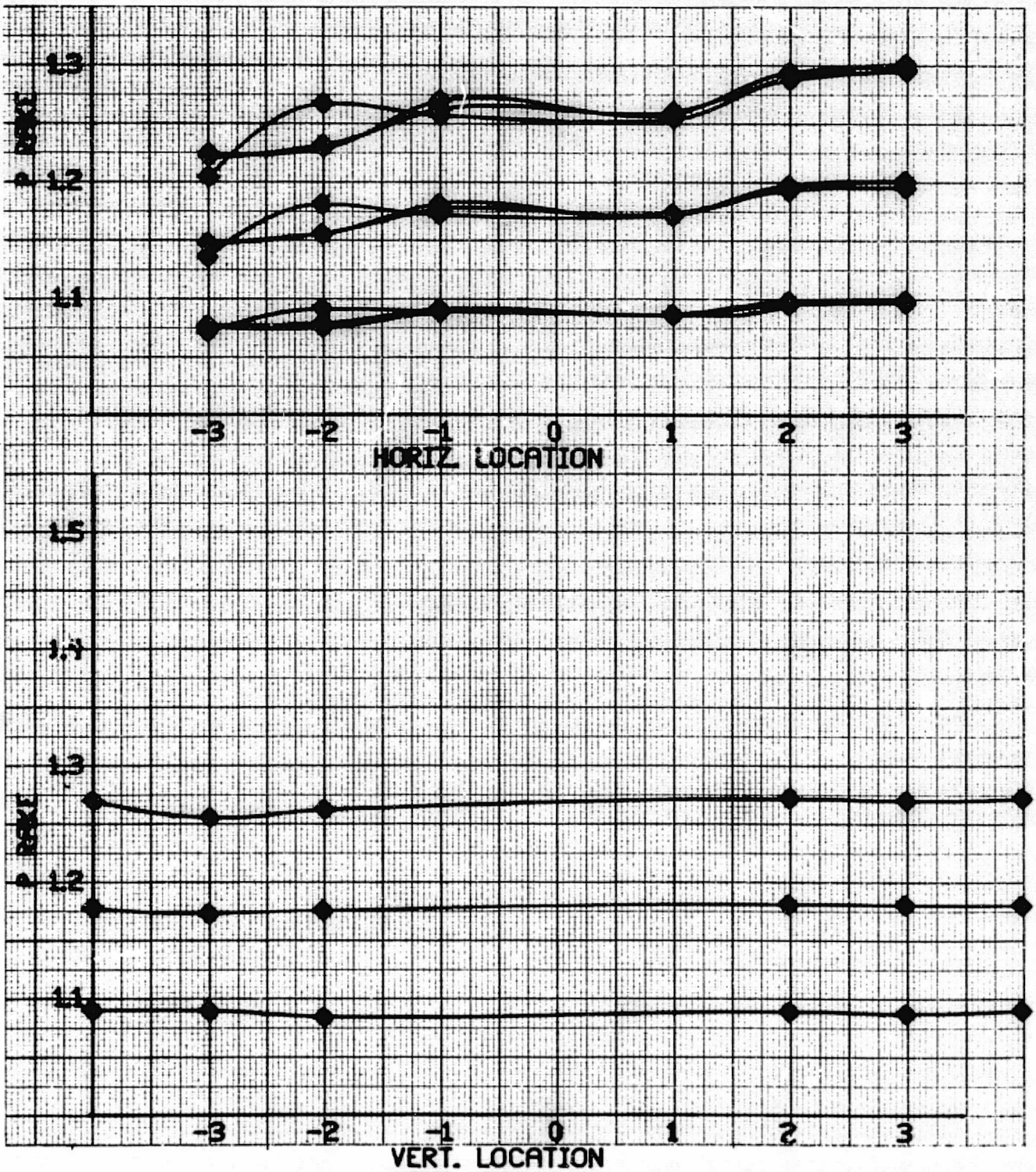

Figure 70. - Nozzle C (with vanes) exit total pressure ratio versus probe location for 0° nozzle angle.

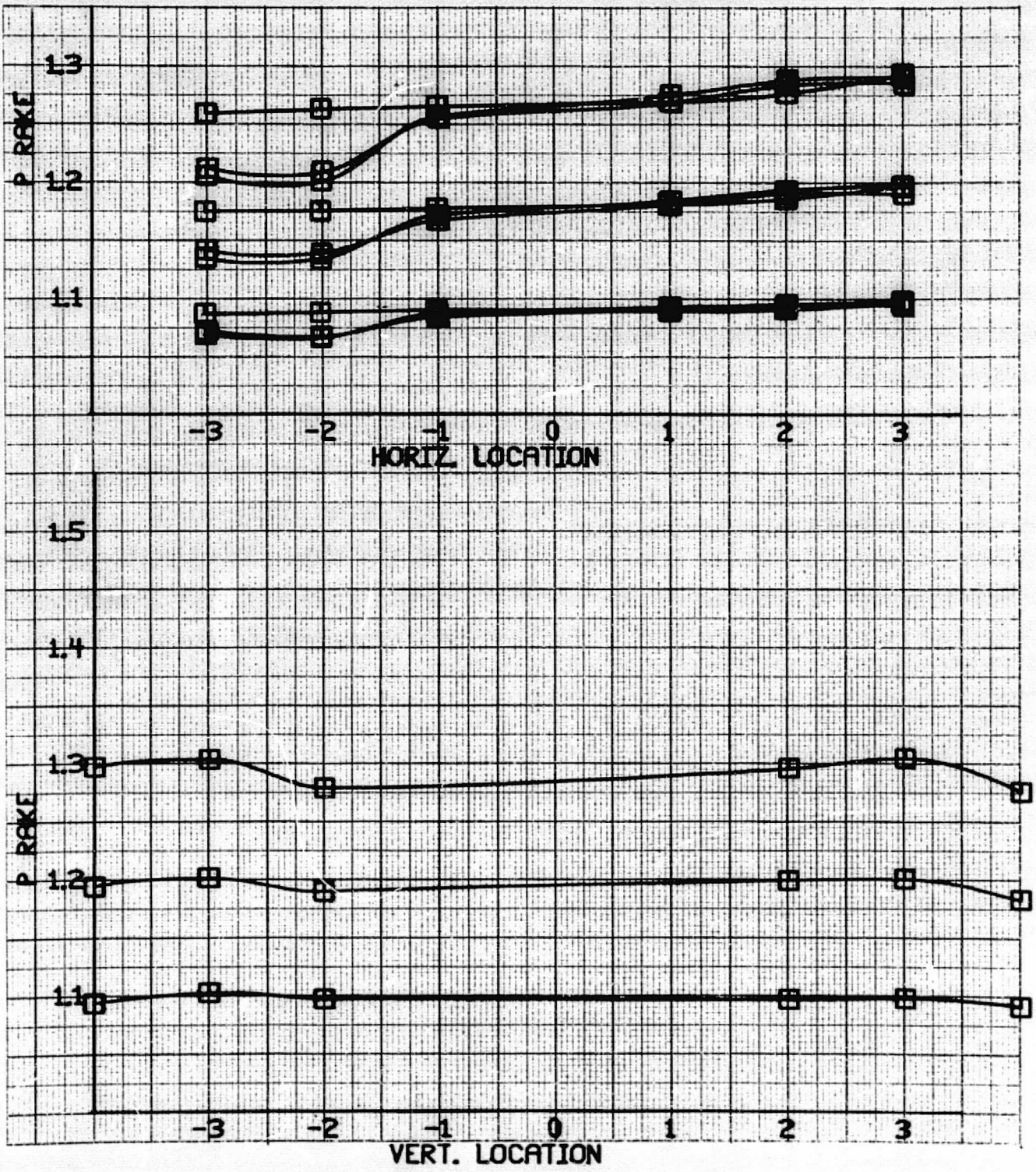

Figure 71. - Nozzle D exit total pressure ratio probe location for 0° nozzle angle.

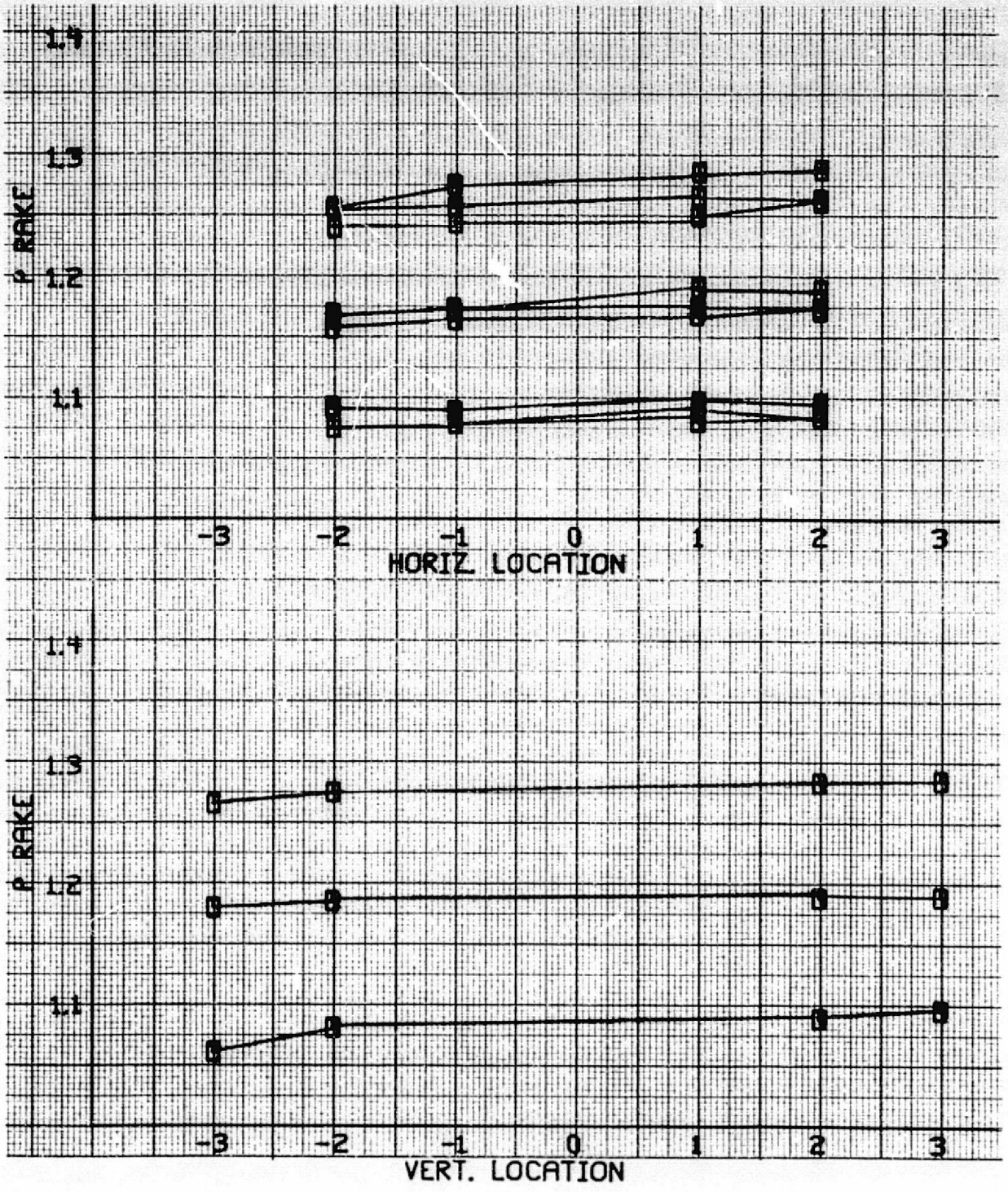

Figure 72. - Twin nozzle exit total pressure ratio versus probe location for 0° nozzle angle.

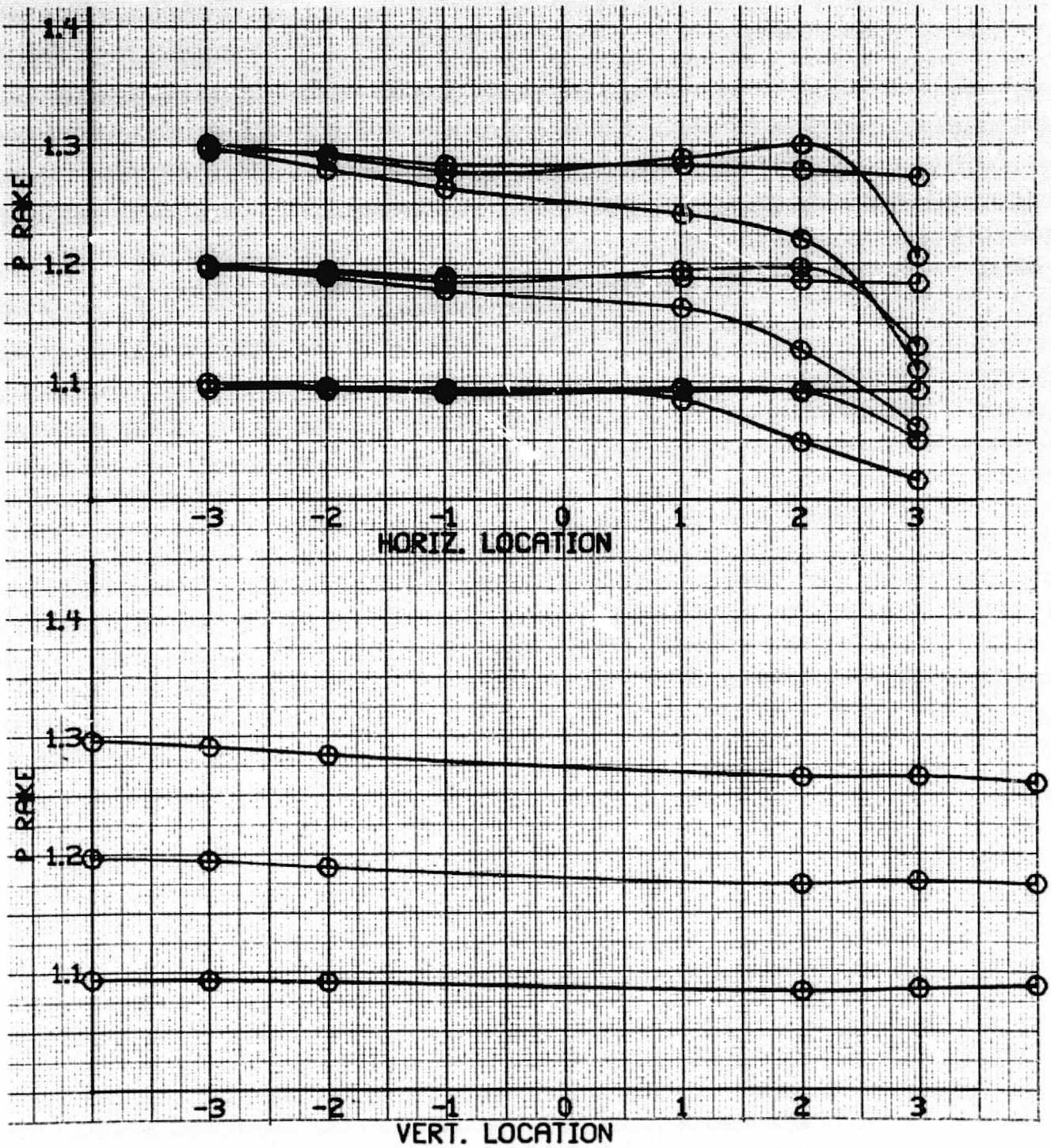

Figure 73. - Nozzle B exit total pressure ratio versus probe location for 90° nozzle angle.

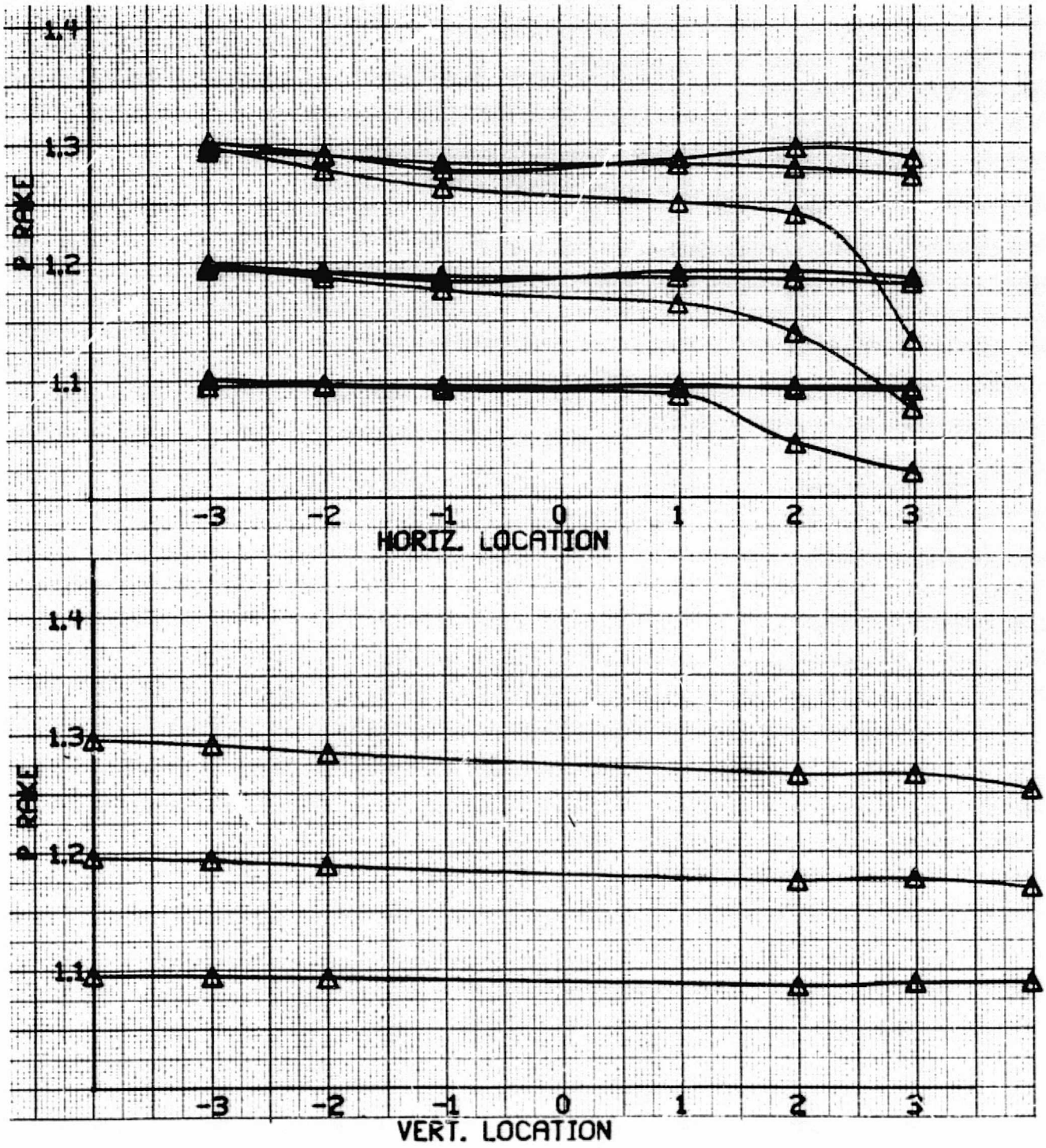

Figure 74. - Nozzle B exit total pressure ratio versus probe location for 90° nozzle angle.

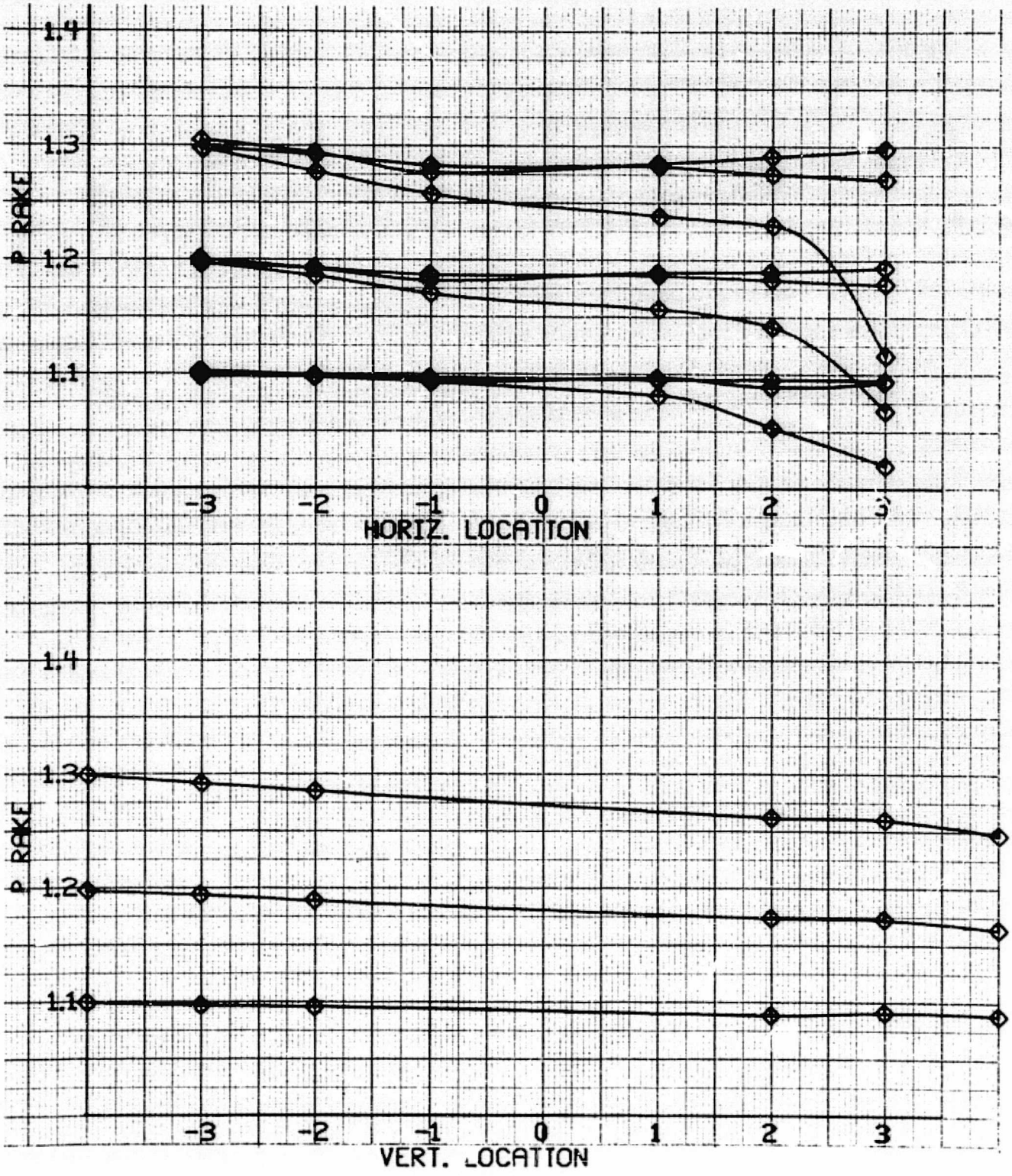

Figure 75. - Nozzle C exit total pressure ratio versus probe location for 90° nozzle angle.

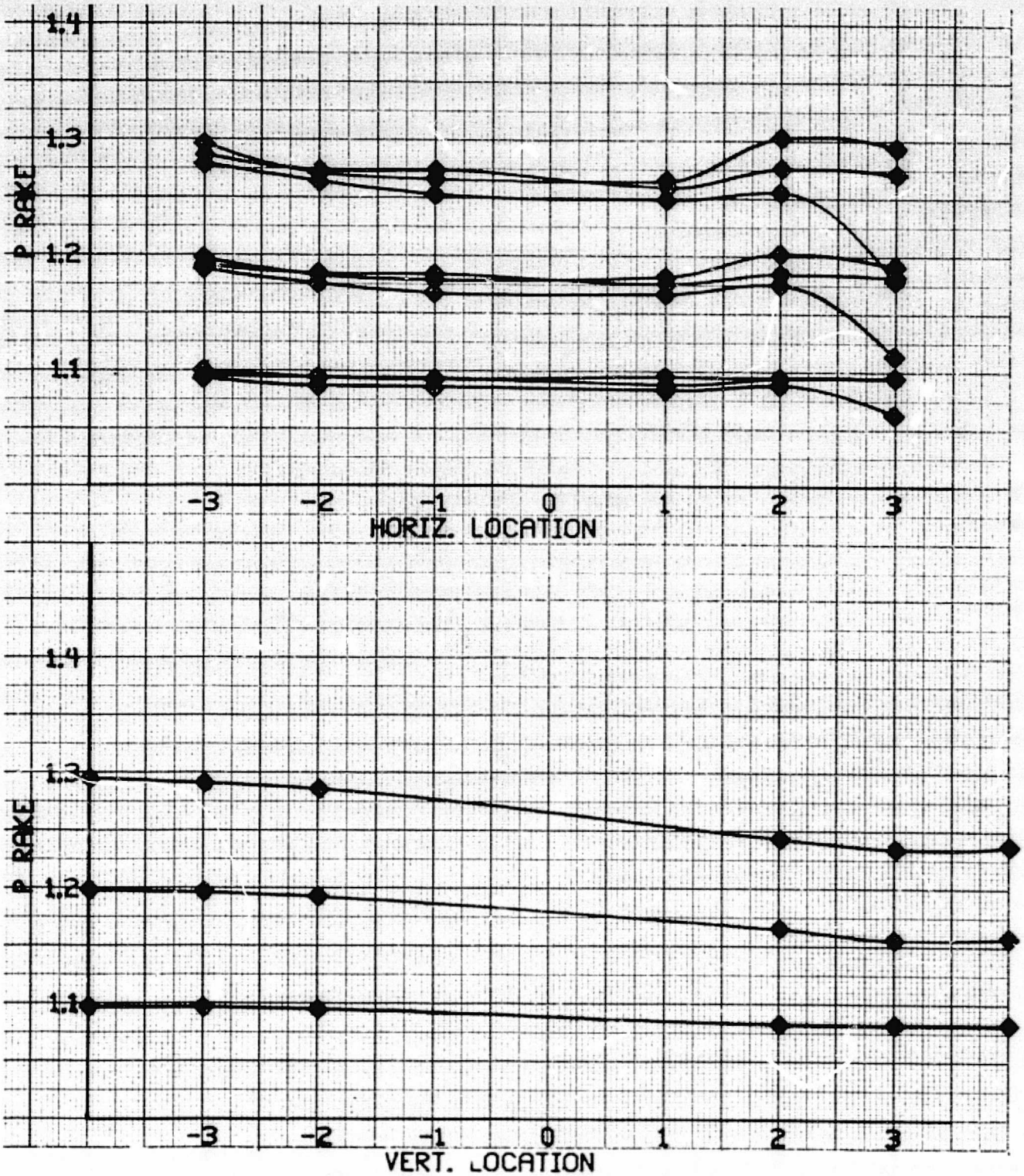

Figure 76. - Nozzle C (with vanes) exit total pressure ratio versus probe location for 90° nozzle angle.

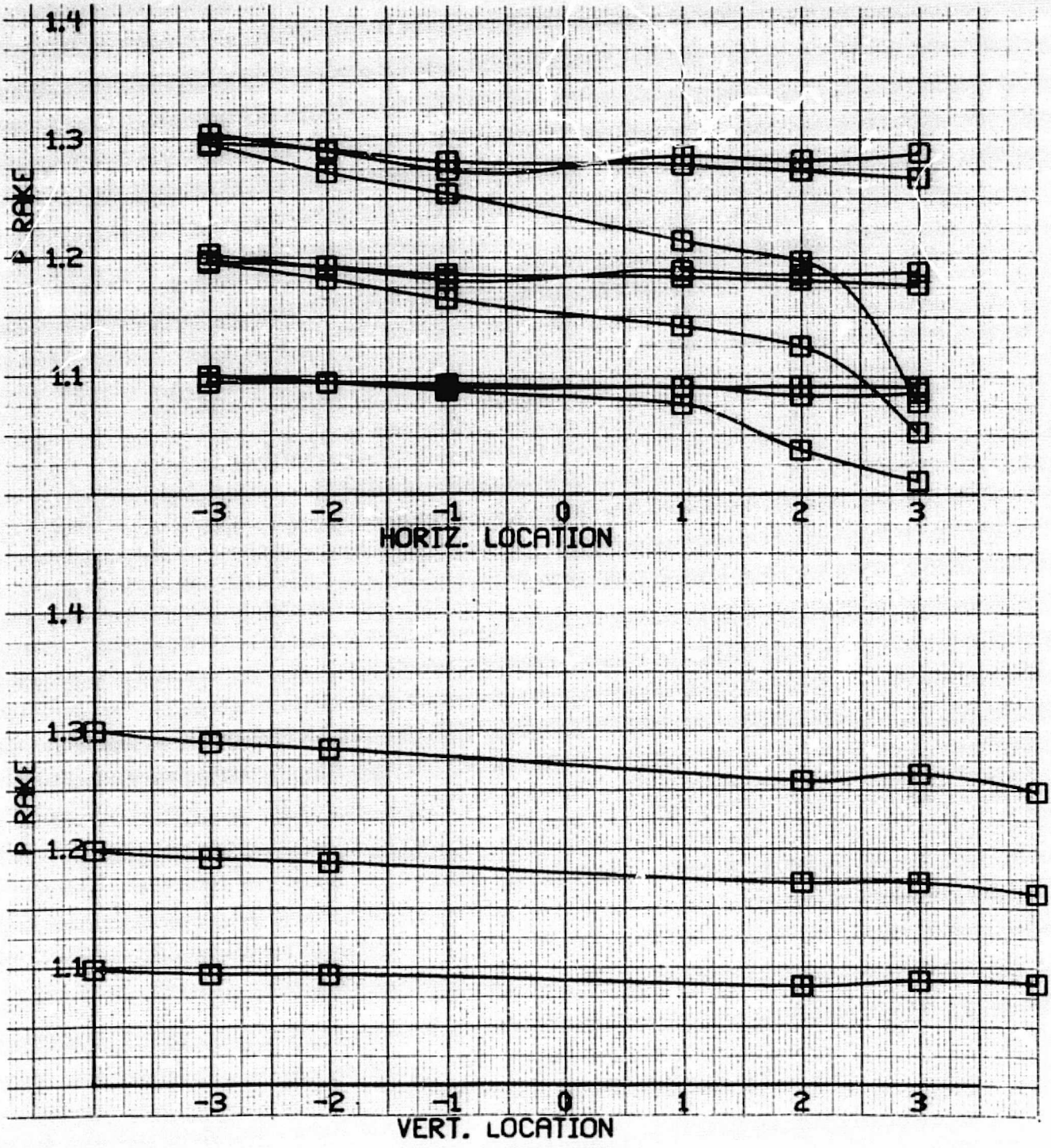

Figure 77. - Nozzle D exit total pressure ratio versus probe location for 90° nozzle angle.

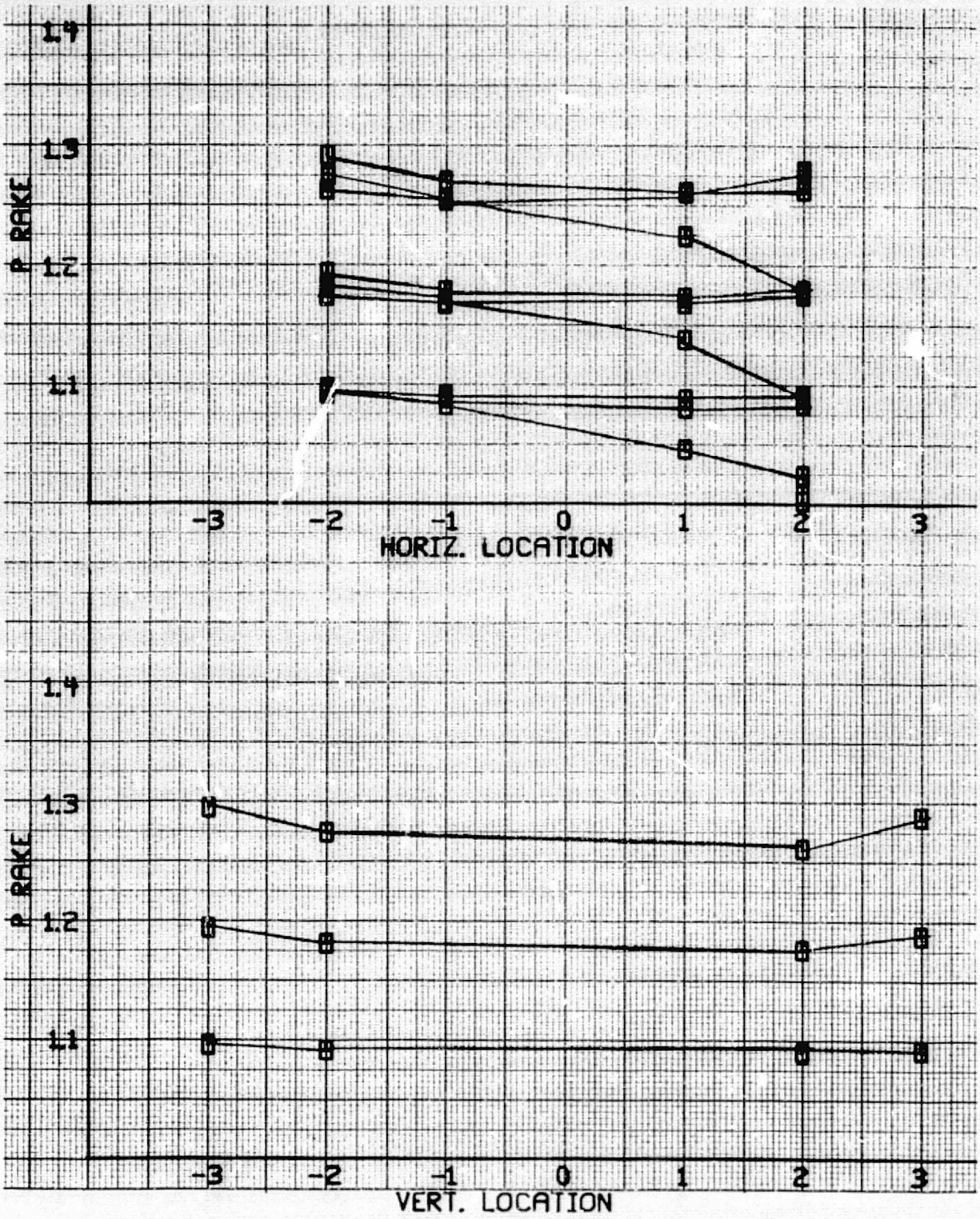

Figure 78. - Twin nozzle exit total pressure ratio versus probe location for 90° nozzle angle.

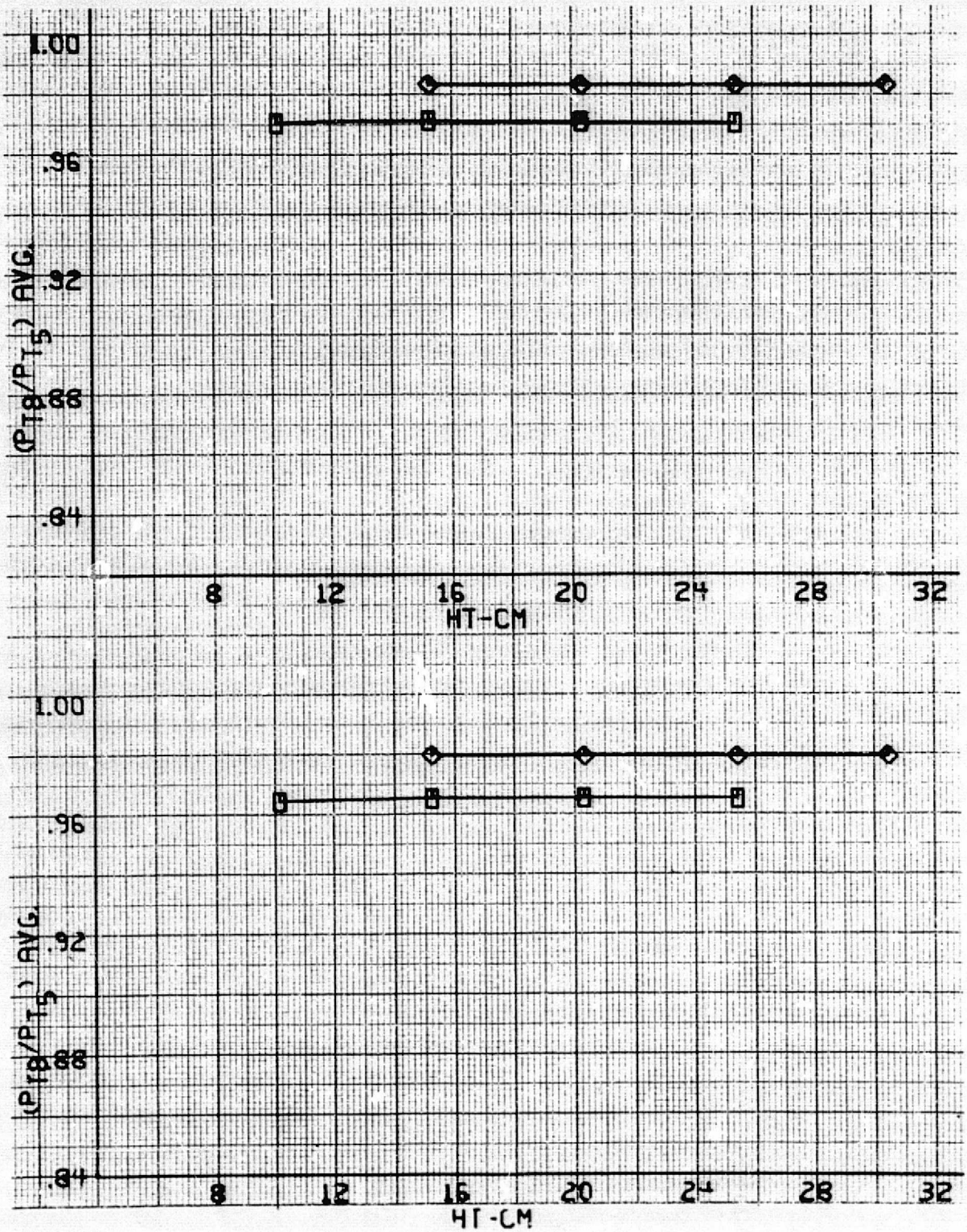

Figure 79. - Exit to inlet total pressure ratio versus ground height at 90° nozzle angle.

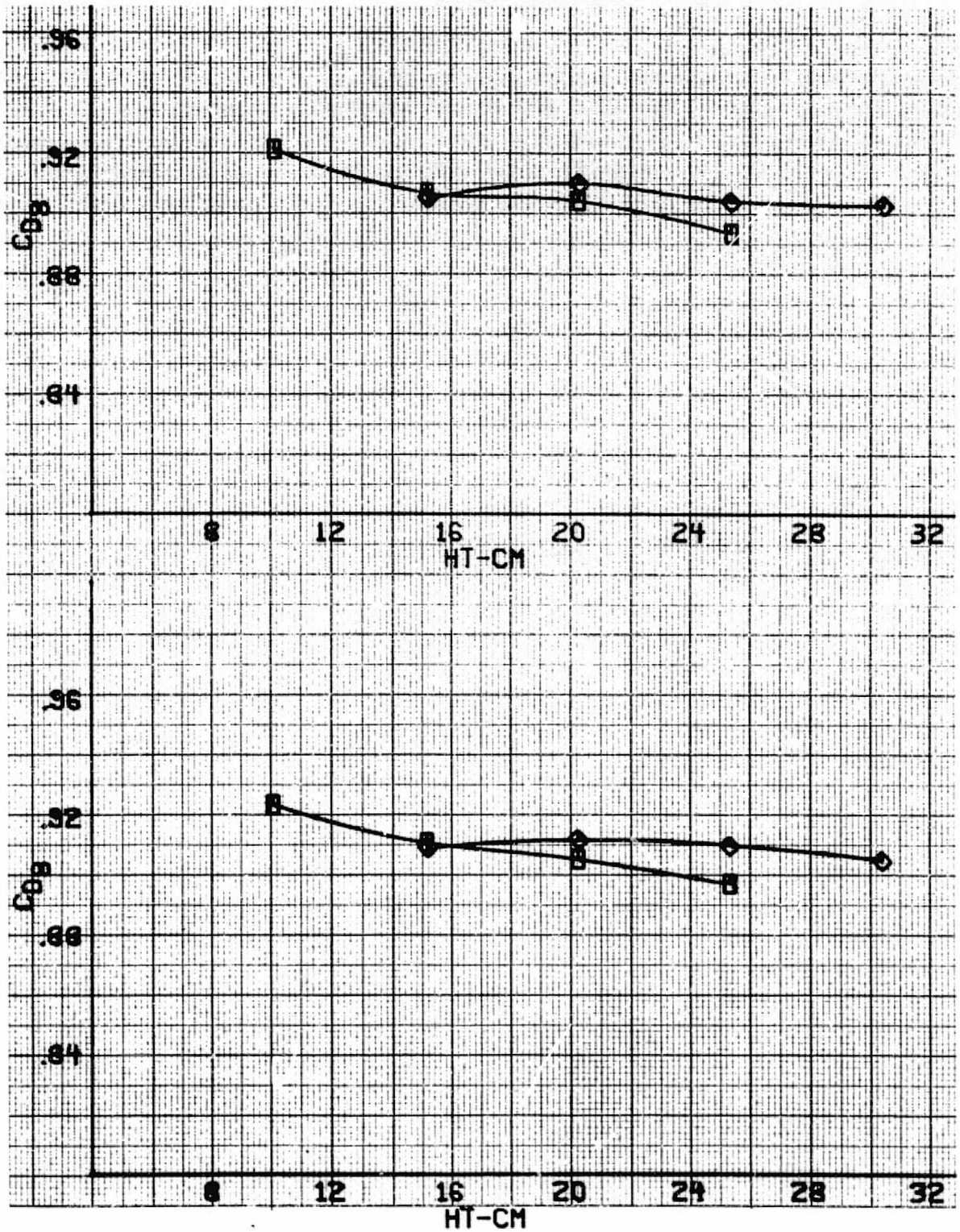

Figure 80. - Exit discharge coefficient versus ground height at 90° nozzle angle.

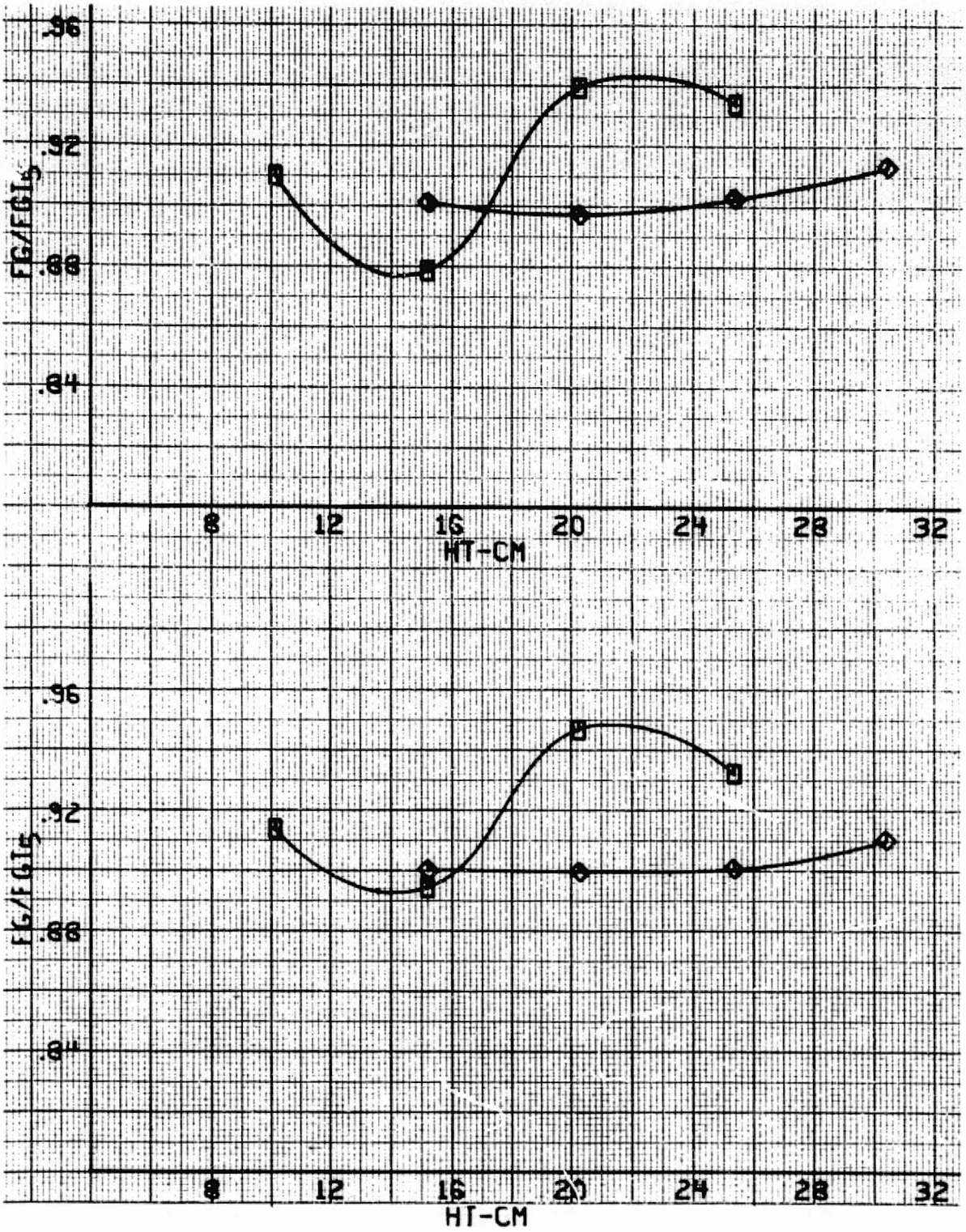

Figure 81. - Diffuser inlet discharge coefficient versus ground height at 90° nozzle angle.

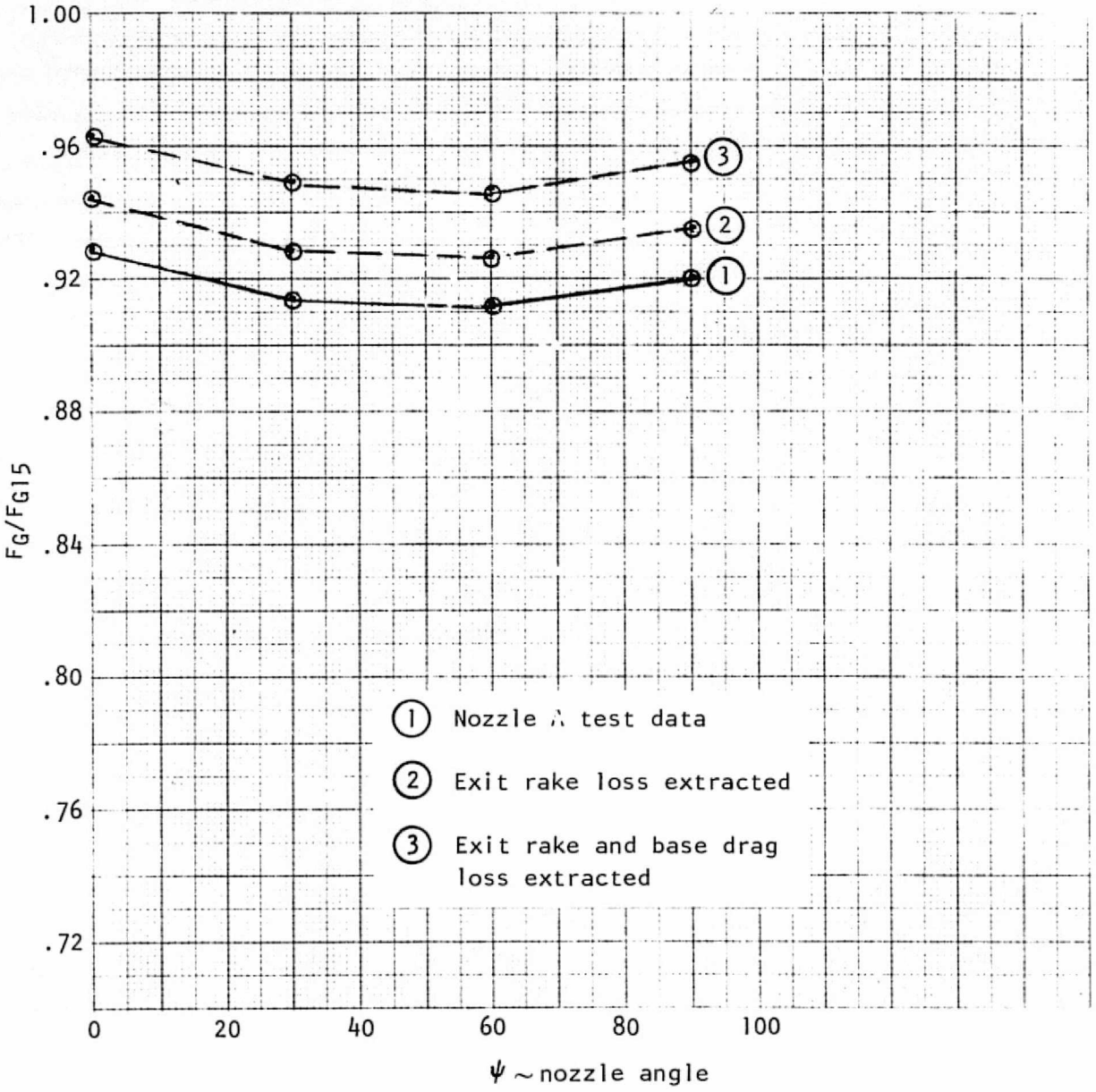

Figure 82. - Nozzle A diffuser inlet thrust coefficient at PT5/PA = 1.2 with exit rake and base drag loss extracted versus nozzle angle.

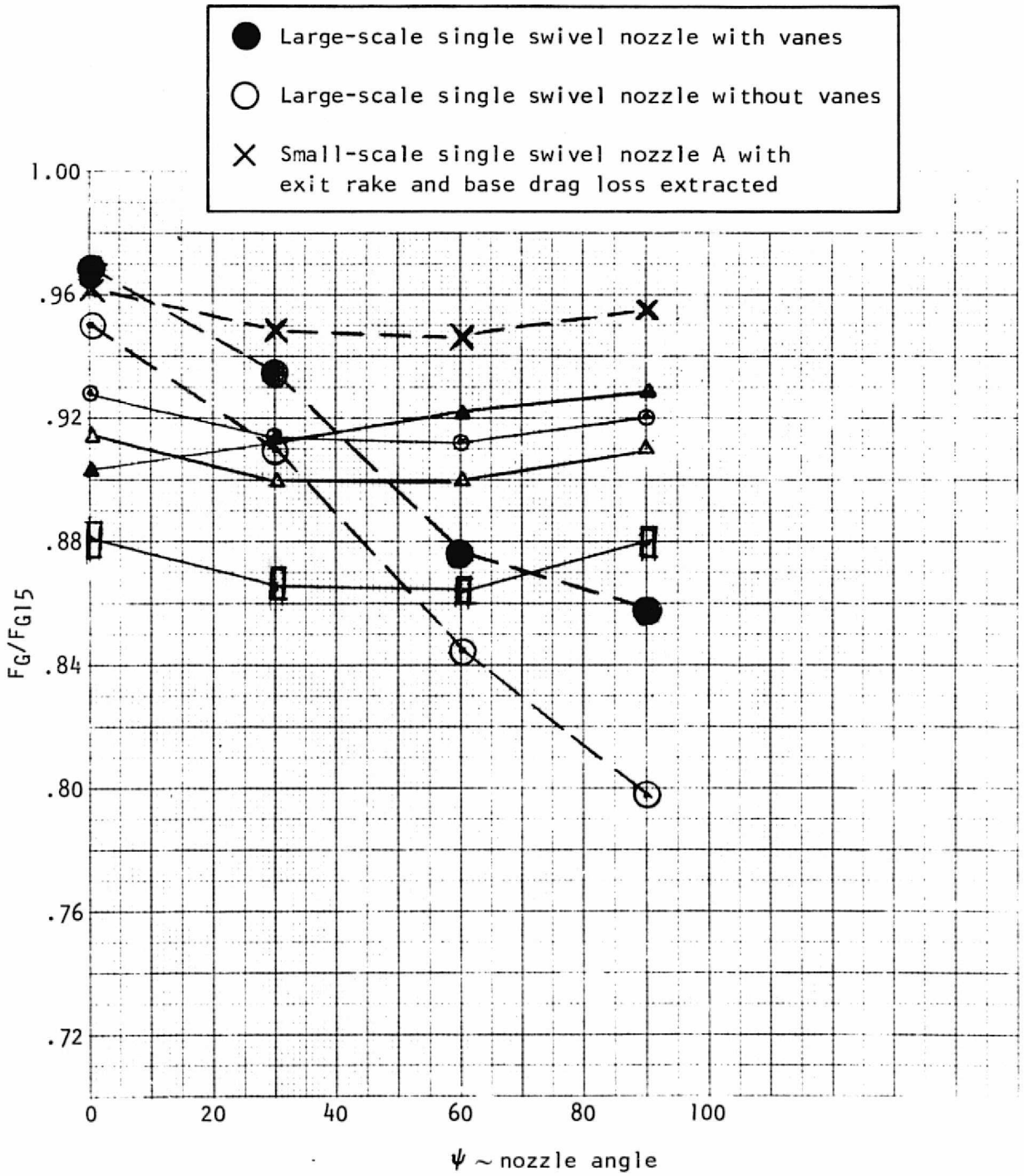

Figure 83. - Large-scale hardware and small-scale model diffuser inlet thrust coefficients at PT5/PA - 1.2 versus nozzle angle.